Pontifícia Universidade Católica
do Rio de Janeiro

Paula Stofer Cordeiro de Farias

Experimental characterization of linear interfacial waves in a stratified turbulent gas-liquid pipe flow using Particle Image Velocimetry.

Tese de Doutorado

Thesis presented to the Programa de Pós-Graduação em Engenharia Mecânica of PUC–Rio in partial fulfillment of the requirements for the degree of Doutor em Ciências – Engenharia Mecânica.

Advisor: Prof. Igor Braga de Paula

Co-advisor: Prof. Luis Fernando A. Azevedo

Rio de Janeiro

October, 2019

Paula Stofer Cordeiro de Farias

Experimental characterization of linear interfacial waves in a stratified turbulent gas-liquid pipe flow using Particle Image Velocimetry.

Thesis presented to the Programa de Pós-Graduação em Engenharia Mecânica of PUC–Rio in partial fulfillment of the requirements for the degree of Doutor em Ciências – Engenharia Mecânica. Approved by the Examination Committee.

Prof. Igor Braga de Paula
Advisor
Departamento de Engenharia Mecânica – PUC-Rio

Prof. Luis Fernando Alzuguir Azevedo
Co-advisor
Departamento de Engenharia Mecânica – PUC-Rio

Prof. Daniel Rodríguez Álvarez
Universidad Politécnica de Madrid

Dr. João Neuenschwander Escosteguy Carneiro
ISDB FlowTech

Prof. Rafael Menezes de Oliveira
Departamento de Engenharia Mecânica – PUC-Rio

Prof. Oscar Mauricio Hernandez Rodriguez
Escola de Engenharia de São Carlos – USP

Rio de Janeiro, October 4th, 2019

Paula Stofer Cordeiro de Farias

Graduated in Mechanical Engineering at PUC-Rio in 2007 and obtained a degree of Master in Mechanical Engineering by Pontifical Catholic University of Rio de Janeiro PUC-Rio, in 2010.

Bibliographic data

Farias, Paula Stofer Cordeiro de

Experimental characterization of linear interfacial waves in a stratified turbulent gas-liquid pipe flow using particle image velocimetry / Paula Stofer Cordeiro de Farias ; advisor: Igor Braga de Paula ; co-advisor: Luis Fernando A. Azevedo. – 2019.
170 f. : il. color. ; 30 cm

Tese (doutorado)–Pontifícia Universidade Católica do Rio de Janeiro, Departamento de Engenharia Mecânica, 2019.
Inclui bibliografia

1. Engenharia Mecânica – Teses. 2. Estabilidade linear. 3. Escoamento bifásico. 4. Velocimetria por imagem de partícula. 5. Ondas interfaciais. I. Paula, Igor Braga de. II. Azevedo, Luis Fernando A. III. Pontifícia Universidade Católica do Rio de Janeiro. Departamento de Engenharia Mecânica. IV. Título.

CDD: 621

In memory of my grandfather, Cyro.

Acknowledgments

First of all, I would like to thank my mentors, Professor Igor Braga de Paula and Professor Luis Fernando Azevedo, for their ability to teach, inspire and motivate.

The technicians, Leonardo and Marcio, for the partnership.

Friends and students of the university, for the daily friendship and research support.

My friend Anis, for a year of high-level knowledge sharing, learning and the Chapter 6 full of experience.

Petrobras and CNPq for the financial support.

My husband Flavio, who with love and affection also dived in this intense project.

My sons Miguel and Matheus, who were born and in the middle of these pages, grew up. They gave me maturity. Revealed my ability. In the form of a hug, a smile, at the end of the day, they reloaded everything I needed.

And lastly my life references, my parents and my sister, who with love and joy, taught me how to overcome harmoniously the difficulties day by day.

Abstract

Farias, Paula Stofer Cordeiro de Farias; de Paula, Igor Braga (Advisor); Azevedo, Luis Fernando Alzuguir (Co-advisor). **Experimental characterization of linear interfacial waves in a stratified turbulent gas-liquid pipe flow using Particle Image Velocimetry**. Rio de Janeiro, 2019. 170p. Tese de Doutorado — Departamento de Engenharia Mecânica, Pontifícia Universidade Católica do Rio de Janeiro.

The occurrence of slug regime in horizontal pipelines is of special interest for the oil and gas industry due to the unwanted operational risks associated with this flow. Hence, an intense effort has been devoted to the study and to model this flow regime. Predictive tools based on linear Kelvin-Helmhotz stability have been widely applied in the literature for prediction of slug onset. These models are derived from stability analysis of well-defined disturbances. However, for pipe flows, a limited number of experimental studies devoted to investigate the evolution of disturbances that lead to the initiation of slugs is available. In addition, no studies are found using of well define disturbances, which could provide accurate information for validation of models and numerical simulations. The present work addresses the problem by the studying of the evolution of controlled waves excited at the liquid interface. To this end, an oscillating paddle was employed. The work focuses the characterization of interfacial waves within the linear regime, which correspond to the regime of most models available in the literature. The amplitude threshold for linear waves was experimentally estimated. The driving signal of the oscillating paddle was synchronized with image acquisitions, enabling phase locked measurements of the waves and hence the use of ensemble averaging techniques. Phase-locked measurements of the velocity field in the liquid and gas layers were performed using off-axis Particle Image Velocimetry (PIV) technique and Shadowgraph. Mean flow, streamwise and wall normal fluctuations were measured simultaneously in the liquid and gas phases. For a range of flow rates and exciting wave frequencies the combined techniques employed allowed the extraction from the measured velocity fields, the coherent part of flow fluctuations related with the exciting waves. The results obtained have shown, seemingly, for the first time, that interfacial modes in both phases are nearly independent of near wall disturbances within the range of parameters covered in this work. Characterization of nonlinear waves was briefly investigated indicating changes in the mean velocity. Moreover, a correlation for wave friction factor based on wave and flow parameters was obtained, leading to an improvement on the liquid height

and pipe head loss estimation when are combined into the closure relations used for the 1-D models. The experimental methodology proposed in this work is a valuable tool to produce accurate information that can be used to validate and improve theoretical models and numerical simulations. It can contribute to the understanding of the physical mechanisms involved in the transition from stratified to slug flows.

Keywords

Linear stability; Two-phase flow; Particle Image Velocimetry; Interfacial waves.

Resumo

Farias, Paula Stofer Cordeiro de Farias; de Paula, Igor Braga (Orientador); Azevedo, Luis Fernando Alzuguir (Coorientador). **Caracterização experimental de ondas interfaciais em escoamento estratificado turbulento gás-liquido utilizando Velocimetria por Imagem de Partícula**. Rio de Janeiro, 2019. 170p. Tese de Doutorado — Departamento de Engenharia Mecânica, Pontifícia Universidade Católica do Rio de Janeiro.

A ocorrência do escoamento slug em tubulações horizontais é de especial interesse para a indústria de petróleo devido aos riscos operacionais indesejados associados a esse padrão de escoamento. Portanto, nas últimas décadas um intenso esforço foi dedicado ao estudo e modelagem do escoamento slug. Ferramentas preditivas baseadas na estabilidade linear de Kelvin-Helmhotz foram amplamente desenvolvidas na literatura para prever a transição para esse regime de escoamento. Esses modelos são derivados da análise de estabilidade modal de perturbações bem definidas. No entanto, para escoamento em tubulação, um número bastante limitado de estudos experimentais dedicados para investigação da evolução de perturbações que originem o regime slug está disponível. Além disso, estudos a partir da introdução de perturbações bem definidas, que podem fornecer informações precisas para validação de modelos e simulações numéricas, foram encontrados. O presente trabalho abordou o problema da transição para o regime slug a partir da caracterização da evolução de ondas interfaciais. Essas perturbações controladas foram excitadas com um modo de geração na interface do escoamento estratificado utilizando uma placa oscilatória. O trabalho se concentra na caracterização de ondas interfaciais no regime linear, que corresponde ao regime de estudo da maioria dos modelos disponíveis na literatura. Portanto, um limiar de amplitude para ondas lineares foi estimado experimentalmente. O acionamento da placa oscilatória foi sincronizado com as aquisições de imagens, permitindo medições sincronizadas em fase. As medições do campo de velocidade foram realizadas usando a técnica de Velocimetria de Imagem de Partículas (PIV) e Iluminação de Fundo (Shadowgraphy). O perfil de velocidade e turbulência do escoamento foram medidos simultaneamente nas fases do liquido e do gás. A sincronização em fase permitiu a extração do perfil de flutuação de velocidade coerentes as ondas interfaciais. Os resultados obtidos são originais e mostraram, pela primeira vez na literatura, que os modos interfaciais em ambas as fases são quase independentes dos modos cisalhantes, dentro da faixa de parâmetros abordados neste trabalho. A caracterização de ondas não

lineares foi brevemente investigada, indicando mudanças no perfil do escoamento médio. Além disso, foi obtida uma correlação para o fator de atrito das ondas interfaciais, levando a uma melhoria na estimativa da altura do líquido e da perda de carga do tubo quando combinadas nas relações de fechamento dos modelos 1-D. A metodologia experimental proposta neste trabalho é uma ferramenta valiosa para produzir informações precisas que podem ser usadas para validar e aprimorar modelos teóricos e simulações numéricas. O estudo pode contribuir para a compreensão dos mecanismos físicos envolvidos na transição do escoamento estratificado para slug.

Palavra-chave

Estabilidade linear; Escoamento bifásico; Velocimetria por Imagem de Partícula; Ondas interfaciais

Summary

List of figures

List of symbols

A_L – Liquid cross-sectional area [m^2]

A_G – Gas cross-sectional area [m^2]

c – Wave celerity [m/s]

D – Pipe diameter [m]

F_s – Sampling frequency [Hz]

f_a – Aliased frequency [Hz]

f_i – Interface friction factor

f_s – Sampled signal [Hz]

f_{wave} – Wave friction factor

g – Gravity acceleration [m/s^2]

h_h – Harmonic amplitude [m]

$\overline{h_l}$ – Mean liquid height [m]

h_g – Gas height [m]

k – Wavenumber [rad/m]

K – Kirby parameter

L – Pipe length [m]

N – Number of images

Re_G – Gas Reynolds number

Re_L – Liquid Reynolds number

S – Mean velocity profile distortions

t – Time delay between image frames [μs]

U_b – Bulk velocity [m/s]

U_r – Ursell number

U_{sg} – Gas superficial velocity [m/s]

U_{sl} – Liquid superficial velocity [m/s]

U_τ – Wall shear velocity [m/s]

u^* – Streamwise random turbulence component [m/s]

u' – Streamwise velocity fluctuation [m/s]

v^* – Wall normal random turbulence component [m/s]

v' – Wall normal velocity fluctuation [m/s]

Greek characters

β – Pipe inclination [deg]

ΔP – Pressure drop [Pa]

Δx – Image field of view [pixel]

λ – Wavelength [m]

ρ_G – Gas density [Kg/m^3]

ρ_L – Liquid density [Kg/m^3]

σ – Surface tension [N/m]

τ_G – Gas shear stress [Pa]

τ_i – Interface shear stress [Pa]

τ_L – Liquid shear stress [Pa]

τ_w – Wave shear stress [Pa]

$\phi_{u'}$ – Streamwise direction wave induced fluctuation [m/s]

$\phi_{v'}$ – Wall normal wave induced fluctuation [m/s]

ω – Wave frequency [Hz]

1
Introduction

The simultaneous transportation of gas and liquid in horizontal pipelines is present in many engineering applications such as boilers, nuclear reactors, evaporators and in oil and gas pipelines. An important characteristic of two-phase flows is the existence of a variety of flow regimes defined by the flow rates, fluid properties, geometrical parameters of flow lines, among other flow variables. The classification of these regimes is based on the distribution of phases within the pipe cross section (Wallis and Dobson, 1973). Typically, two-dimensional maps of flow regimes are useful as a quick guide for flow pattern prediction (Baker 1954, Mandhane et.al 1974, Taitel and Dukler 1976), hence they are widely employed in industry.

In the oil and gas industry, multiphase flows in pipelines are usually found in many stages of production. Unwanted operational conditions may appear under some flow regimes. Gas-condensate pipelines, for example, operate primarily in the stratified flow regime. Due to temperature and pressure drop, the condensation of saturated gas vapor results in a continuous change of pressure drop along the pipeline and hence influence the operating conditions (Raimondi, L., 2017). Thus, the knowledge of the flow regime is important for the proper operation of pipelines, as well as for its design, since these regimes can significantly influence pressure drop, heat transfer, hold-up, shear stress levels and other relevant production parameters.

Among several regimes, slug flow in horizontal pipelines is of special interest due to its common occurrence in oil and gas industry and to operational risk related with intermittent stresses on structure and possible overloads of oil separators caused by long liquid slugs. During the last decades, intense effort has been devoted to study and to model the slug flow characteristics in order to increase safety and profit margins in pipeline operations (Havre et al., 2000). This regime can be initiated by two main mechanisms: changes of pipe orientation (terrain induced slugs, severe slugs) or by shear induced effects (hydrodynamic slugs). The formation of hydrodynamic slug is attributed to natural growth of hydrodynamic instabilities at the fluid interface of a stratified flow regime (Wallis, 1969).

Traditional slug flow models are mostly based on the ‘‘unit-cell’’ analysis. In this approach, a periodic control volume, incorporating the long gas bubble and the liquid slug, travelling at a known speed, enables a steady-state solution analysis based on mass and momentum balances (Wallis, 1969). However, steady-state models are not able to predict the transition between flow patterns and numerical models for transient multiphase flows have been developed in the the early ‘90s.

The ‘‘slug tracking’’, and ‘‘slug capturing’’ are most used strategies for transient slug flow models (Issa and Kempf, 2003). In ‘‘slug tracking’’ category, the movement, growth and vanishing of slugs are analyzed based on the Lagrangian tracking of individual slugs. Hence, the position of each slug tail and front is monitored along the pipe within the framework of the two-fluid model. The commercial code OLGA (Bendiksen et al., 1991) is one example of the application of slug tracking model. In the other hand, models based on “slug capturing” assumes that slug flow regime is predicted by growth of hydrodynamic instabilities.

For horizontal pipelines, there is already a general agreement in the literature that disturbances at the interface of a stratified regime can play a major role in the initiation of slugs. The transition from stratified to slug regimes are modelled by the one-dimensional, transient, two-fluid model applying empirical closure relations for wall and interfacial shear stresses. Thus, predictive tools based on linear Kelvin-Helmhotz stability have been widely applied since the 70´s to predict the conditions for slug initiation. From a literature survey, several models and empirical correlations can be found for predicting the onset of slugging (Wallis and Dobson 1973, Lin and Hanratty 1986, Taitel and Dukler 1976, Barnea and Taitel 1993, Kadri et al. 2009). The two-fluid model is well established (Ishii, 1975) however, it was not conclusively demonstrated its capability of predicting accurately the development of slug flow from the growth of instabilities in stratified flow regime. To overcome this, an alternative procedure adopted is to predict the conditions necessary for the existence of slugs in pipelines. However, it is interesting to emphasize that conditions necessary for slug existence and for slug initiation do not converge for similar values. This is clear if one considers the possibility, for instance, of hysteresis. Thus, once the slugs are formed they can disappear at lower velocities than those required for its initiation (Valluri et al., 2008).

Recently, prediction of flow regimes in pipeline flows have reached a certain level of maturity but there is still a high demand for improvements of available

models (Ayati et al. 2017). In addition, there is a high demand for more accurate models for predicting head loss in wavy stratified flows. Due to the complexity of the problem it is, indeed, very difficult to establish a unique model which can be used for a wide range of flow parameters. Several works have been carried out over the past 50 years dedicated to investigate, to validate and to model flow dynamics, focusing on the initiation of intermittent flows. A common procedure adopted for validation of theoretical and numerical models is to correlate the instability of a given base flow with experimental conditions required for first appearance of slugs (see Sanchis et al. 2011 for a review). To this end, statistical data about superficial velocities at which slugs first appear and slug shedding frequencies have been extensively used. For instance, Barnea and Taitel (1989 and 1993), Funada and Joseph (2001) and Kadri et al. (2009) compare predictions from linear stability models with measured slug statistics. Although shear rates related to phase velocities can influence the growth of disturbances via linear instability mechanisms, it is rather unclear whether these mechanisms are solely responsible for slug initiation. Moreover, accurate stability predictions are still rather difficult because turbulence can actively modify the base flow and hence the wave development. Thus, a deep knowledge about relevant physical mechanisms related with slug initiation is still demanded for the development of more sophisticated and effective tools for slug control.

For a straightforward validation of models and simulations, it would be more convenient to have an experimental database about the development of interfacial waves, since most of the models are derived from the modal stability analysis of well-defined disturbances. Although many experimental investigations address the characterization of waves in stratified flows, no information about modal disturbances is found. Typically, for modal analysis, a controlled experiment is required (see Drazin 2002, for a review). However, the setup required to introduce disturbances with characteristics approaching that of the most unstable modes, according to the stability analysis, is not found in the literature. Thus, there is an evident lack of experimental data for validation of recent models based on modal linear stability analysis, like those reported in works of Kaffel and Riaz (2015) and of Barmak et al. (2016). In this scenario, it is clear that experimental characterization of controlled interfacial waves is important for validation of slug predictive models.

1.1
Objective

The aim of the present work is to address the instability problem related with slug initiation by introducing controlled waves at the liquid interface, for a horizontal stratified gas-liquid pipe flow. Conditions selected for this study are close to transition from stratified to intermittent flow regimes. Several experimental techniques such as shadowgraphy, excitation of controlled disturbances and two-phase Particle Image Velocimetry are combined in this thesis to provide original information about the flow at the initial stages of evolution of unstable interfacial waves. At these stages, waves are assumed to have small amplitudes. This condition is similar to those adopted in most models found in the literature for prediction of slug initiation. Thus, the idea is to provide detailed information that can be directly compared against existing models and numerical simulations. This is important for a proper validation of these tools. Moreover, the original information produced within this work might help to shed some light on the physical description of the phenomenon and to improve models used for stratified flows, which are also highly important for industry.

1.2
Methodology

The methodology employed in this thesis consists of studying the evolution of controlled perturbations introduced at the gas-liquid interface of a stratified flow. The idea is to characterize the waves, which are involved in the process of slug transition under different sets of flow parameters, namely, mixture velocities, wave frequencies and amplitudes. The approach adopted is inspired on the classical work of Klebanoff et al. (1962) that introduced controlled disturbances in a boundary layer using a vibrating ribbon. In the experiments related to the present thesis, a moving paddle positioned at the gas-liquid interface replaces the vibrating ribbon. Although the technique is well established for boundary layer studies, controlled perturbations with a well-defined spectral content have never been applied for experimental investigation of two-phase flows.

The characterization of the flow and the measurement of the evolution of the disturbances, at early stages of slug formation, was performed using non-intrusive optical techniques known as Shadowgraphy and Particle Image Velocimetry (PIV). The acquisition of images was synchronized with the wave generation, hence enabling phase-locked acquisitions. Phase -locked acquisition

is a very useful instrumentation technique. It can be used whenever an imaging acquisition system is phase-coherent with a reference signal. In the present study, the reference signal is derived from the periodic stimulus of the wave generation source. Thus, temporal and spatial evolution of the disturbances generated by the oscillating plate could be captured. In this work, it was chosen to start the investigation with a simple set-up for studying the evolution of interfacial oscillations. Afterwards, PIV measurements were carried out in the liquid layer only. Finally, velocity fields were measured in the gas and liquid layers simultaneously. It is important to mention that in all cases the measurements were synchronized with the excitation of the disturbances.

One of the main advantages of phase-locked measurements is the capability to extract coherent oscillations from noisy signals. This advantage was used to study the effect of waves on mean velocities and turbulence. Velocity fluctuations related with wave frequency could be analyzed separately from the turbulence. In the linear regime of wave evolution, these are waves induced fluctuations that would be directly comparable with eigenfunctions given by the solution of stability analysis based on Orr-Sommerfeld equations. Moreover, some other features of interfacial waves were measured by applying digital image processing techniques. Characteristics such as wavenumber, celerity, wave amplification, and induced pressure drop were also obtained.

In summary, the methodology adopted in the present work is an original contribution to two phase flow studies. It provided a valuable experimental database for comparison with models and numerical simulations. This might contribute to the validation and improvement of existing tools used for slug prediction. To the best of the authors knowledge, this is the first time that such data are reported in the literature. Details of the wave generation procedure, optical techniques and test bench assemblies are reported in the next chapter.

1.3
Thesis Structure

This manuscript is divided into ten chapters. Chapter 2 presents a literature survey about physical mechanisms related to stability of stratified flows and its relevance for slug initiation are outlined. A description of the setup and measurement techniques applied in this work is provided in Chapter 3. In Chapter 4 a discussion about image processing strategies adopted is described. Next, Chapter 5 is devoted to present data reduction and post processing procedures. The evolution of interfacial linear waves is studied in Chapter 6. Chapter 7

proposes a nonlinearity parameter to define a threshold for linear wave regime. The parametric variation of parameters is reported in Chapter 8. In Chapter 9 the increment of friction factors related with interfacial waves is measured. Finally, in Chapter 10, a summary of the main conclusions are presented and suggestions for further studies are provided.

2
Review of mechanisms related to the transition from stratified to slug flow

In this chapter a general overview of two phase flow and of physical mechanisms related to initiation of slugs are provided and a survey of models used for prediction of slug formation is discussed.

2.1
Two-phase flow

Two-phase flows are found in several industrial processes and usually are composed of two immiscible phases flowing simultaneously in a system. In pipe flows, different flow regimes might be found depending on the conduit geometry, fluid properties and velocities, among others. An extensive review of two-phase flows regimes is found in the book by Wallis (1969).

In the oil industry, the design of fluid transportation systems is still a challenge. One of the most difficult problems is the prediction of the flow patterns, which is necessary for equipment design and pipeline operation. A wide variety of gas-liquid two-phase flow patterns has been observed in the literature and they can be didactically separated into three categories: dispersed flow (dispersed bubbles), separated phases (annular and stratified) and slug flow. In the work of Wallis and Dobson (1973) and Taitel and Dukler (1976), a complete flow pattern review for horizontal two-phase flow can be found for the reader and will be shortly presented in the following.

- Disperse bubble flow: The gas phase is dispersed in a continuous liquid phase. Due to gravity, the bubbles tend to move to the top of the tube.
- Plug flow or elongated bubble flow: The gas phase is distributed as elongated bubbles flowing at the top of the pipe with wavelengths of the order of the tube diameter.
- Slug Flow: Flow regime characterized by an intermittent series of liquid plugs (slugs) separated by a relatively large gas pockets. The liquid slugs have a bullet shape that occupies almost the

entire cross-sectional area of the pipe and may contain small entrained gas bubbles.

- Stratified flow: Characterized by low flow rates, the less dense phase, gas, flows on the top of liquid phase. The phases are segregated and flow separated by a continuous interface which can be smooth at lower flow rates, or wavy, as flow rate increases.
- Annular flow: The gas phase flows at the center of the pipe cross-section while the liquid phase flows in the form of an annulus around the gas phase, as a thin film wetting the pipe wall. In horizontal flow, due to gravity, this film is thicker on the pipe wall bottom.

The sketches of flow regimes for two-phase flow in a horizontal pipe are illustrated in Figure 4.

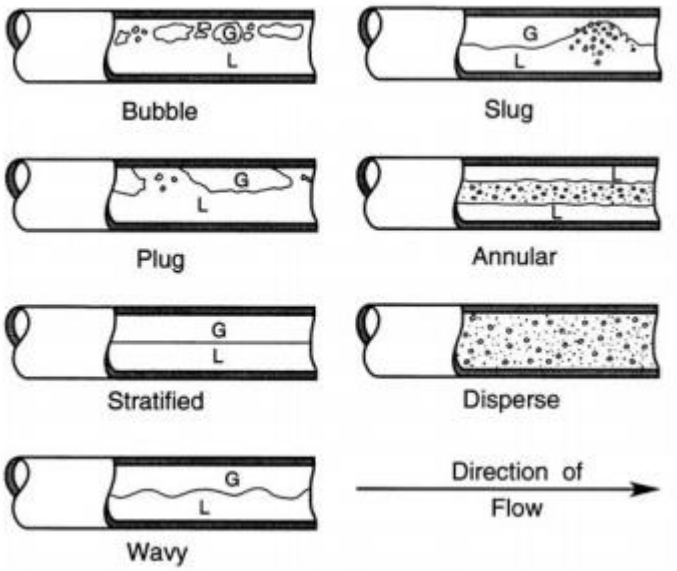

Figure 4 – Sketches of flow regimes for two-phase flow in a horizontal pipe. Extracted from Weisman (1983).

Two-phase flow-pattern maps are widely used tools in industry to predict flow regimes. These are generally two-dimensional charts designed for a quick identification of flow regimes in a specific system according to flow and fluid properties. Over the past decades, a substantial number of studies have been devoted to investigate transition between flow regimes based on various flow parameters. In the period between 1960´s to 1980's several of these maps were proposed for prediction of flow regimes. Most flow pattern maps proposed within this period were developed for adiabatic conditions (Hewitt and Roberts, 1969; Baker,1954; Taitel and Dukler,1976).

Geometrical parameters of flow lines and fluid properties, such as liquid viscosity, surface tension and density, can significantly affect the transition boundaries of two phase flows. An alternative to maps based on mechanistic models is to trace critical conditions for transition between regimes according to extensive experimental observations. One example of this approach is the map proposed in the work by Mandhane et al. (1974), which is illustrated in Figure 5. The map proposed in Mandhane et al. (1974) is based on experimental data from different tests rigs. They observed that some results from different test benches can show discrepancies. Thus, it became clear that there is no unique flow pattern map which is valid for a wide range of flow parameters and test conditions. Thus, the accuracy of this approach is also limited.

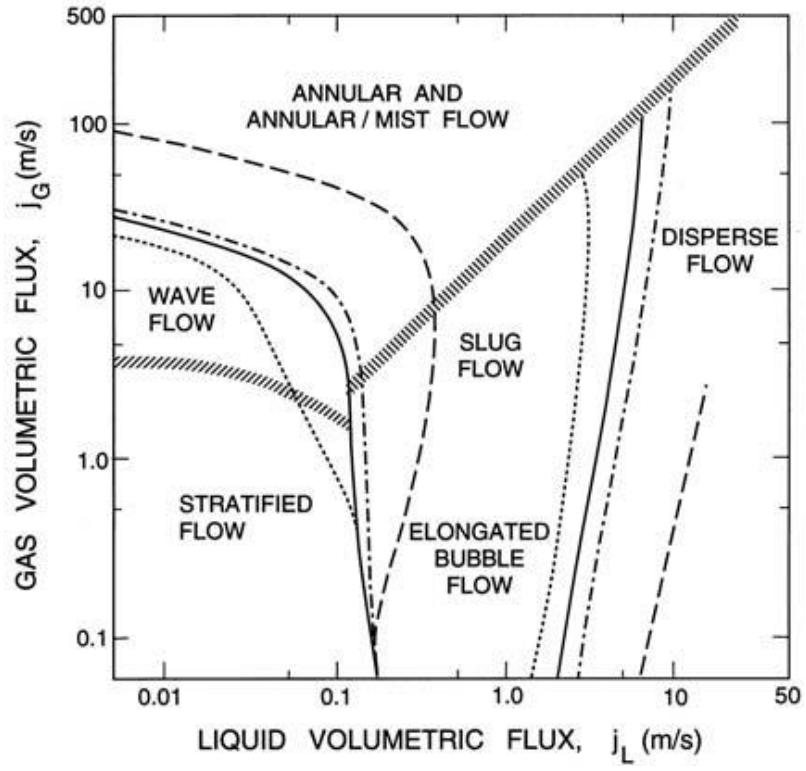

Figure 5 – Flow regime boundaries for various pipe diameters: 1.25cm (dotted lines), 2.5cm (solid lines), 5cm (dash-dot lines) and 30cm (dashed lines). Extracted from Mandhane et al. (1974).

According to Mandhane et al. (1974), the transition from stratified to slug flow is one where considerably large discrepancies between different data sets were found. The origin of these discrepancies motivated the development of several models for the problem.

In the oil and gas industry, the slug flow pattern is important due to its frequent occurrence in typical operational regimes of pipelines and are a concern

for the industry. In offshore production facilities, for example, the occurrence of intermittent flow can increase the operational risk due intermittent stresses on structure and possible overloads of oil separators caused by long liquid slugs.

The usual technique adopted in industry for suppression of slugs is via a sudden expansion of the pipe section. This creates a vessel like structure known as “Slug Catcher”. However, this equipment does not prevent slug formation neither its effects on pipelines upstream of the catcher. The development of more sophisticated and effective strategies for predicting the occurrence of slugs can be interesting to avoid undesirable flow behavior. A description of the physical mechanisms underlying slug formation is demanded for development of accurate predictions and for design of flow control technologies.

In oil industry flowlines, slug flow can be initiated by transient effects during pigging operations (operation induced slugs), by changes of pipe orientation (terrain induced slugs, severe slugs) or by shear induced effects (hydrodynamic slugs).

In case of terrain induced slugs, there is liquid accumulation in the lower region of pipelines situated in hilly terrains. Once the liquid blocks the pipe cross section, the gas is trapped. The pipe pressure upstream the liquid plug increases until it becomes sufficient to overcome the hydrostatic liquid head. Then, the liquid is expelled until a new blockage plug is formed (Bai et al, 2005).

The formation of hydrodynamic slug is attributed to hydrodynamic instabilities at the fluid interface (Wallis, 1969). In this case, disturbances at the interface can grow due to flow instabilities and lead to slug formation. The relevance of the mechanisms related to hydrodynamic instability in slug flow initiation is largely supported by many authors in the literature (Wallis and Dobson 1973, Taitel and Dukler 1976, Barnea 1987, Barnea and Taitel 1993, Rodrigues 2008).

The present thesis focuses on mechanisms related to the initiation of hydrodynamic slugs. Thus, some basic concepts about hydrodynamic stability are required to clarify the connection between instability of interfacial waves and the formation of slugs. The next sections present a review of hydrodynamic stability concepts. Those who are familiar with the subject can skip to section 2.3.

2.2
Hydrodynamic instability

“For any problem of viscous flow under given steady conditions there must, in principle, exist an exact steady solution of the equations of fluid dynamics.

These solutions formally exist for all Reynolds numbers. Yet, not every solution of all the equations of motion, even if exact, can actually occur in Nature. Those which do, must not only obey the equations of fluid dynamics, but also be stable" (Landau and Lifshift 1959).

In fact, steady solutions of equations of motion represent an equilibrium system of forces. However, this balance can either be stable or unstable. An unstable system does not return to its initial equilibrium state if perturbed, whereas a stable system does return. These general concepts apply to both solid and fluid mechanical systems.

In two-phase flow studies, hydrodynamic instability aims at predicting unstable conditions that may lead to a change in the flow regime. A complete description of transition phenomenon in two phase flows would open great prospects for industry. Unfortunately, due to mathematical difficulty inherent to this physical problem, the transition scenarios are not expected to be fully understood in the very near future.

Yet, the development of transition models is important for engineering purposes. Thus, the development of models based on stability analysis of simplified flows are an interesting solution. To this end, simplifications are applied to the problem mathematical formulation. The basic ideas employed in the analysis of flow instabilities are similar to those adopted for mechanical systems. In both frameworks, a common way to address the problem is by introducing disturbances with small amplitude and to observe whether they grow or decay. Based on this approach one can find in the literature two classical approaches for flow stability analysis. The first uses energy variation of the perturbed flow immediately after the flow is disturbed, whereas the other search for long time response based on the solution of an eigenvalue problem. A detailed review of these approaches can be found in any classical book of hydrodynamic stability (e.g. Drazin, 2002).

In the energy method, if the base steady flow has lower energy than the perturbed flow, an energy input is required to produce the perturbation. Hence, the flow is assumed to be stable. An analogy can be traced with the mechanical system of a ball on a valley. There, the gravitational potential energy is at a minimum. On the other hand, if energy of the perturbation reduced the energy of the base flow, the energy released can be converted into a kinetic energy of the disturbances. This is analogous to a mechanical system of a ball on the top of a hill. By applying this concept, the energy balance can be adopted to determine whether the flow is stable or not.

In the second method, the equations of fluid motion are decomposed in normal modes (e.g. Drazin 2002, Mendonça 2000) and the resulting eigenvalue problem is solved. The stability analysis consists of finding solutions that may grow or decay in time or space.

Both classical methods (energy and normal modes) always assume that disturbances are small with respect to base flow quantities and hence the problem can be linearized (Kundu et al. 2012). This simplified problem is known in the literature as Linear Stability Theory (LST). However, critical conditions for the flow to become unstable might vary according to the method adopted. In the following section, the definition of critical flow conditions according to different stability analysis is briefly described.

It is important to mention that in the case of two-phase flows in pipelines, it is not yet defined what can be considered as a small amplitude. Therefore, it is not clear to which extent results given by linear stability analysis are valid. This is an open question in the literature that will be addressed in this work.

2.2.1
Discussion about critical conditions for onset of instability

The classic experiment of Osborne Reynolds (1883) suggested that there is a non-dimensional parameter which is related with laminar to turbulent flow transition of single phase flows in pipes. Later this parameter became known as Reynolds number. The critical value is related to the conditions where transition was observed. Subsequent works demonstrated that the critical Reynolds number could vary according to the inlet conditions, but there is a lower bound below which the flow is always laminar (for a review see Schlichting, 1979). Thus, it becomes clear that flow stability may depend on the initial energy of the perturbation. Based on these observations and on the premises of classical stability analysis methods, a flow can be classified into different states according to its stability. In the book of Schmid and Henningson (2001) four different classifications are suggested: i) unconditionally stable with monotonic damping of disturbances, ii) unconditionally stable, iii) conditionally stable and iv) linearly unstable. A graphical visualization of these definitions can be seen in Figure 6(a). The sketch of Figure 6(b) illustrates the evolution of disturbances according to different stability states.

According to Figure 6(a), region I is delimited by the Reynolds number given by energy stability analysis. In this approach, the critical condition is given by the

initial derivative of the energy after the introduction of a disturbance into the system. Thus, a stable flow implicitly assumes a monotonic decay of disturbances (Line 1 in Figure 6b).

The right end of region II in Figure 6(a) is delimited by the global Reynolds given for unconditionally stable flow. This critical Reynolds number is assumed to correspond to the lowest Reynolds number at which any instability can be sustained. In this case, the perturbations are stable regardless of their initial energy (E_v at t=0). Line 2 in Figure 6(b) suggests that perturbations in this region can grow for a moment, but in an infinite time they will decay, thus the flow is expected to be globally stable. For Reynolds number greater than Re_G the perturbations can be either damped (region III) or amplified (region IV) depending on the initial disturbance energy. This behavior is clearly represented by lines 3(a) and 3(b) in Figure 6(b). The critical Reynolds defined by linear stability delimits these two remaining regions. Above this Reynolds number regime there exists at least one infinitesimal disturbance that is unstable, as illustrated by line 4.

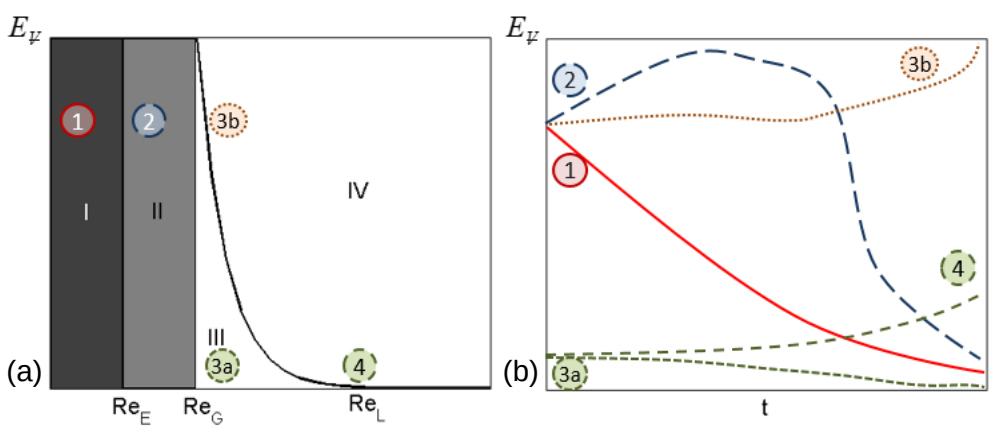

Figure 6 – Different definitions of critical Reynolds numbers adapted from Schmid and Henningson (2001).

It is important to emphasize that the instability of a single phase flow does not determine the occurrence of turbulence nor the transition location. The Critical Reynolds defined by linear stability analysis only establishes the limiting conditions from where perturbations may start to grow. Thus for complete description of the transition process, non-linearity might be also important. The same statement should hold for two phase flows.

The focus of this work is in the linear regime of unstable stratified flows. In the selected studied cases, disturbances introduced in the base flow are regarded as infinitesimal. The next subsections present an introduction to linear stability theory in single-phase flows. Initially, the review focuses on basic concepts and

definitions that are important to understand some classical strategies commonly adopted to study instabilities of stratified two phase flows.

2.2.2
Linear hydrodynamic stability theory for parallel single phase and viscous flow

The main objective of linear instability analysis is to determine whether a system is unstable or not to infinitesimal disturbances. This is justified by the hypothesis that if the system is unstable to small disturbances, it will be also to the large ones.

Classical linear hydrodynamic stability theory applied to shear layer flows are developed from the Navier-Stokes equations (Drazin, 2002). To determine whether the flow has stable solutions, the flow is decomposed into a permanent part (U), called the base flow, and an oscillatory part ($\tilde{u}$), named as perturbation. For this analysis the base flow is usually known. Terms indicated by tilde represent the fluctuations of the variables and are the unknowns of the equations. By replacing the variables into the Navier-Stokes equations and the continuity equation, one can obtain the disturbance equation for parallel flow.

$$\frac{\partial \tilde{u}}{\partial t}+U\frac{\partial \tilde{u}}{\partial x}+\tilde{v}\frac{\partial U}{\partial y}+\left[\tilde{u}\frac{\partial \tilde{u}}{\partial x}+\tilde{v}\frac{\partial \tilde{u}}{\partial y}\right]=-\frac{\partial \tilde{p}}{\partial x}+\frac{1}{\mathrm{Re}}\left(\frac{\partial^2 \tilde{u}}{\partial x^2}+\frac{\partial^2 \tilde{u}}{\partial y^2}\right) \tag{2.1}$$

$$\frac{\partial \tilde{v}}{\partial t}+U\frac{\partial \tilde{v}}{\partial x}+\left[\tilde{u}\frac{\partial \tilde{v}}{\partial x}+\tilde{v}\frac{\partial \tilde{v}}{\partial y}\right]=-\frac{\partial \tilde{p}}{\partial x}+\frac{1}{\mathrm{Re}}\left(\frac{\partial^2 \tilde{v}}{\partial x^2}+\frac{\partial^2 \tilde{v}}{\partial y^2}\right) \tag{2.2}$$

$$\frac{\partial \tilde{u}}{\partial x}+\frac{\partial \tilde{v}}{\partial y}=0 \tag{2.3}$$

Where,

$$U=U(y)\,,\tilde{u}=\tilde{u}(x,y,t),\tilde{v}=\tilde{v}(x,y,t) \tag{2.4}$$

Assuming that the perturbation is infinitesimal, non-linear terms can be neglected. Then the most general form of a two dimensional disturbance is a wave with amplitudes varying along the shear layer, $\hat{u}(y),\hat{v}(y)$ and $\hat{p}(y)$, which propagates along the time and space axis with frequency ω and wave number k.

$$\tilde{u}(x,y,t)=\hat{u}(y)e^{i(kx-\omega t)} \tag{2.5}$$

$$\tilde{v}(x,y,t) = \hat{v}(y)e^{i(kx-\omega t)} \tag{2.6}$$

$$\tilde{p}(x,y,t) = \hat{p}(y)e^{i(kx-\omega t)} \tag{2.7}$$

Replacing these solutions back into the stability equations, leads to an ordinary fourth-order equation known as Orr-Sommerfeld equation (Orr, 1907; Sommerfeld, 1908).

$$k(U-c)(\hat{v}''-k^2\hat{v}) - U''k\hat{v} = -\frac{i}{\mathrm{Re}}(\hat{v}^{IV} - 2k^2\hat{v}'') - \hat{v}''k^4\hat{v} \tag{2.8}$$

Where, $c = \omega/k$.

The stability analysis is now reduced to an eigenvalue problem of the system of differential equations in perturbation variables. Depending on the preferential dimension for wave growth, the Orr-Sommerfeld equation can be solved using temporal or a spatial instability framework (Mendonça, 2000). Spatial growth is associated with convective instabilities, whereas temporal growth is related to absolute instabilities. The classification convective and absolute describes how the wave growth is observed within the domain of analysis.

In the convective instability, for instance, disturbances travel downstream and exhibit growth or decay as they propagate along the flow direction. In the absolute instability, the disturbances can propagate in all direction, and they can be seen in whole domain (Drazin, 2002). Figure 7 illustrates these processes and help to clarify the difference between both classifications.

In the absolute instability representation in Figure 7(a), the wedge containing the disturbance range the right and left sides, and such, after some time, the disturbance spreads to the entire domain. Thus, the best formulation analysis in this case is represented by a temporal instability evolution. The convective instability is illustrated in Figure 7(b). In the diagram, the disturbance wedge is located to the right side. At some location, in the x-axis, after the disturbance passage, the undisturbed flow field is restored. In this case, the stability analyses is better represented by the spatial formulation.

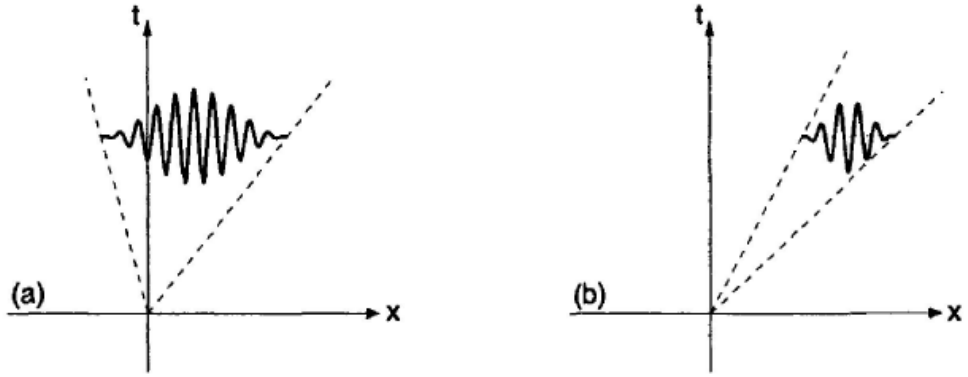

Figure 7 – Symbolic sketch of the time-space development of (a) absolute instability and (b) convective instability (Drazin, 2002).

Considering a spatial stability formulation, the solution to the Orr-Sommerfeld equation exists for a given wave frequency. Thus, the wave number is a complex eigenvalue.

$$\omega = \omega_r \tag{2.9}$$

$$k = k_r + ik_i \tag{2.10}$$

So,

$$\tilde{u}(x, y, t) = [\hat{u}(y)\exp(-k_i x)]\, e\exp(ik_r x - i\omega_r t) \tag{2.11}$$

The imaginary term, k_i, gives the amplification rate of the perturbation. If, $k_i < 0$, a linear disturbance can grow and the flow is considered unstable. On the other hand, if $k_i > 0$, the linear disturbances decay and the flow is stable.

Linear stability models applied to two-phase flow are also developed from Navier-Stokes equations resulting in Orr-Sommerfeld type equations for each phase. Both systems are usually coupled through interfacial conditions (Yiantsios, S. G. & Higgins, B. G. 1988, Rodríguez, 2015 and 2017). More details on two-phase flow modeling are given in the Section 2.3.

2.2.3

Non-linear Stability

Development of disturbances with infinitesimal amplitude can be described by linear theory. If the disturbance amplitudes become large, then nonlinear terms that were neglected in the linear theory may be no longer negligible. Hence, predictions given by LST may no longer represent the physical phenomenon.

In the non-linear framework, disturbances having different frequencies might not evolve independently (Schmid and Henningson, 2001). In addition, nonlinear self-interactions of the dominant mode can distort the mean flow (Drazin, 2002).

In some situations, a weak nonlinear regime might exist. Typically, in these cases, the time scales related with the amplitude variation of disturbances are longer compared to their oscillation period (Jurman et al., 1991). For this scenario, simplifications can be applied to the nonlinear set of conservation equations without loss of fidelity in the representation of the physical phenomenon. Within this regime, resonant interactions can occur and lead to a change of regime. For two phase flows, the resonance of disturbances was described recently in the work of Campbell and Liu (2014).

For the investigation of highly nonlinear flow regimes, the solution of the equations is challenging and hence numerical solution of the Navier-Stokes equations is adopted (Schmid and Henningson, 2001). Nonlinear stability analysis is out of scope of this work and further details can be found in the book of Schmid and Henningson (2001). However, the basic ideas addressed in this section are rather important to assist in the definition of an amplitude threshold for validity of models based on linear stability theory.

2.3
Modeling of slug initiation based on hydrodynamic stability

The work of Boomkamp and Miesen (1996) presents an extensive literature review about the physical aspects associated with stability of two phase flows. They investigated five different mechanisms of energy transfer from the base flow to the disturbances. Each mechanism has its origins in one of the following flow features: density stratification, velocity profile curvature, viscosity stratification, shear effects, or a combination of viscosity stratification and shear effects. Thus, it can be inferred that stability analysis of stratified two-phase flow is indeed a complex subject due to the multiplicity of parameters involved.

Linear stability analyses are commonly used to model the complex interfacial wave transition from a smooth stratified to wavy and slug flow regimes. Typically, linear models address separately one of the mechanisms described by Bookamp and Miesen (1996). These models have been derived considering the interaction of various forces such as buoyancy, inertia, surface tension and viscosity. In the most classical models (Lin and Hanrraty, 1986), the growth and decay of an infinitesimal wave on flat liquid layer of finite depth follow the

approach proposed by Lord Kelvin and Hermann Von Helmholtz in late 19th century for shear layers (Drazin, 2002).

Next section presents a literature survey of the most relevant models and experimental investigations devoted to improve our understanding of physical mechanisms responsible for initiation of slug flow in two-phase flows.

2.3.1
Inviscid linear stability theory

The "classical theory" of Kelvin-Helmholtz instability is based on the analysis of small amplitude and monochromatic perturbations at the interface between two fluids. Neglecting viscous effects, velocity potentials are derived to represent the two-dimensional flow in each phase, and compatibility conditions are required to be satisfied at the interface (McCready and Uphold, 1997; Brennen 2005). Generally, KH instabilities involve interactions between buoyancy, surface tension and Bernoulli effects.

An inviscid stability analysis for predicting the onset of slugging, based on classical Kelvin-Helmholtz instability theory, was introduced during 1970's in the works of Kordyban and Ranov (1970), of Wallis and Dobson (1973) and of Taitel and Dukler (1976). The inviscid Kelvin-Helmholtz (IKH) theory considers that slugs are generated when the suction pressure generated over a wave by the Bernoulli effect (Wallis and Dobson, 1973) is large enough to overcome the downward stabilizing influence of gravity forces (Kordyban and Ranov, 1970). The Bernoulli effect in a stratified flow is illustrated in the Figure 8.

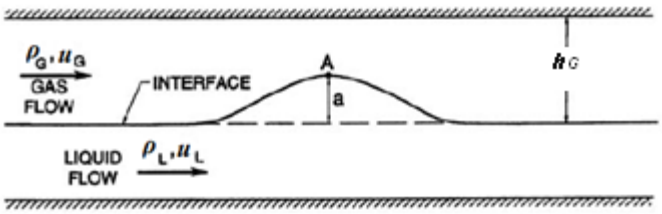

Figure 8 – Sketch of a solitary disturbance in a confined stratified flow. Extracted from Brennen (2005).

According to Kelvin-Helmholtz theory, Milne-Thomson (1960) provides a stability criteria for waves with an infinitesimal amplitude (a), formed on a flat liquid layer flowing between horizontal parallel plates. Their criteria is reproduced in Equation (2.12). The formulation considers the hypothesis of long waves. In this hypothesis the wavelength is much higher than the wave amplitude ($\lambda >> a$), in order to neglect surface tension effects. Thus, just the forces in phase with

the wave height contribute for the system stability and the flow will become unstable if,

$$u_G^2 > g h_G \Delta\rho / \rho_G \qquad (2.12)$$

Where, h_G is the distance between the upper plate and the equilibrium liquid level, g is the acceleration due to gravity and $\Delta\rho$ is difference in the densities of the two fluids.

Taitel and Dukler (1976) compared this transition prediction against experimental charts reported in Mandhane et al. (1974) and found a fair agreement. The authors used the critical conditions for flow instability, given by inviscid Kelvin-Helmhotz analysis, to represent the transition between flow regimes in a flow pattern map.

Kordyban and Ranov (1970) derived a criterion for transition based on inviscid linear stability analysis and predicted the onset of instability for known wave length and liquid level. The authors also assumed that waves were long with respect to liquid depth in order to neglect surface tension effects. Predictions were compared against flow maps of Baker (1954) and Schicht (1969) and the agreement was reasonable. However remarkable discrepancies were observed when compared against the experimental results of Wallis and Dodson (1973).

2.3.2
Viscous Linear Stability theory

The available literature related to models based on viscous linear stability theory is vast. Therefore, the discussion about these models is didactically separated here in one-dimensional and two-dimensional models.

2.3.2.1
Models based on averaged cross-sectional quantities

A viscous KH analysis was developed in attempt to improve models for predicting the transition from stratified to slug regime (Lin and Hanratty 1986; Barnea and Taitel 1993). Most one dimensional models used for instability analysis of stratified flows are based on the two-fluid model developed by Ishii (1980). The authors used the concept of the two-fluid model by considering the phases separately in terms of two sets of conservation equations, governing the balance of mass, momentum and energy in each phase. According to Ishii (1980),

flow parameters can be represented by their average over the pipe cross-sectional area. This allows the reduction of the system of equations into one single dimension. However, the predictions obtained via the two-fluid model depend on the reliability of the closure relations used to model the base flow and the interactions between the liquid and gas phases, which have significant influence on the solution (Barmak et al., 2016).

According to Lin and Hanratty (1986) the Inviscid Kelvin-Helmholtz theory incorrectly predicts the stability of stratified gas-liquid flows to infinitesimal long wavelength disturbances. The authors emphasized that viscous effects have important influence on the wave velocities and this is not predicted by inviscid theory. Therefore, they introduce wall and interfacial drag terms into the analysis in what they call a Viscous Long Wave (VLW) model. In their model, the wavelength is considered to be very large in comparison with the liquid depth. Thus, a shallow water approximation is adopted, and the surface tension is neglected. The destabilizing effect of the liquid inertia is used to explain why inviscid Kelvin-Helmholtz theory predicts high critical gas velocities for the initiation of slugs in air-water flows. However, for very large liquid viscosities flows, the same transition predictions are given by viscous and inviscid models. Hence, they suggest that for stability calculations of highly viscous liquid flow the inertia effects are negligible.

Bendiksen and Espedal (1992) examined the linear stability criterion applying different mean flow models using several types of interfacial friction factors. The sensitivity of the transition predictions was found to be high. Also, this study shows that there are still discrepancies between the experimental findings and the theoretical predictions, especially for high-pressure and large-diameter pipes.

In the work of Barnea and Taitel (1993), surface tension effects and interfacial shear stresses were considered in an attempt to improve the transition predictions. The transition criteria obtained was simple and easy to implement, hence it is attractive for practical applications. However, it is still sensitive to closure relations and discrepancies with experimental observations are still observed (Ayati et al., 2017). In the present thesis, the model developed by Barnea and Taitel (1993) is used to assist the analysis of some experimental results and its formulation is briefly outlined in the appendix.

Many of these analyses assume that the wavelengths are much larger than the pipe diameter, the so-called long-wavelength approximation. However, in the literature, extensive studies devoted to characterization of the interfacial waves

of stratified flows (Strand 1993, Ayati et al. 2015, Sanchis et al. 2011, Hanratty 1983, Andritsos and Hanratty 1987) show the possible existence of short wavelengths, not related to the K-H instability.

Andritsos and Hanratty (1987) reported an important contribution characterizing different types of wave patterns observed for gas-liquid stratified flow in a horizontal circular pipe. They reported observations of 2-D regular wave regime, 3-D large amplitude irregular wave regime and atomizing flow. The 2-D waves are described in their work as regular waves whose wavelength decreases and amplitude becomes larger as the gas flow increases. These waves led to the occurrence of roll waves which coalesced in some cases to form slugs.

Sanchis et al. (2011) applied interface tracking to characterize the waves close to slug transition. In their study, long-wave length stability theory fails to predict the occurrence of hydrodynamic slugs in the experiments.

Funada and Joseph (2001) give a detailed report of the viscous potential flow analysis of KH instability in a rectangular duct. In their study a stability criterion comparison between model and experiments was presented and expressed by a critical value of the relative velocity. Viscous potential flow analysis is shown to give a good approximation to fully viscous flows in cases where the gas shear is negligible. For the authors, the effects of surface tension are always important and determine the stability limits for the cases in which the volume fraction of gas is not too small. Their work also reported the strong effect of the viscosity of the liquid on the growth rate. The criterion for stability of stratified flow given by viscous potential flow analysis suggests that the model can fit well to the experimental data with thin liquid layer when the gas fraction is greater than 70%. However, it over predicts the transition limits when the liquid layer is thick.

Later, Soleimani and Hanratty (2003) revisited viscous long wavelength theory to predict the initiation of rollwaves and consequently the slug onset. They observed that the critical liquid height for slugging is found to decrease with increasing gas velocity. At low gas velocity, the liquid height is large enough to sustain stable slugs. However, at large gas velocity the height of the liquid at the transition to roll waves is below the critical height required for the existence of stable slugs. Consequently, there is a large range of liquid flow rates for which the stratified layer contains roll waves. For the authors, under these flow rates slugs will appear if conditions are favorable for the coalescence of roll waves. Thus, the coalescence condition depends on velocity and frequency of roll waves.

Kadri et al. (2009) introduce a wave transition model aiming to predict the transition from stratified to slug or roll-wave regimes for different pipe diameters and different gas and liquid superficial velocities. The model is based on the time required for a long wavelength wave to grow and reach the top of the pipe. It considers also the time required for a wave crest to overtake a subsequent wave propagating downstream. If the crest overtakes the downstream wave end before hitting the top of the pipe, a roll-wave is formed, otherwise a slug is formed. In that study, it is clear that there is still a discrepancy between experimental findings and predictions for pipes with large diameters and high flow rates. According to the authors, the models are sensitive to the interfacial friction factor. Therefore, the accuracy of the predictions could be improved if the interfacial friction factors at transition would be known for a wide range of flow conditions.

In the literature, friction models correlations for the broad range of fluid properties and flow conditions available for one-dimensional two-fluid models (Biberg et al, 2008) is lack. In other to fill this gap, Biberg (2007) proposed proposed an algebraic-logarithmic model for a stratified turbulent flow that incorporates wave effects using an interfacial turbulence level. Thereby, it can provide the cross sectional velocity distribution and yields mechanistic expressions for wall and interfacial shear stresses. The mathematical model derived by Biberg et al. (2007) allow for simulation of large pipeline systems with the consistency and accuracy of a cross-sectional model, whereas maintaining the computer performance of a traditional 1-D model. However, the model still demands further validation against experimental results. Just recently, detailed velocity fields became available in the literature (Ayati et al. 2014, Birvalski et al. 2014). Unfortunately, a quantitative comparison between those experiments and Biberg's model are not yet found in the literature.

One-dimensional two-fluid models for multiphase flow in pipelines have found a wide range of application for two-phase-flow simulation in oil and gas industry. Commercial multiphase flow simulators, such as OLGA (Bendiksen et al, 1991) and LedaFlow (Kjølaas et al. 2013), are widely used for predictions of steady-state pressure drop, liquid holdup, and flow-regime transitions. In some cases observed in the field, hydrodynamic slugs generated in the flowline may grow substantially and generated large scale flow instabilities and issues in the processing facility (Danielson et al., 2012). According to the authors, in these cases, a "slug capturing" approach to simulate the system behavior seems more appropriate than standard approaches. However, care must be taken when simulating the transition from stratified to slug flow. Discrepancies between

models and experiments are still reported, especially near the transition from stratified to slug flows (Sanchis et al., 2011).

2.3.2.2

Models based on 1-D Orr-Sommerfeld equations

In the one-dimensional two-fluid model the flow quantities are integrated over the cross-sectional area of the pipe, based on the area averaging of mass and momentum equations (Ishii, 1975). Thus, variations in the radial direction are affected by averaging process and loss of information are inevitable. Hence, empirical correlations and simplified models are used to reintroduce the effects of mass and momentum transfer at the interface between two fluids and the wall. Biberg friction relations and velocity profiles factors for example, is used by some authors as given by the corresponding mean velocity distributions (Biberg, 2008). The smaller waves effects are incorporated into friction models through interfacial turbulence parameters. However, gradients in radial direction are known to play an important role on shear flows, for instance, they are essential in LST analysis of single phase flows (see equation (2.8)). Thus, a natural step for the development of these models is to consider the flow gradients in the radial direction.

Linear stability analysis of stratified two-phase flows in a horizontal channel was investigated in the works of Yiantsios and Higgins (1988), Boomkamp et al. (1997), Kaffel and Riaz (2015) and of Barmak et al. (2016). In these studies, the problem is reduced to Orr-Sommerfeld equations for the stream function disturbances, defined in each layer, and coupled via boundary conditions.

Yiantsios and Higgins (1988) investigate the stability of two superposed fluids with different viscosity in a plane Poiseuille flow. Interfacial modes diagram of neutral stability were reported and the critical Reynolds number for shear and interfacial modes were compared to experimental data of Kao and Park (1972). In their work discrepancies between theory and experiments predictions were observed and discussed.

Kaffel and Riaz (2015) studied the effect of viscosity ratio and Reynolds numbers on interfacial and near wall modes. They analyzed also the possibility of interaction between different modes. A possible coalescence of near wall and interfacial modes was identified in both stable and unstable region of the wave spectra. Mostly, this interaction occurred for shallow liquid layers, which do not correspond to the usual conditions for slug initiation.

Barmak et al. (2016) investigated the most critical disturbances for slugging under different flow conditions. According to their findings, unstable perturbations do originate either at the interface (“interfacial modes of instability”), or in the bulk of one of the phases (“wall modes”). The preference for each mode was not clearly distinguishable a priori. In addition, influence of the channel height in the neutral stability curve was more evident for cases with low liquid flow rates.

The works of Kaffel and Riaz (2015) and of Barmak et al. (2016) considered a laminar and fully developed flow, even though the Reynolds numbers were high in some cases. Thus, the prescribed velocity profiles of base flow represent an additional source of discrepancy of these models.

2.3.3
Investigation of non-linear stages

According to Bontozoglou (1991) non-linear effects, which are not included in most models, can play a crucial role in the transition process. An overview of some theoretical and numerical literature studies on non-linear stability related to stratified to slug transition is outlined in this section.

Jurmann et al. (1992) analyze experimentally the evolution and the interaction between interfacial waves in a rectangular channel. Measurements of the bi-coherence spectrum of interfacial waves indicate that the overtone and the fundamental mode can exhibit phase coherence. This suggests that energy can be transferred from the fundamental mode to the linearly stable first overtone by nonlinear mechanisms. This process dissipates energy and can stabilize the fundamental wave growth. At high flow rates, in wavy flows this might be observed. In case of high amplitude of fundamental waves, a subharmonic mode may be excited (Jurmann et al., 1992). In this case, the energy transferred from interactions between the subharmonic and the fundamental mode may lead to fast growth of this subharmonic.

According to McCready and Uphold (1997), the generation of subharmonics and low frequency modes by nonlinear interactions can be important for the transition to slugs. However, they emphasize that this mechanism demands linearly unstable waves that extract energy from the base flow.

Later, Valluri et al. (2008) studied the slug onset by numerical simulation in laminar horizontal channel flow. The work reported that the coalescence of short and small amplitude waves can lead to large amplitude waves that further may

evolve to slugs. Also, the authors highlight the relevance of accurate estimation of shear stresses along the interface to improve stability models.

More recently, Sanchis et al. (2011) suggested that nonlinear wave-wave interactions could induce rapid growth of fluctuations in the liquid level and initiate slugs. This paper investigates experimentally the properties of waves at low gas flow rates, which through a wave coalescence mechanism, lead to hydrodynamic slugging transition. K-H stability theory was used in comparison with experimental results and failed to predict the occurrence of slugging initiated by wave-wave interaction.

Campbell and Liu (2014) used the method of multiple scales to study an inviscid stratified flow through a horizontal channel. They show that in some situations, the linearly stable sub-harmonic mode can grow faster than exponential. The mechanism is captured by their model which is capable to predict the generation of long waves that, in principle, would be stable according to linear stability theory.

Campbell and Liu (2016) showed by direct numerical simulations that, indeed, the resonance coupling allows the energy generated by linear instability to be transferred to the long waves. This strong energy cascade forces the waves to overcome the stabilizing influence of viscosity and permits a rapid wave amplification. However, it is not clear yet how these interactions play a role in viscous fluids. In addition, the resonance usually demands a phase locking of interacting modes. It is known from experiments that in some cases, the slugs are suddenly initiated and therefore the resonance process of few waves might be different in the presence of multiple modes. Thus, there are some open questions about this topic that demand further investigations.

Ayati (2018) present a statistical and spectral study of interfacial waves in stratified turbulent air-water flow in a horizontal pipe. The study focus on regimes with high gas velocities within wavy flow regime. The author investigates the influence of the gas flow rate on statistical and spectral properties of interfacial waves using conductance probes. Interfacial mode interactions suggest that weakly non-linear (triadic) interactions in the form of overtone and sub-harmonic interactions might play an important role for initiation of roll-waves. However, it is still not clear how this mechanism is linked to the initiation of slugs.

The linear and nonlinear models aforementioned were mostly guided by experimental observations of the physical phenomenon. Indeed, the characterization of slugs and its initiation process have been subjected to intense

investigation. Thus, in next section, a survey is presented of the relevant experimental contributions to the understanding of the problem.

2.3.3.1
Characterization of stratified flows at nearly transitional conditions

The number of experiments reported in the literature regarding wave-turbulence interaction in confined two-phase flows have increased during the past years. However, additional studies are still demanded before the complete picture of the phenomenon can be drawn. Detailed experimental investigations are important for validation and calibration of theoretical and computational models. In this section, selected studies will be discussed to provide an overview about the most important experimental contributions to the field. The focus here is on instability-related experiments in stratified flows.

Relevant works related to experimental characterization of interfacial waves in confined stratified flow are didactically separated here in two groups, according to the geometry adopted. Rectangular channels were often used in fundamental studies (Kordyban and Ranov 1970, Wallis and Dobson 1973, Jurman et al. 1991 and Fernandino and Ythehus 2008), whereas pipe flows were typically used for development of engineering correlations (Lin and Hanratty 1987, Andritsos et al. 1986, 1987, Fan et al. 1993, Ujang et al. 2006). It is not clear to which extend the results obtained in different geometries are comparable. Thus, recent works focused on a detailed characterization of the flow field in circular pipe flows (Birvaski et al. 2014; Ayati et al. 2014, 2015, 2017). The present thesis is included in this last group of works.

Visual observations performed in works of Hanratty (1983) and of Andritsos and Hanratty (1987) allow the identification of three sub regimes in stratified flows, namely; (i) 2-D regular waves (ii) large-amplitude irregular waves and (iii) atomizing flows. Those authors conjectured about the physical mechanisms related to each sub regime. For sub-regime (i) waves are assumed to be generated by wave-induced pressure oscillations in the gas, that are in phase with the wave slope. Therefore, energy is transferred from gas to the liquid via velocity fluctuations normal to the interface. If the energy input exceeds viscous dissipation, regular 2-D waves can appear. In sub regime (ii) roll waves are assumed to be formed if all destabilizing effects are in phase with the wave height, to overcome the stabilizing effect of gravity. Sub-regime (iii) is assumed to occur

if pressure variation induced by waves overcome the stabilizing effect of surface tension. Thereby, small wavelets travelling on the top of the roll waves can be atomized. According Andritsos and Hanratty (1987) the prediction of the pressure drop and shear variation along a wavy surface constitute a key problem for the determination of liquid film stability.

Later, Strand (1993) suggested the existence of six sub regimes, based on the time signal obtained from conductance probes. The sub regimes of stratified flow reported in that work are: smooth, small amplitude 2D wave, large amplitude 2D wave, 3D wave, pebbly wave and unstable large 2D wave region. Recently, Ayati et al. (2015) also used the waves power spectra densities in order to categorize the stratified flow sub regimes. The study also applied conductance probes, and the results supported the observations of Strand (1993).

Andritsos and Hanratty (1987) measured interfacial waves at some stations along the pipeline using conductance probes. Results are reported for different liquid viscosities and pipe diameters. According to their findings, viscosity tends to increase the gas velocity required for the initiation of regular 2-D waves, and to decrease the range of flow conditions for which they do exist. Linear stability theory was used as comparisons against transition conditions identified in the experiments. The results show that the large amplitude waves could be roughly predicted by inviscid K-H analysis for low fluid viscosities.

Ujang et al. (2006) studied experimentally the initiation and the subsequent evolution of hydrodynamic slugs in horizontal and pressurized pipelines. The work elucidated the effects of pressure on slug initiation and evolution. Results indicate that high pressures tend to introduce a slight delay on the slug initiation, but once they are formed their intermittency period was weakly affected.

Non-intrusive optical techniques have developed significantly during the last decades. The evolution of digital cameras and image processing capacity, combined to high energy and high frequency light sources, have been producing a remarkable progress in the analysis of complex flows. Quantitative measurement of flow fields using optical techniques have proven to be rich sources of experimental data, which can be used to better understand the physical phenomena involved in two-phase flows (Carneiro et al. 2011, Birvaski et al. 2014; Ayati et al. 2014, 2015, 2017, Fernandes et al., 2018). The literature review in this section discusses some experimental works devoted to study waves in stratified flows, as listed below,

- Laser Doppler Anemometry – LDA: Strand (1993)
- Laser Doppler Velocimetry – LDV: Fernandino and Ytrehus (2006)

- High resolution photography: Sanchis et al. (2011)
- Particle Image Velocimetry Technique: Sanjou and Nezu (2011), Ayati (2014, 2015, 2018) and Bisvalski et al. (2014, 2015).

Strand (1993) used Laser Doppler Anemometry (LDA) to capture the velocity profiles in the liquid phase, describing flow structures near the interface. The axial velocity profile in the gas phase was also measured using a pitot tube, while wire resistance probes were applied to capture the wave evolution information. The study indicates that 2D waves with large amplitudes can deform the velocity profile.

Fernandino and Ytrehus (2008) studied wave-turbulence interaction in a stratified air-water duct flow. The author applied the Laser Doppler Velocimetry (LDV) technique to measure mean velocity and turbulence structures in the liquid phase for different types of interfacial waves. For high airflow rates, the mean liquid velocity profile near the interface and near the wall increases, whereas at the center region it shows a deficit, resulting in S-shape profile. The author suggests that further investigations are needed to explain the reason for this behavior. They highlight that investigations of critical wave amplitudes and wavelengths might be more relevant than the usual determination of transition from smooth to a stratified wavy regime.

Sanjou and Nezu (2011) performed Particle Imagery Velocimetry (PIV) measurements in an open-channel flow combined with wind-induced waves to investigate the effects of air–water interactions on turbulence structures through the whole depth region. Despite setup differences, the characteristic S-shaped profile of the mean flow was also observed in the study.

Sanchis et al. (2011) examined the effects of wave interaction on the formation of hydrodynamic slugs in two-phase pipe flow using high resolution photography. The method yielded accurate measurements of the global wave parameters of the flow, such as the mean liquid level or the average wave speed, which gave detailed information about possible resonance mechanisms. Unfortunately, they could not substantiate that wave resonances were, indeed, responsible for subharmonic growth.

Very recently, Ayati et al. (2014, 2015, 2018) and Birvalski et al. (2014, 2015 and 2016) employed Particle Image Velocimetry technique to obtain detailed velocity field measurements, wave and turbulence characterization for a stratified air-liquid flow.

Birvalski et al. (2014, 2015) used multiple cameras to measure simultaneously velocity fields in the liquid layer and close to the interface. A conditional averaging technique based on the wave phase was applied in order to decompose the velocity field into three components: time-averaged velocity, wave-induced fluctuations and turbulence-induced fluctuations. The phase-averaging was performed using the simple method of decomposition which assumes a linear relation between the interface position and the wave-induced velocities. Therefore, the part of the velocity signal that does not correlate with the surface displacement is considered to be turbulence. According to Birvalski et al. (2014) the axial fluctuations close to the wall showed practically no phase-dependence, suggesting no influence of the waves on wall turbulence.

Birvalski et al. (2016) extended their previous study to capture velocities in the gas and liquid layers. The authors also measured the wave statistics, including wave amplitude and wavelength, in the transition between different sub-regimes. The cases with relatively low wave amplitude were seen to follow the log-law and have a logarithmic profile shape through the bulk of the liquid. For cases with higher waves, the results deviate from the logarithmic shape at approximately half of the liquid layer. The gas velocity profile did not show a substantial difference between the sub regimes. Reported difficulties in measurements near the interface due to light reflections limited the study scope and detailed velocity profiles near the interface are not presented.

Ayati et al. (2014, 2015, 2016, 2017) performed simultaneous Particle Image Velocimetry (PIV) measurements of stratified turbulent air/water flow in horizontal pipe. Conductance probes and hot-wire anemometry were combined to investigate the influence of waves on the liquid and gas turbulence. Conductance probes provided wave statistics, while a hot-wire probe measured velocity fluctuations in the air phase with high temporal resolution, enabling the investigation turbulence coherence with the wave spectra.

Ayati et al. (2014, 2017) observed that the pressure drop, the bulk velocity and the interfacial axial turbulence level are coupled. They suggested that the interface waviness might have a direct effect on the overall pressure drop. The results indicated a qualitative linear correlation between pressure drop with streamwise turbulence intensity and the gas bulk velocity. According to the author, this behavior was limited to the operated flow conditions, and additional studies are required to provide information that could be useful to improve friction factors correlations, since turbulence structures are strongly linked to interfacial shear stress.

Ayati et al. (2015, 2017) observed the turbulence intensity behavior from measurements performed near the interface and near the wall, for different stratified flow sub regimes. For smooth stratified flows, the peak in turbulence intensity close to the wall was larger than the peak close to the interface. The opposite trend was observed in wavy flows. This effect was related to an equivalent surface roughness that enhances and thickens the turbulent boundary layer near the interface. However, no quantitative measurements of equivalent roughness height were provided. This effect was not parametrically assessed in their study since wave amplitude could not be controlled.

Recently, conditional averaging based on phase coherence has been employed to study the effect of waves on the turbulence in stratified flows (Ayati et al. 2016, Birvalski et al., 2015 and Vollestad et al., 2018). This technique was developed as an attempt to track the wave influence on flow turbulence. In those studies, the waves appear spontaneously at the interface. Therefore, there is no control of the wave parameters. Typically, for modal analysis, a controlled experiment is required. However, the setup required to introduce controlled disturbances to enable the stability analysis of the most unstable eigenmodes was not found in the literature.

According to this literature survey, one can observe that several experimental studies have been conducted in the past decades, but the information reported are not often directly compared with model predictions. For instance, linear and nonlinear models provide growth rates, wavelengths, disturbance profiles and so on. This information is not yet found in the literature. Thus, there is a clear lack of experimental database to assist with the validation or improvement of theoretical and numerical tools used for simulating stratified flows and slug onset.

Several open questions regarding the instability of interfacial waves in stratified flows still demand further investigation. For instance, the link between wall turbulence and interfacial waves is not yet quantified. In addition, it is not clear how the different wave mechanisms described by several authors do perform in the presence of a broad spectra of interfacial waves. Another issue that demands further clarification is the accuracy of the base flow model proposed in the work of Biberg (2007).

In view of the current state of affairs, it appeared that a work, in a regime of controlled waves, would be extremely important to shed some light on the physical processes involved in the generation and in the spatio-temporal evolution of interfacial waves. This thesis aims to fill this gap. In the present work,

controlled disturbances are introduced near the pipe entrance and their subsequent evolution is measured for different flow conditions. It is expected that the experimental methodologies developed here can contribute to a better understanding of the transition process from stratified to slug flow regimes. The present work also intends to provide an accurate database that can be used for validation of models and numerical simulations.

3
Experimental Facility

In present work different experimental setups were used. One for measuring time resolved evolution of interfacial waves, other for measuring velocity fields in liquid layer only, and in the last one for capturing velocity fields in the gas and liquid layers, simultaneously. This chapter is devoted to present equipment, assemblies and techniques adopted in this thesis. First, it is presented a general overview of the common test bench components and, thereafter elements of each particular experimental setup.

3.1
General test bench arrangement

The test bench consists of a closed water loop circuit with an open air circuit for the gas. The rig was built with circular pipes oriented in horizontal direction. For this thesis, two loops were used: (i) one for measurement of interfacial waves and (ii) another for measurement of velocity fields in gas and liquid. The first, was built with FEP (Fluorinated Ethylene Propylene) pipes setup with 50.8 mm of internal diameter. The total length of this apparatus was 8 m. The second setup was built with transparent Plexiglas tubes of 50 mm and 12-m-length.

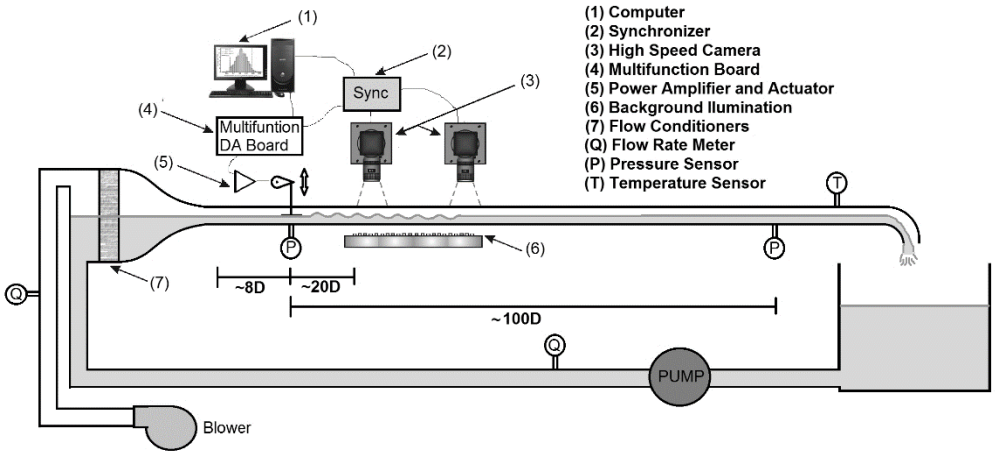

Figure 9 – Schematic view of the test bench.

.

According to the sketch of the Figure 9, air was supplied to the test section by a 2 HP Aspo® centrifugal blower which can reach velocities up to 40 m/s. Superficial liquid velocities up to 0.5 m/s were provided by a Netzsch® 3HP progressive cavity pump. At the outlet of the test section, the mixture of air and water was directed to a high volume tank. An schematic drawing of the system is illustrated in Figure 10. From the high volume vessel, the water was pumped to an intermediate reservoir by a ¾ hp centrifugal Dancor® pump, whereas air was vented out to the laboratory. The two-tank setup minimized the presence of air bubbles in the liquid phase.

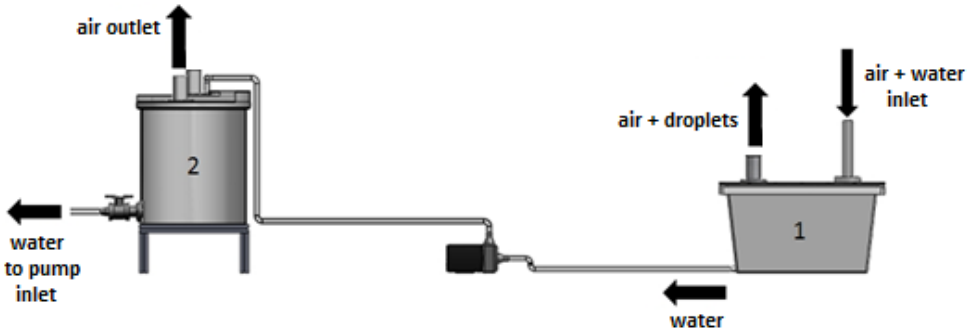

Figure 10 – Schematic view of the air and water mixture separation.

Water flow rates were measured using two redundant flow meters, a calibrated turbine (model SVTL L19, Contech®) and a rotameter (Conaut®). This redundancy was important to check the turbine calibration during test campaigns. Air flow rates were also measured using a turbine (model SVTG G19, Contech®) and a rotameter (Applitech ®), and the same principle of redundancy was applied.

Temperature variations in the flow could influence the superficial tension and viscosity. Preliminary tests showed that a 1ºC variation affected the growth of interfacial waves. In order to maintain a constant temperature condition during the experiments, a Neslab® chiller (model Melin M75) was installed in the test bench. The chiller circulated cooled water through an inox coil that was immersed in the intermediate tank. A Pt-100 resistive temperature sensor was used for monitoring the water tank temperature. The chiller was adjusted to keep the tank temperature set point, to within ±0.1 ºC.

Aluminum profiles supported the entire pipe section. This structure ensured a rigid assembly and allowed for a fine leveling of the test section

Other key components of the test bench that deserve a detailed description are the inlet contraction, the wave maker and the system synchronization. These components are described in following subsections.

3.1.1

Inlet contraction

The design and construction of the experimental setup are of fundamental importance for a successful measurement of controlled disturbances. The main concern of the design was the minimization of uncontrolled fluctuations of the gas-liquid interface at the pipe inlet. A straightforward design methodology for low disturbance mixing sections was not found in the literature. Even adaptation of concepts used in the design of wind and water tunnels for two-phase flows has not been found. Therefore, the design of the inlet mixing section was conducted employing concepts from the design of quiet wind and water tunnels. The literature related to this subject is vast and well established. The methodology described in the work of Albayrak (1991) was selected for the designing of an axisymmetric contraction nozzle. Flow conditioners such as honeycombs and screens, were selected in agreement with designing guides from the literature (Lumley and MacMahon, 1967 and Groth and Johansson, 1988). The drawing in Figure 11 illustrates the final design of the nozzle machined from polypropylene.

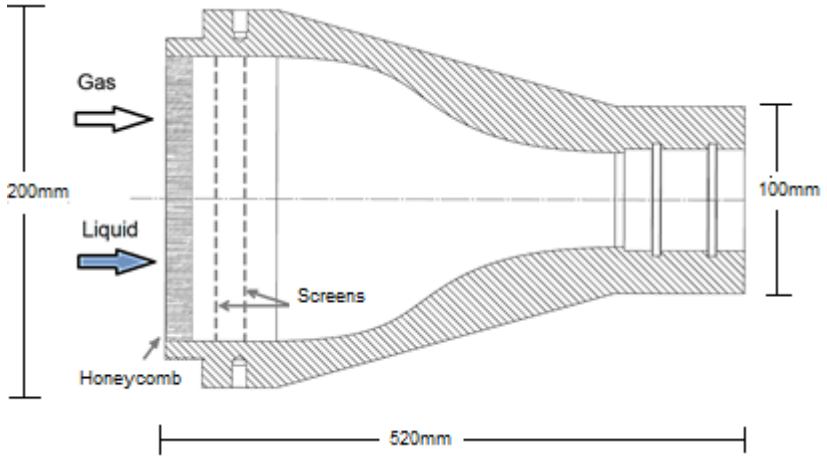

Figure 11 – Contraction nozzle design.

The noise reduction effect at the test section inlet obtained with the installation of the contraction nozzle can be assessed with the aid of Figure 12. In this figure, the transition map from Mandhane et al. (1974) was used as a reference for the transition limits observed in this work. Critical flow conditions observed with and without the use of the contraction nozzle are represented by solid triangles and open circles, respectively. For comparison purposes, experimental results reported in the work of Bendiksen (1984) were also plotted in the figure as solid squares.

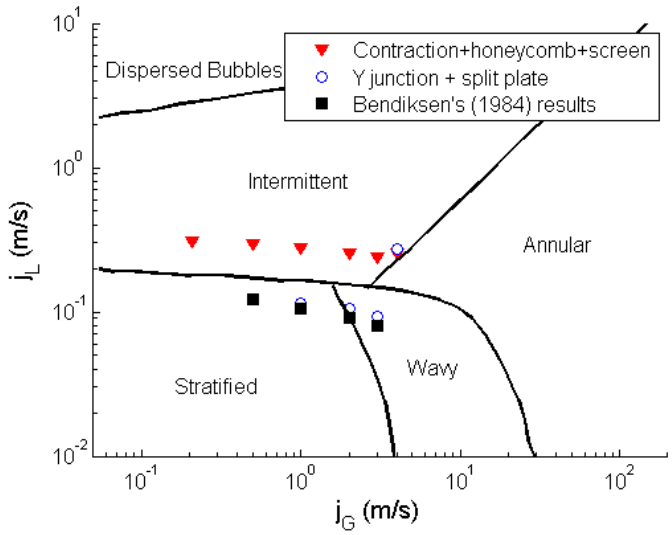

Figure 12 – Flow pattern map extracted from Mandhane (1974). Experimental points indicate the location of the transition measured experimentally in the present work, and in the work of Bendiksen (1984).

According to Figure 12 the use of the contraction nozzle as a mixing section shifted the transition conditions towards higher liquid velocities. This observation is an indication that an effective reduction of inlet disturbances was achieved with the contraction design employed. These are considered excellent results that were of fundamental importance to allow for the study of the transition process under controlled disturbances.

3.1.2

Wave generation

Controlled disturbances were introduced at the liquid-gas interface near the pipe entrance using an oscillating paddle. Relatively low energy is required to excite disturbances if the plate is positioned on the interface. Therefore, the disturbances are mostly introduced near the interface and not in the whole liquid layer. A sketch of the wave generation assembly and its evolution are shown in Figure 13. The oscilating paddle was composed by a stell plate machine with open holes and its top view geometry sketch is shown in Figure 14. The paddle was fixed in the rod set with a slight angle. This geometry and assembling guaranteed that the waves were mainly generated downstream of the excitation point, preventing the generation of counter-current disturbances.

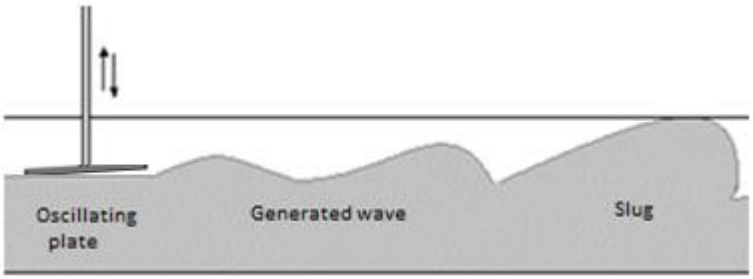

Figure 13 – Sketch of the wave generation process.

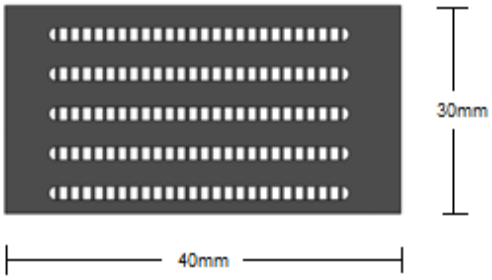

Figure 14 – Top view plate geometry sketch.

One of the most influential parameters in the development of interfacial waves is the mean liquid level. Thus, it is important to maintain this parameter constant during measurements. However, this can be quite challenging when operating at conditions close to transition to slug flows. Depending on the liquid and gas flow rates, waves could grow and initiate slugs further downstream from the excitation location. Such slugs are capable to capture a high amount of liquid as they propagate along the pipe and can significantly affect the flow conditions at stations upstream of its initiation. In order to avoid the influence of slugs on the results, disturbances were introduced in the flow as wave trains, and not as continuous waves. The wave train consists of a series of individual wave cycles, separated by a time delay of approximately one minute. Data acquisitions were synchronized with the central part of the wave train, where the waves displayed constant amplitude and spectral content. This procedure was adopted to ensure that no data was acquired when slugs were present in the pipe. In this way, it was expected that pressure waves caused by the eventual presence of slugs in the end of the pipe section, would not influence the results obtained.

3.1.3

Wave maker

A multifunction D/A board NI USB 6212 was used to control the movement of the oscillating plate generating arbitrary waveforms. A power amplifier with

unity gain was used to drive the actuator, that consisted of a head positioning system of a common hard disk drive. An illustration of the wave maker is shown by Figure 15. The actuator rotation axis was coupled to the knob of a radial potentiometer to monitor, in real time, the movement of the actuator. Thus, its displacement could be measured and waves at frequencies from 3 to 12 Hz could be generated.

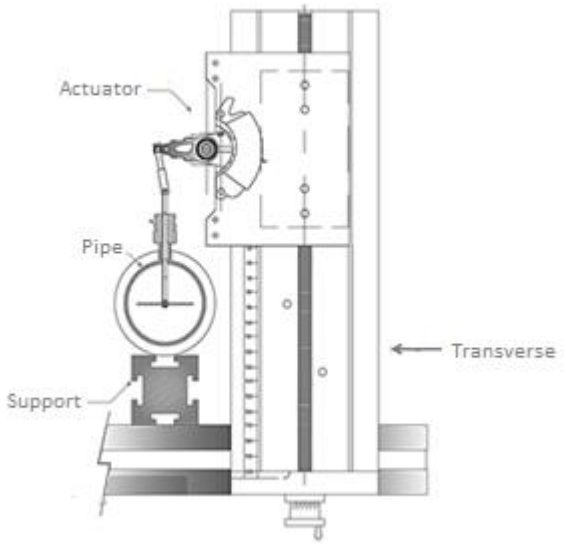

Figure 15 – Assembly of the controlled wave generation system implemented.

3.1.4
System synchronization

The wave image acquisition by the cameras was synchronized with the disturbance generation using an in-house routine developed in Labview, and a BNC575 synchronizer produced by Berkley Instruments. The BNC 575 allows the generation of digital signals for accurate triggering of waveform generation and image acquisitions. Insight 4G ® software from TSI was used to capture images from the cameras. A constant time delay was set between the initiation of the disturbance and the image triggering. This was necessary to ensure that the center of excited wavetrain was within the camera field of view.

Ensemble averaging techniques were adopted. The periodicity of the waves within a series of acquired images allowed to resolve measured excited disturbances exactly at the disturbing frequency using standard fast Fourier transform algorithms. Post-processing details will be outlined in Chapter 5.

3.2
Optical techniques

Measurement techniques based on flow imaging are a rich source of experimental information. However, multiphase flows represent a challenging condition that, in some cases, preclude the successful application of these techniques. Differences of fluid refraction indexes, which causes light scattering at interfaces, are a major source of problems. Thus, non-conventional solutions are often needed to overcome the inherent difficulties of the problem.

Different measurement techniques were combined in this thesis. For capturing time resolved information about the interface evolution, shadowgraphy was used. Two variants of the PIV technique were employed for measuring detailed information of velocity fields in the liquid and, later, in the gas and liquid layers. These versions of PIV can be regarded as planar and off-axis PIV. The techniques have been widely applied to single-phase flows, but in the current thesis a significant effort has been made to extend their application to two-phase flows with similar visualization quality. This section includes a brief presentation of these techniques.

3.2.1
Shadowgraph technique

A non-intrusive shadow technique is an optical technique based on the principle of light attenuation at the interface between two fluids. The implementation relies on flow imaging by a camera opposed to a background illumination, as illustrated in Figure 16. The light passing through the flow is strongly attenuated at interfaces, which can be detected by image processing techniques. Additional information about the technique can be found in the work of Nogueira et al. (2003). In the present thesis the background illumination was provided by panel of light emitting diodes (LEDs).The panel was formed by an 2500 mm x 120 mm acrylic plate with 86 LEDs equally spaced in 2 rows, which provide proper contrast and homogeneous background illumination for image acquisition. A power supply of 12V and 80A was used to power the panel illumination system.

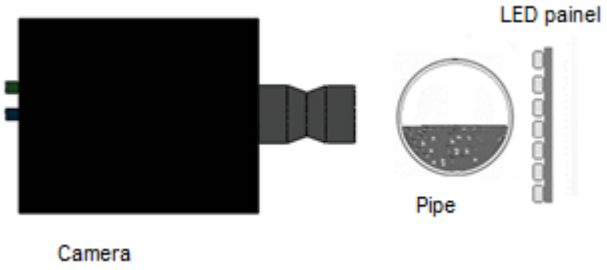

Figure 16 – Schematic view of optical assembly for shadowgraphy.

3.2.2

Particle Image Velocimetry – PIV

Particle Image Velocimetry (PIV) has been widely used for measuring velocity fields in single and two-phase flows. The technique consists of capturing the displacement of tracer particles by application of pulsed illumination, usually provided by a laser light plane, at two subsequent instants. It is assumed that the tracer particles move with local flow velocity between the two frames (Raffel et al., 2007). The particle positions registered at each pulse of illumination are acquired with a camera. The procedure is illustrated in Figure 17.

For a digital PIV processing, each recorded frame is divided in small sub-areas, called interrogation windows. The average displacement of tracer particles, is estimated for each interrogation window by a cross correlation between image frames. Velocity vectors in pixels are obtained by the ratio of estimated displacement and the time delay between illumination pulses. The conversion to real coordinates can be made with a proper calibration of images

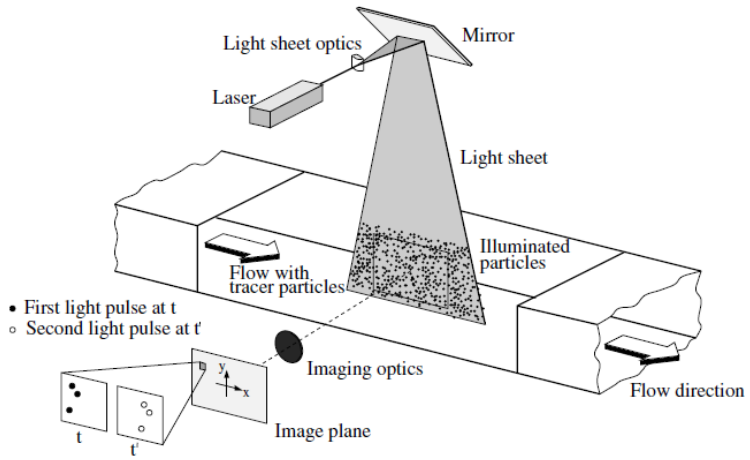

Figure 17 – Experimental arrangement for particle image velocimetry. Extracted from Raffel et al., 2007.

A set of routines developed in Matlab® language were used for processing and post-processing of all PIV data reported in the present study. The choice for a code developed in our laboratory was due to its greater flexibility when comparing with commercial softwares. More details about image processing and post-processing are given in Chapters 4 and 5, respectively.

Although PIV is a well-established technique for single phase flows, its application to two phase flows is more restricted due to optical constraints. Some comments about these restrictions are provided in next subsections.

3.2.3
Reduction of optical distortions

The use of optical techniques for qualitative or quantitative visualization of confined flows, such as pipes or channels, invariably faces the problem of optical distortions. These distortions are introduced by differences in refractive indices between different fluids, and between fluids and conduit walls. Here, different solutions were adopted for minimization of optical distortions. This topic is addressed in the following subsections.

3.2.4
Refraction index matching

The matching of refraction indexes of liquid and pipe walls is an interesting solution that allow for visualization through curved walls with minimized optical distortions. According to Hewitt et al. (1990), a FEP (Fluorinated Ethylene Propylene) material has refraction index similar to that of water. In industry, this material is used to manufacture pipes for the chemical industry. The material has a reasonable transparency level hence is a good candidate for application in flow visualization. Thus, pipes made of FEP were selected for the test bench used in shadowgraphy tests.

The drawback of FEP material is its moderate transparency that reduces significantly the light reflected by tracer particles. This attenuation is acceptable for light reflected by tracer particles in liquid. However, tracer particles for gas are about 10 times smaller than those used in water. Thus, the opacity of FEP precluded measurements in the gas phase. Therefore, other solution was necessary for application of PIV technique to both phases.

3.2.5

Reduced pipe wall thickness

For visualization of tracer particle displacements in the gas phase, it is necessary to use a very transparent pipe because particles are rather small and, consequently, the intensity of light reflected is weak. In terms of transparency, Plexiglas pipes perform much better in comparison to FEP pipes. However, the refraction indexes of Plexiglas and water are rather different. To overcome this problem, the wall thickness of the pipes was machined and polished. The resulting wall thickness was reduced to only 0.5 mm from its original 3 mm. According to Ocaña (2011), this reduces significantly optical aberrations and light scattering at the wall, and enables near wall measurements.

3.3

Optical assemblies

In the following subsections, an overview of all optical arrangements adopted in this work is presented. The objective is to describe and illustrate setups used for shadowgraphy and for PIV measurements.

3.3.1

Setup for measurement of wave evolution — Shadowgraphy

The shadowgraph technique was applied in a test section pipeline assembled with FEP pipe with an internal diameter of 50.8 mm and 8-m-length (approximately 150D). Images of the liquid film were captured using two high frame rate cameras with 1.3 MP resolution (IDT Motion Pro X3.) The cameras were mounted on the same base, as shown in Figure 18, and separated by 200 mm. Both cameras were mounted on a support that was placed on a horizontal traverse. The traverse had a travelling range of 2m. In the assembly, the most upstream position corresponded to 20D from the disturbance source, while the furthest downstream position corresponded to approximately 60D.

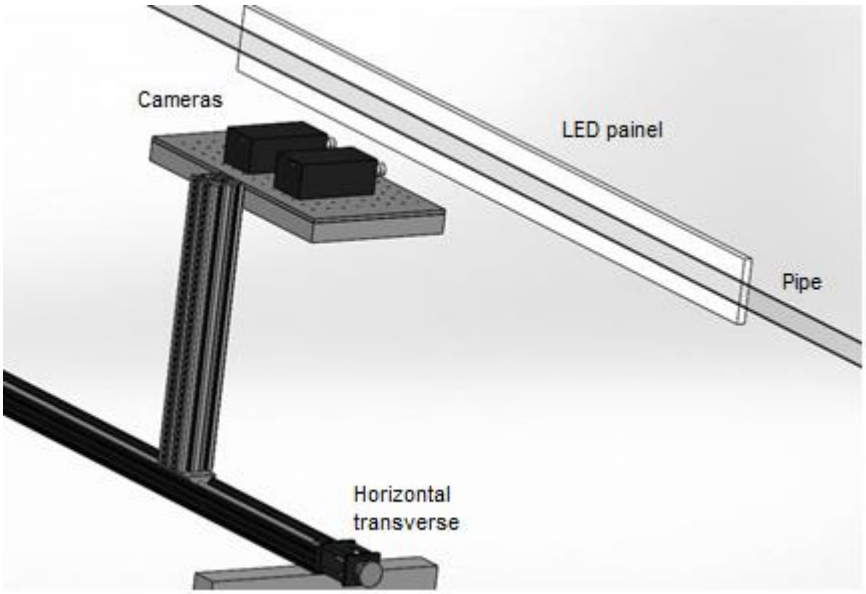

Figure 18 – Shadowgraph visualization setup.

A 2.5-m long panel assembled with 86, high-power white light emitting diodes (LED) was built and employed as background illumination source. The size of the panel covered the range of the traverse, so that the interface evolution could be captured by the cameras along a 2-m length in the pipe.

A typical image obtained in the present thesis using the shadowgraph technique is reproduced in Figure 19. This image gives an idea about the level of intensity contrast achieved. The gas-liquid interface is clearly distinguishable in the image, enabling the application of digital image processing techniques for its automatic detection.

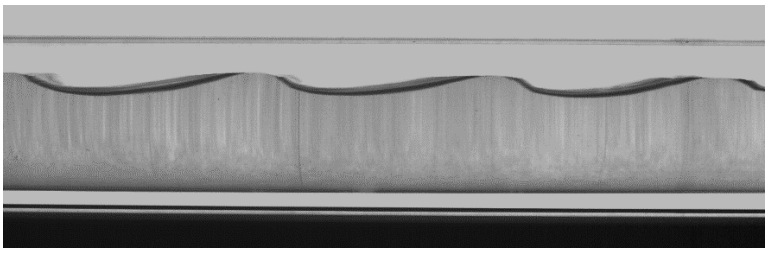

Figure 19 – Typical captured longitudinal image of a passing wave obtained by applying the shadowgraph technique implemented.

3.3.2

Setup for PIV measureme nts in the liquid layer— Planar PIV

Velocity fields in the liquid phase were measured using a standard planar PIV setup and FEP pipes. This setup included one TSI Powerplus 4 MP camera

with resolution 2048 X 2048 pixels and a double cavity Nd-YLF Evergreen® laser, which is capable of delivering 200 mJ/laser pulse at a frequency of 15 Hz.

At the visualization region, the pipe was encased with a 350-mm-long rectangular transparent box filled with water, in order to match the refracting index of the FEP pipe. This configuration, reduces distortions caused by the pipe wall curvature, and allow for the liquid film visualization at regions close to the pipe wall. Figure 20 illustrates the geometry of the test section. The visualization box was built with Plexiglas, except for the lower and the upper walls that were built of glass. Glass was chosen due to its resistance to the incidence of high power laser beams, unlike Plexiglas.

The laser beam emitted by the system was transformed into a light plane of small thickness (approximately 0.5 mm) using a cylindrical lens followed by a spherical lens. The cylindrical lens transformed the beam into a divergent plane, while the spherical lens controlled the thickness of the beam. A mirror mounted at 45° deflects the laser plane which penetrates longitudinally in the centerline of the pipe. The PIV camera was mounted orthogonally to the plane of illumination.

Due to optical alignment, the camera and the laser optics were placed at a fixed streamwise location corresponding to 100 D from the pipe inlet. The field of view imaged was set to 1.4D X 1D. The water was seeded with spherical polyamide particles with an average diameter of 50 µm and nearly neutraly buoyant . Image pairs were acquired with a sampling rate of 5 Hz, a value limited by the maximum rate of acquisition allowed by the camera in use. Figure 21 assists in the description of the visualization arrangement employed for the planar PIV measurements in the liquid phase.

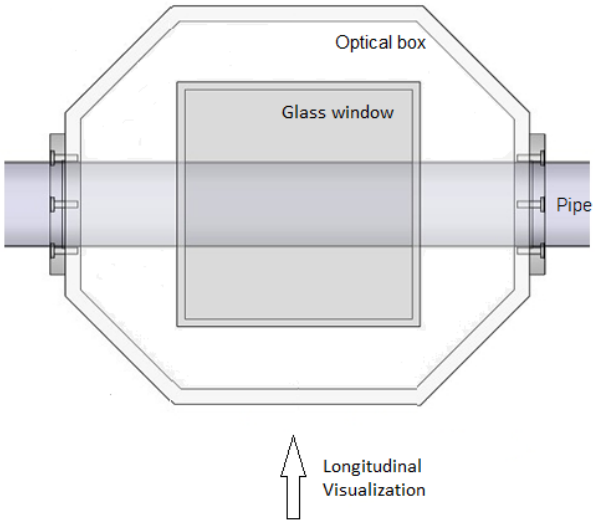

Figure 20 – Upper view of the optical box design for planar PIV measurements.

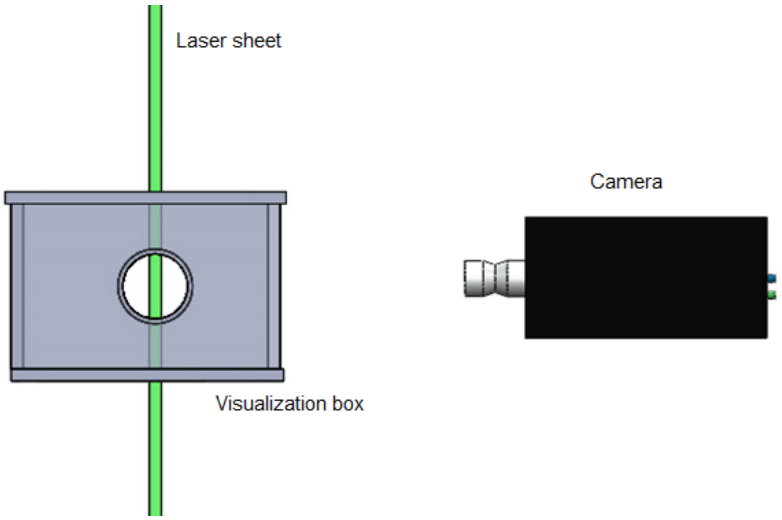

Figure 21 – Schematic visualization for the application of the planar PIV technique

3.3.3

Setup for off-axis PIV measurements in gas and liquid

Preliminary experiments demonstrated that tracer particles in the gas phase flowing in the FEP tube were poorly imaged by the camera, due to light attenuation through the material. Acrylic pipes present a much better transparency to the light scatter by the seeding particles and were employed in the simultaneous PIV measurements of the velocity fields in the liquid and gas phases.

An off-axis PIV setup was implemented, as illustrated in Figure 22. This setup included two TSI Powerplus 4 MP cameras with 60 mm Nikon. The setup focus distance was 640 mm. This particular camera arrangement was selected

to allow for velocity measurements in both phases at positions close to the interface. In this configuration, the cameras were tilted with respect to the plane orthogonal to the laser light sheet. The magnitude of the tilt angle was 15 degrees, as illustrated in Figure 22. Each camera was used to measure velocity in one of the phases. Thus, images of the liquid layer were captured using the lower camera, whereas images of the gas were captured by the upper camera. Scheimpflug adapters were mounted on each camera to allow for the focusing of the images on the illumination plane. The field of view of each camera at a given streamwise position was 2D X 1D.

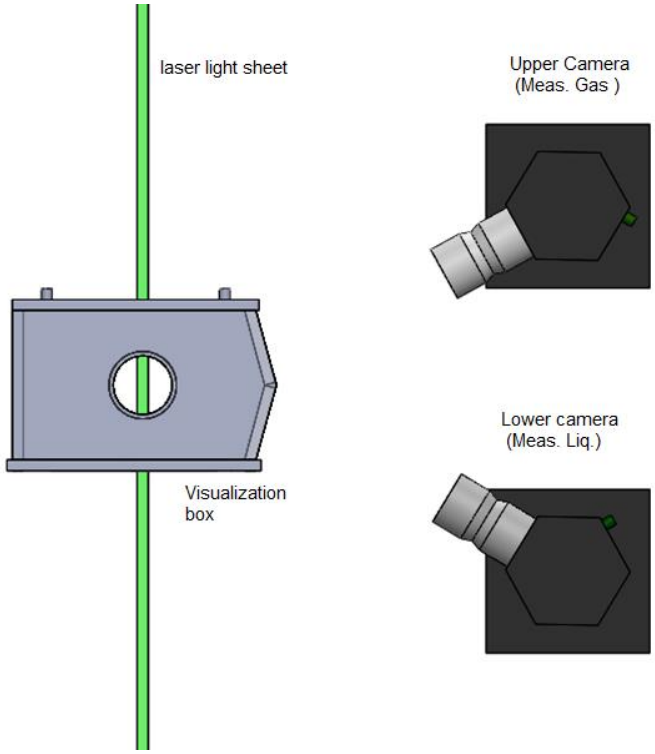

Figure 22 – Schematic view for the off-axis PIV setup employed in the simulataneous velocity measurements in the gas and liquid phases.

To reduce optical distortions, the pipe was encased by a transparent box. The box extended along 2 m of the test section. The box side walls facing the cameras were inclined at 15 degrees in order to be parallel to the camera lens planes. Inside the visualization box the pipes were segmented into pieces of 400 mm connected by specially designed flanges. Each piece had its wall thickness reduced to 0.5 mm from its original 3 mm, along an extent of 250 mm. Thereby, it was possible to perform PIV measurements in 5 different stations along the pipe streamwise direction. For minimization of optical distortions half of the box was filled with water, so that there was only air and walls within the optical path from

the flow to the upper camera. Conversely, the optical path from the flow to the lower camera contained only liquid and walls. Due to perspective effects, the images had to be dewarped before being processed with PIV. More details of this procedure are provided in Chapter 5.

The cameras were mounted on a horizontal traverse with a travel range of 2000 mm. The off-axis visualization setup overview is illustrated in Figure 23. In order to keep the light plane aligned during the system displacement, the lenses and mirrors were also mounted on the traverse. This setup enabled the measurement of velocity fields within a streamwise range of about 2000 mm. In the present work, the visualization was kept at the furthest downstream measured station located at 62 D from the inlet.

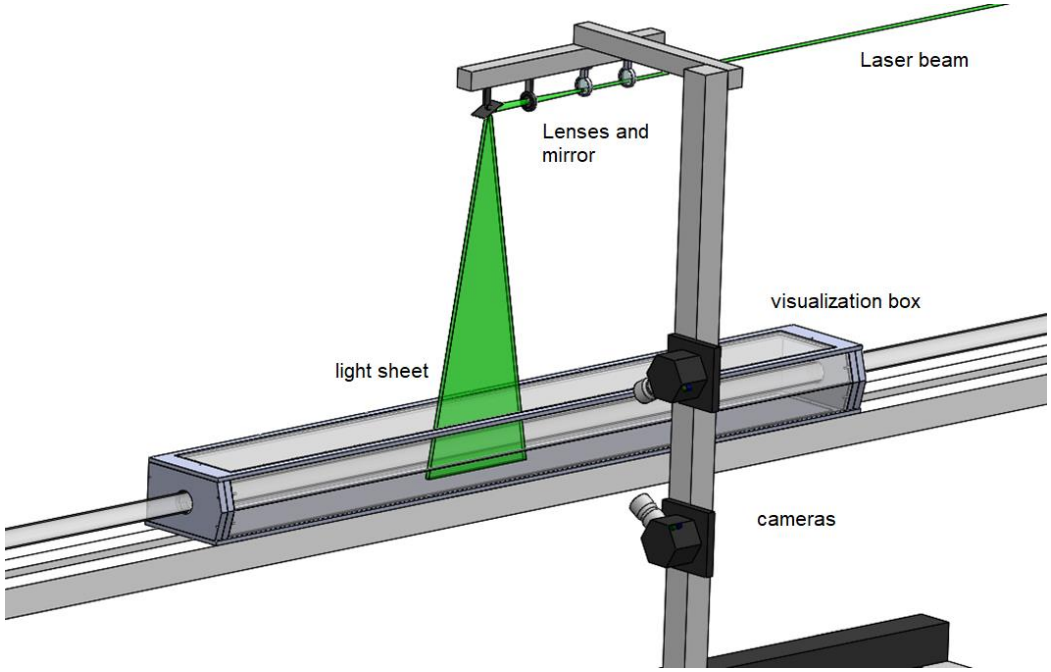

Figure 23 – Schematic view of the off-axis setup employed for simultaneous PIV measurements it the gas and liquid phases.

For PIV measurements the water was seeded with spherical polyamide particles of 20µm. The polyamide has nearly the same density as water, therefore the particles were nearly neutrally buoyant. Seeding particles for gas were provided by GTech ultrasonic humidifiers. These humidifiers are capable to generate water droplets with diameters of about 3 µm. According to Ayati et al. (2014), water droplets in air phase behave as passive particles following the dominant turbulent fluctuations faithfully. For uniformization of the fog concentration, the ultrasonic humidifiers were placed inside of a tight box. The fog injection was adjusted by pressurized air and a flow control valve, as

illustrated in Figure 24. The flow rate of the compressed air was measured by a rotameter from Omega® (model D6563). Figure 25 provide an overview of the entire test section assembly.

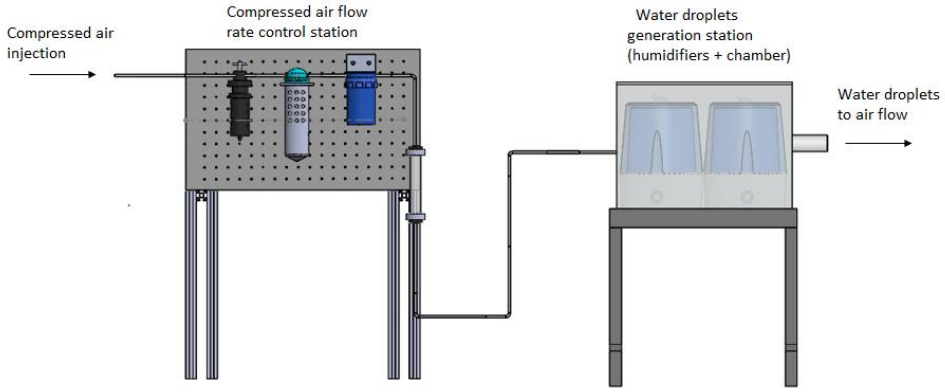

Figure 24 – Water droplets seeding station.

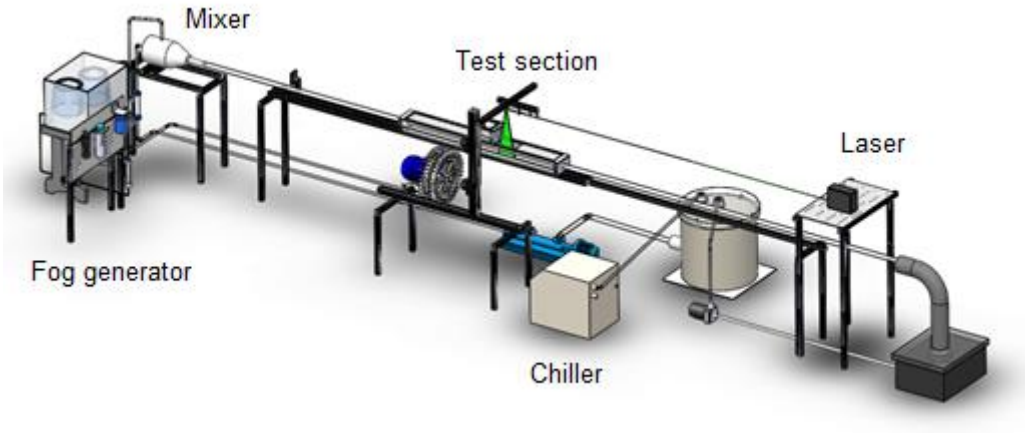

Figure 25 – General view of the test section for off-axis PIV measurments.

4
Image processing

The experiments carried out in this work demanded original strategies for characterization of interfacial waves. To this end, several techniques were combined for processing the acquired flow images. This section outlines the procedures employed for measuring the liquid interface and velocity fields.

4.1
Interface detection

The flow measurements involved a large number of images, therefore the gas-liquid interfaces had to be detected automatically using digital image processing. To this end, a number of in-house routines were developed in Matlab® programming language.

Prior to the image processing, it was necessary to apply some processing procedures for intensity and histogram equalization. Basically, the pre-processing techniques employed apply a transformation to the original image histogram in order to use the full grayscale range of the image. In addition, this procedure not only removes any bias that could have been introduced by differences in illumination intensity, but also facilitates the determination of the binarization threshold for identifying the gas-liquid interface contours (see Gonzales et al. 2009 for a review of the standard image processing routines).

Figure 26 shows a typical camera image captured by Shadowgraphy technique. As can be seen in the figure, a shadow is formed at the front and at the back of the pipe walls. Hence, an image often has two regions with high gradient of illumination. The upper edge originated from the back wall intersection, whereas the lower one is related with front wall intersection. These edges are indicated in the figure by light red and dark blue dash dotted lines, respectively. In this part of the study, the foremost interface/wall intersection that is assumed as the interface position of interest. This assumption restricts the range of study to 2D, or nearly 2D waves, because 3D waves can't be well captured with this procedure. Further, in off-axis measurements, the interface

detection problem is solved by the camera tilting which enables visualization of the illumination plane at the centerline of the pipe.

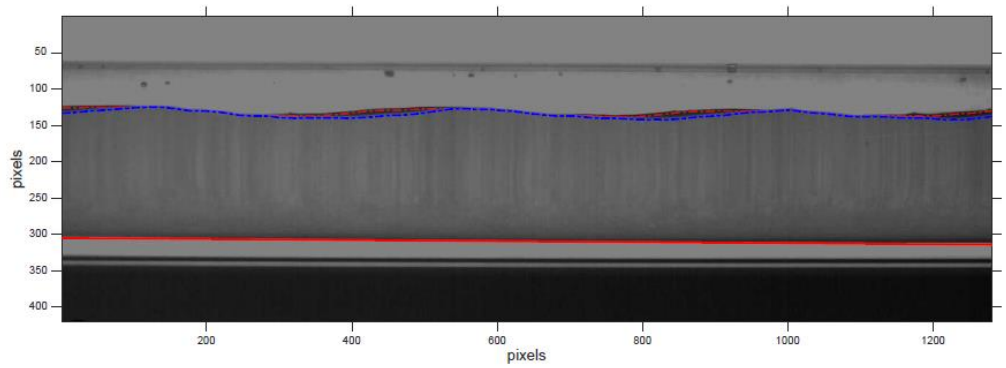

Figure 26 - Interface detected by binarization threshold (blue dashed-dotted) and distinction from back wall reflection (red dashed-dotted). The detected pipe bottom (red line) provided the reference level y=0. Flow conditions: U_{sg} = 1.0 m/s and U_{sl} = 0.21 m/s. Field of view of approximately 5D.

The high quality of the level of synchronization obtained between acquisition and disturbance generation is demonstrated in Figure 27. The figure shows a set of interface contours obtained from 60 different images captured at a distance of 15 D from the disturbance source. Each image corresponds to a different wave event, generated with a time interval of the order of 30 seconds. An excellent agreement was found showing that, indeed, excited waves were phase-locked with respect to data acquisitions. Some degree of scattering was observed, but this could be considered as normal because both phases were turbulent and hence non-controlled disturbances were always present in the flow.

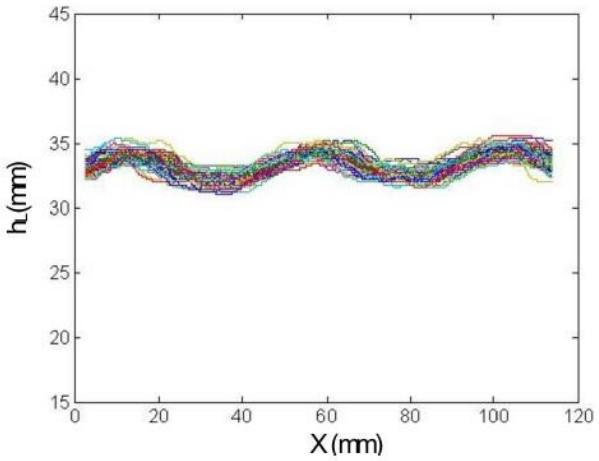

Figure 27 - Example of interface detection from 60 different images from different wave-generated events. Flow conditions: U_{sg} = 1.0 m/s and U_{sl} = 0.21 m/s.

In order to measure the liquid height from the captured images, it was necessary to perform an image calibration procedure. The procedure aimed at determining a correspondence between dimensions in a real plane with those given in pixels at the camera image plane. The pixel correspondence in millimeters was directly obtained by measuring in the image the known external pipe diameter. It should be mentioned that all measurements within this set of tests were performed under the same calibration conditions, i.e. the same distance from the lens to the illuminated plane and magnification. Prior to every new measurements campaign, the image calibration was checked.

4.2
Image processing for Off-axis PIV

This subsection describes the procedures applied in the off-axis PIV measurements.

4.2.1
Perspective correction procedure

An external calibration was essential for estimation of liquid height from the captured images in an off-axis arrangement. The procedure was required because the insertion and alignment of a calibration target within a pipe with, at least, 2 m long was not convenient. For this external calibration, a copy of the visualization box having only 300 mm long was produced. This copy could be placed over the original visualization box, as illustrated in Figure 28. Due to the reduced length of the calibration box, a calibration target could be easily inserted and aligned with the laser light sheet. Guiding pins were machined and installed on both boxes to ensure an accurate positioning and alignment of the laser.

For a vertical movement of the imaging system, the cameras were mounted on a vertical traverse. Since the distance between both boxes' centers was known, a calibration performed with images from the upper box could be transferred to the lower one. To this end, the image system had to be moved down by the exact distance between the boxes centers.

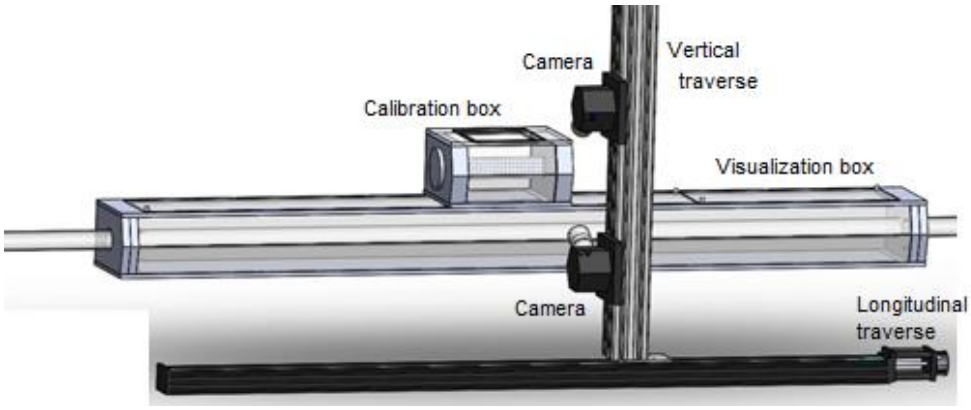

Figure 28 - Off-axis calibration assembly.

A calibration target was machined in the form of a half cylinder. A grid of dots equally spaced was glued on the flat face of this half cylinder. This calibration target was inserted into the pipe, as illustrated in the Figure 29. The laser light sheet was carefully aligned to cross simultaneously the center line of the pipes in both, the calibration and visualization boxes.

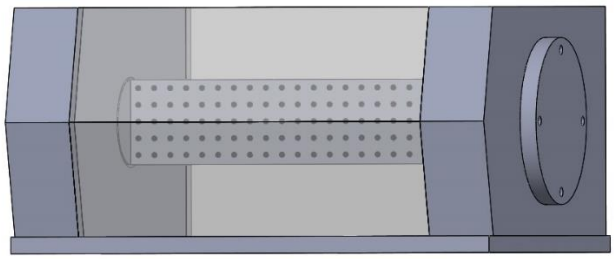

Figure 29 – Calibration target employed for image calibration in the off-axis PIV measurements.

For calibration of the lower camera, the calibration box and the pipe were completely filled with water. Afterwards, one image of the target was captured. For calibration of the upper camera, the calibration box and the pipe were both emptied and one image of the target was captured. It is relevant to mention that the optical path for gas and liquid at calibration conditions were the same as in flow conditions. To guarantee this condition, the visualization box was half filled with water during the experiments, as already described. The water level in the box was adjusted according to the mean liquid level within the pipe.

An in-house Matlab® code, based on Soloff's method (Raffel et al., 2007) was used to correct for image perspective and for small optical distortions. The calibration routine automatically detected the dots on the calibration images. The points in the image plane and in the real plane were fitted by third order

polynomials. An example of the correction provided by this procedure is illustrated in Figure 30.

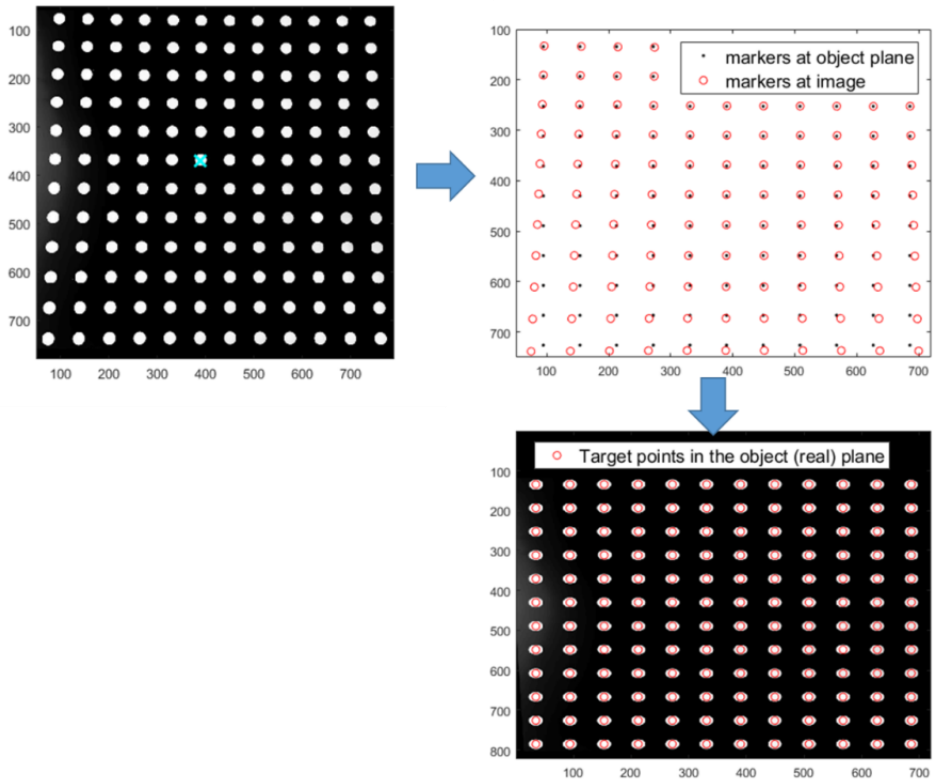

Figure 30 - Example of calibration procedure used to correct for image distortions.

The upper left image of Figure 30 shows the image of a uniformly spaced grid inside the pipe with thin walls. The distorted image was acquired by a camera inclined with respect to the target plane. The upper right image shows a comparison of markers in the original image against those expected for a target with constant dot spacing. The lower right image illustrates how the target points overlap those at the image after the application of a correction procedure. This operation has to be applied to each captured image.

4.2.2

Image masking for off-axis PIV measurements

After correcting perspective and distortions, additional image processing procedures were applied. These procedures removes particles of the gas from the image captured by the camera used for measuring the liquid layer, and vice versa. This procedure consisted in generating a dynamic image mask to shade in black the undesired image area. To this end, the interface position that was automatically detected in the images of liquid flow was used. For images captured

by the lower camera this undesired area was above the interface, and for the upper one it was the opposite area.

The center mark of the calibration target and the magnification of each camera were both used to convert the interface location from images of the lower camera to images of the upper one. Figure 31 illustrates this masking procedure applied to typical liquid and gas images captured by the off-axis setup.

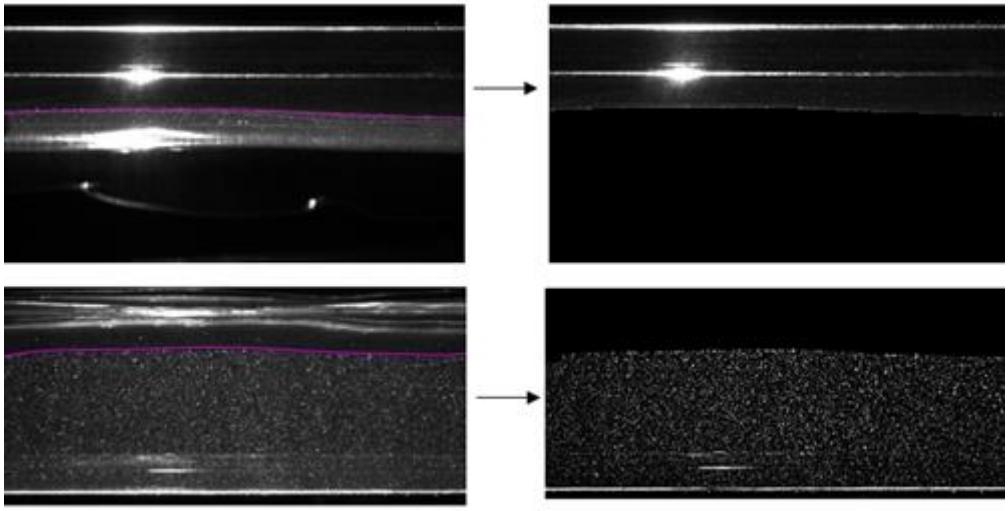

Figure 31 – Example of masking procedure. Left : Original image acquisitions. Right: Images after masking. Upper figures correspond to gas images and bottom ones to liquid.

4.2.3

PIV algorithm

The images for PIV measurements were recorded using Insight 4G®, a commercial software from TSI's. However, this software does not allow either to use an adaptive image masking, or different magnification between both cameras. Thus, off-axis PIV processing was performed with an in-house developed code. The PIV algorithm developed was based on cross-correlation processing with a multi-pass adaptive procedure (See Raffel et al., 1997 for a review). The algorithm was validated previously against benchmarks available at www.pivchallenge.org.

Velocity fields were obtained using a final interrogation area size of 16 x 16 pixels (approximately 1.2 mm in the actual flow) for liquid phase, and of 32 x 32 pixels for the gas phase. An interrogation window overlap of 75% was selected. Thereby, vector grid spacing was, approximately, 0.3 mm and 0.6 mm, for liquid and gas measurements, respectively. The choice of window size and time interval between two frames were determined by a series of preliminary tests that are

described in Chapter 8. It is important to mention that outliers were monitored during data processing and did not exceed 5% in all cases analyzed in this work.

5
Data Reduction

The techniques described in previous chapters are capable to produce information about liquid film height with high temporal and spatial resolution. In addition, it is possible also to measure velocity fields in liquid and gas layers. The distinctive and original feature of the measurement procedures developed and employed was the capability of performing measurements that were phase-locked with the imposed disturbances. This chapter describes the strategies adopted for reduction of data collected under this synchronized condition.

5.1
Characterization of liquid film height

In the following subsections, the data reduction methods adopted for analysis of the liquid film are detailed.

5.1.1
Mean liquid height

Mean liquid heights were determined by the temporal and spatial average of the instantaneous film thickness measured, as given by Equation (5.1).

$$\overline{h_l} = \frac{1}{N}\frac{1}{Dx}\sum_{1}^{N}\sum_{1}^{Dx} h_l(x,t) \qquad (5.1)$$

where, N is the number of images and $h_l(x,t)$ is the instantaneous liquid height at a given axial position. The variable Dx is the dimensional length corresponding to the axial field of view. Figure 32 illustrates a typical time trace of measured liquid height in the presence of controlled excitations. The disturbance frequency in this case was 4 Hz. The time trace represents the oscillation of the liquid film at a given spatial location. For the sake of clarity, only the first 200 records are shown in the figure. A sinusoidal oscillation with constant period can be observed in the figure. The observation of the figure gives also an estimate for signal-to-noise ratio obtained for the height signal.

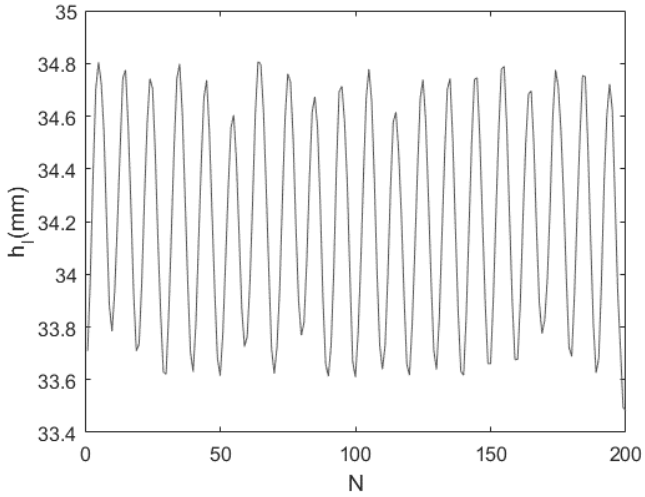

Figure 32 - Typical example of the temporal variation of liquid height determined by the image processing procedure developed. Usg = 0.80 m/s, Usl = 0.14 m/s @ 4Hz disturbance frequency.

5.1.2

Wave amplitude

Phase locked acquisitions combined with controlled excitations allowed the capture of an integer number of periods of the excited waves. This enabled to resolve the wave exactly at its frequency using a standard spectral decomposition via Fourier transform. Figure 33 displays an example of measured liquid oscillation spectrum for an excitation frequency of 4 Hz. As can be seen, the amplitude peak at the excitation frequency is rather sharp and a weak leakage is observed. In addition, a high signal to noise ratio can be observed, indicating that disturbances with 0.7 millimeter (0 to peak) were, indeed, mostly introduced at the selected frequency.

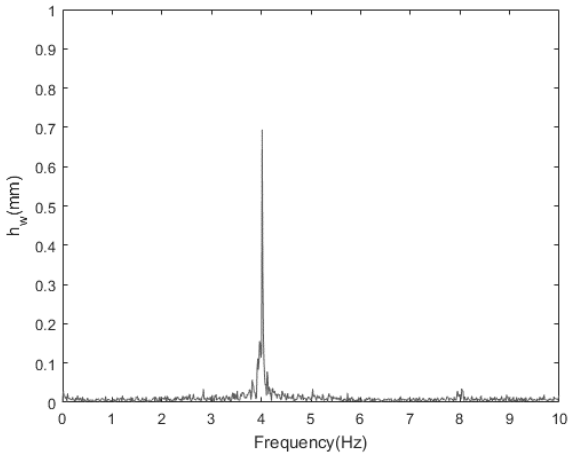

Figure 33 - Spectral of interfacial disturbances @ 4Hz. Usg = 0.80 m/s, Usl = 0.14 m/s.

5.2
Characterization of velocity fields

In order to separate wave related velocity fluctuations from flow turbulence, a simple spectral decomposition was applied to the time series of velocity fields. Thereby, fluctuations could be split into different components namely, mean velocity ($\overline{U}$) and flow fluctuations (u'). The flow fluctuations could be also split into wave induced fluctuations ($\emptyset_{u'}$) and random turbulence (u^*). All the components are shown in Equation (5.2).

$$u(x,y,t) = \overline{U}(x,y) + u'(x,y,t) = \overline{U}(x,y) + \emptyset_{u'}(x,y,t) + u^*(x,y,t) \qquad (5.2)$$

Although several procedures were adopted to reduce noise in the PIV measurements, instantaneous velocity signals obtained significant amount of spurious vectors at image regions where high intensity of light reflection prevailed (see Figure 31). To minimize the influence of spurious data on the results a set of procedures were adopted for detection of removal of outliers from the series of measured velocities. At first, standard algorithms for outlier detection, such as a global filter and a normalized median error (Raffel et al., 2007) were applied. Afterwards, velocity vectors with magnitudes higher than two standard deviations from he mean were excluded. In order to maintain a constant time step, for Fourier transformation, a cubic interpolation of neighboring grid data was performed to replace the outliers. To this end a Matlab® library function *interp1* was used. It is important to emphasize that the percentage of outliers was always lower than 5% (Raffel et al., 2007) of the total number of measured vectors within the area analyzed. Regions of the image where this condition was not satisfied were not analyzed. It can be inferred from Figure 31 that the first half of the image was discarded due to strong reflections in the gas phase.

5.2.1
Time-averaged velocities

The time-averaged velocity, $\overline{U}(x,y)$, is given by the standard relation of equation (5.3). This average velocity is also referenced throughout the manuscript as base flow because flow conditions were kept constant during the test campaigns.

$$\overline{U}(x,y) = \frac{1}{N}\sum_{1}^{N} u_i(x,y,t) \qquad (5.3)$$

5.2.2
Flow fluctuations

The magnitude of flow fluctuations, which include wave induced disturbances and random turbulence, were estimated by the standard deviation, as given below.

$$u'(x,y) = \frac{1}{N-1}\sum_{1}^{N}\sqrt{(u(x,y,t) - \bar{U}(x,y))^2} \qquad (5.4)$$

The number of image pairs acquired (N) was determinated by preliminary experiments in order to guarantee a convergence of first and second order statistic moments about the mean velocity. This analysis is reported in Chapter 8.

5.2.3
Wave induced disturbances

Amplitude of velocity fluctuations related to interfacial waves were obtained via spectral decomposition. Thereby, only part of the spectra related to the wave frequency was analyzed. This enabled to clarify whether interfacial waves were coupled with flow turbulence or not. Figure 34 summarizes the processing scheme adopted.

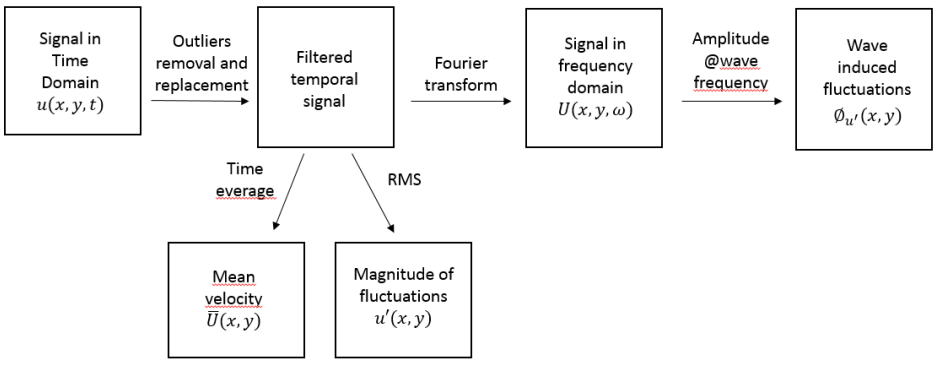

Figure 34 - Digital filtering process scheme.

The cameras and laser employed in the PIV measurements have a limited operational frequency. Therefore, highest acquisition frequency was limited to 5 Hz. This implies in aliased velocity signal at wave excitation frequency. Due to the high signal to noise ratio of coherent liquid film oscillations, the wave

fluctuations were obtained from the aliased wave frequency. The frequency of the aliased signal could be easily retrieved using the following equation:

$$f_a = |nF_s - f_s| \tag{5.5}$$

Here, f_a is the aliased frequency of the sampled signal f_s, while F_s is the sampling frequency and n, is the closest integer multiple of the sampling frequency to the signal being aliased.

6
Characterization of waves in the liquid film

6.1
Experimental conditions matrix

Current investigations were performed for liquid and gas velocities within the range of [0.16; 0.18] m/s and [0.5; 1.0] m/s, respectively. The corresponding Reynolds numbers based on superficial liquid and gas velocities were [12177; 14885] and [2679; 4778]. It is didactically important to display the conditions selected for this investigation in a map of flow regimes, as illustrated in Figure 35.

The reference map in the figure was extracted from the work of Mandhane et al. (1974). The geometry and the fluids adopted in that work are similar to those of current investigation. According to the figure, the range studied here covers the transition from smooth stratified to intermittent flow regimes. At such flow rates, disturbances are close to a neutrally stable condition, yielding weak damping/amplification rates. Thereby, the evolution of disturbances is expected to display a slow variation with the axial coordinate, hence facilitating its measurement along the pipeline.

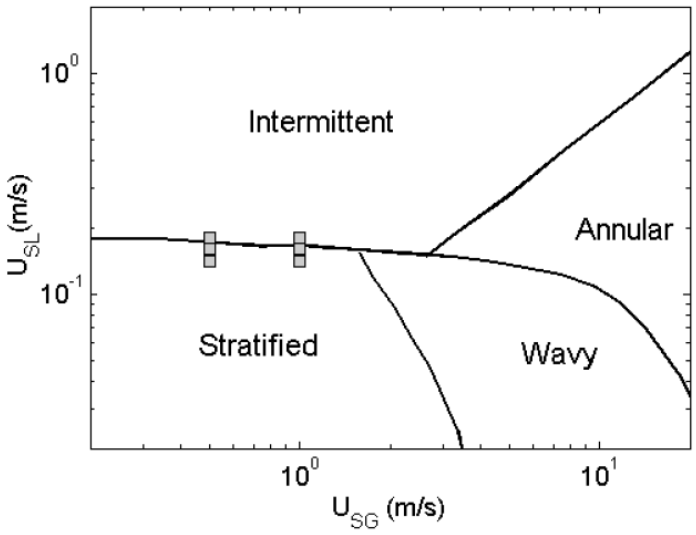

Figure 35 – Flowregime map. Symbols indicate experimental conditions selected for this investigation. Base map extracted from the work of Mandhane et al. (1974).

6.2
Influence of disturbances on transition from stratified to slug flow

The sketch shown in Figure 6 in Chapter 2, illustrates how the definition of critical Reynolds numbers can affect the interpretation of flow instability. In view of the current study, the definition of the critical Reynolds given by linear stability calculations could be related, for instance, with transition from stratified to slug flow. This premise is adopted in most prediction models for slug initiation, as already discussed in the literature review. In this scenario, even infinitesimal waves can lead to slug initiation if a critical condition for the flow instability is reached. Here, a very simple test case was designed in order to examine the influence of initial disturbances on the slug initiation for different flow velocities. In this test, the transition conditions were detected in two situations, one with the source switched off and other with disturbances of high amplitude being introduced in the flow. Since the most unstable frequencies were, in principle, not known for the different velocities, it was chosen to introduce a very short wavepacket. This kind of wavepackets have a rich spectral content, therefore fluctuations in a broad range of frequencies were excited with high initial amplitude.

In Figure 36, the transition points observed in the experiments were compared with the map given by Mandhane et al. (1974) and the linear stability predictions given by the model of Barnea and Taitel (1993).

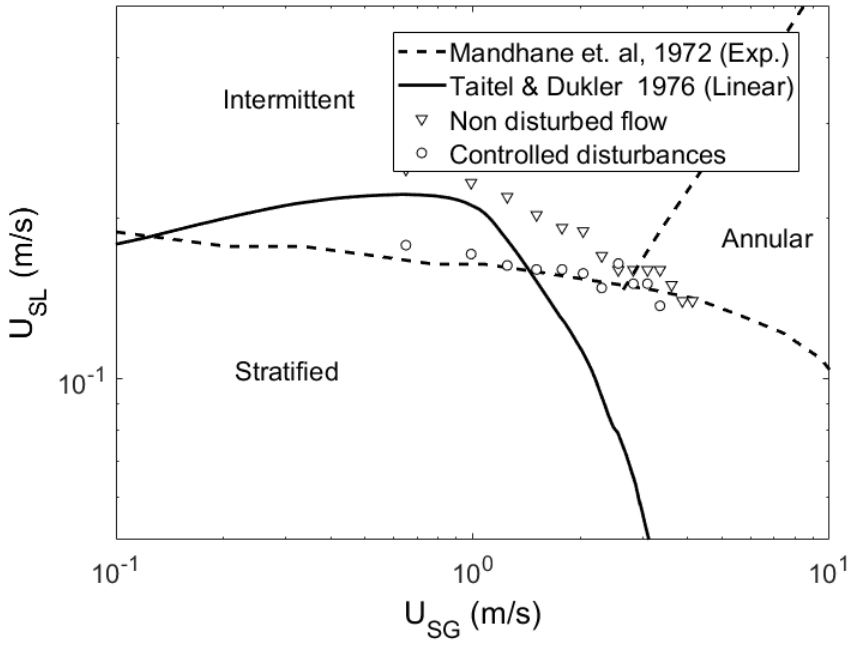

Figure 36 – Influence of disturbances on slug initiation. Experimental transition limits comparared with data from Mandhane et al. (1972) and Barnea and Taitel (1993) LST model.

The map reproduced from Mandhane's work was based on an experimental database from different apparatus. None of the test rigs selected by Mandhane have a specially designed section for mixture of gas and liquid aiming at the reduction disturbances at the pipe inlet. Therefore, very energetic fluctuations were expected to be present in such cases. On the other hand, Barnea and Taitel (1993) have developed a model based on Linear Stability Theory, which predicts the onset of instability for infinitesimal disturbances. Surprisingly the experimental results obtained here, fits very nicely to Mandhane's map when the flow was disturbed, and approach the LST predictions for non-disturbed flow. This picture is very similar to the sketch of Figure 36. For high gas velocities the disturbances generated by shear at the interface are so strong that is impossible to have a condition of non disturbed flow. This is the reason why the experimental points merge at high gas velocities.

From a practical point of view, the results of Figure 35 e Figure 36 suggests the use of Mandhane's criteria for a conservative prediction of slug initiation. If flow conditioners are used at the inlet, then the criteria of Barnea and Taitel (1993) might be more suitable.

It is interesting to observe that all axis are in logarithm scale. Thus, the difference in terms of superficial velocities between the transition lines from the

works of Mandhane (1976) and Barnea and Taitel (1993) reach almost 100%. According to inherent findings, it is clear that linear stability analysis are indeed useful for prediction of slug initiation in cases of absence of interfacial disturbances. However, the accuracy of those models and the validity range of linearized equations is still unclear, due to the lack of controlled experiments. Hence, the results presented in next chapters aim to fill this gap.

6.3
Measurements using shadowgraphy

A non-intrusive shadow technique was employed to provide time resolved temporal and spatial evolution of the disturbances, generated by the oscillating plate, along the streamwise image position. In this subsection the results obtained applying shadowgraph technique are discussed. Prior to the wave characterization, experiments were conducted for assessment of the adopted methodology. Next, these tests are reported in detail.

6.3.1
Assessment of methodology

In view of the high sensitivity of wave development to the flow conditions, a series of preliminary tests were performed in order to assess the quality of the results obtained with the test rig. This is an important part of the experiment because the results must be reproducible for further comparisons with simulations and theoretical models.

6.3.1.1
Paddle oscillation analysis

The frequency content of the paddle oscillation and corresponding liquid height fluctuation are analyzed in the spectra of Figure 37 in order to assess whether generated waves were composed by a single Fourier mode. This is important since the focus of this study is the characterization of waves within the linear regime; therefore, excitation of multiple waves must be avoided. The spectra of the related figures display a sharp peak around the frequencies, indicating that disturbances were, indeed, mostly introduced at the selected frequencies. An apparent leakage around the excitation frequency can be seen in Figure 37a, which corresponds to the spectra of the paddle oscillation. This is due to the modulation of the paddle-driving signal. The apparent leakage is not

observed in Figure 37b because the liquid film height was measured only at the central part of the modulated signal where the amplitude is nearly constant. Small amount (less than 15%) of energy contamination to harmonic components was observed in both figures.

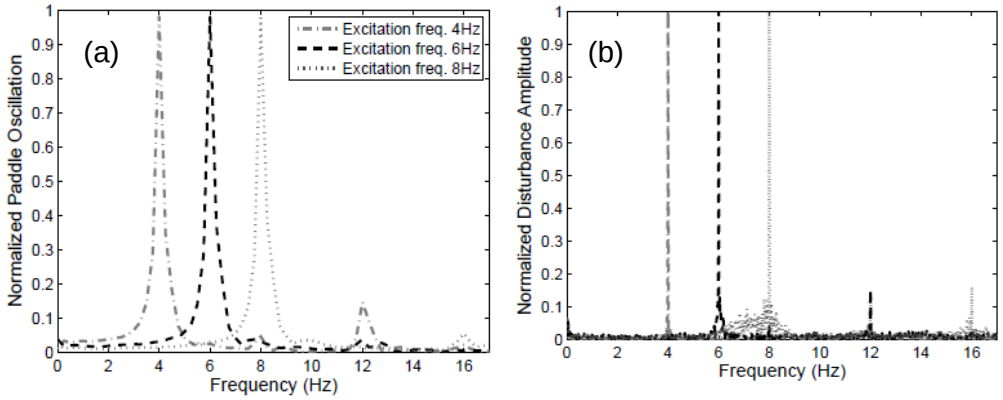

Figure 37 – Normalized Fourier spectra of excited disturbances for three different driving frequencies, namely, 4 Hz, 6 Hz, and 8 Hz. Flow conditions: U_{sg}= 1.0 m/s and U_{sl} = 0.21 m/s. (a) Spectra of paddle oscillation. (b) Initial interface oscillation.

6.3.1.2

Statistics convergence

In order to avoid changes on flow conditions due to slugs, disturbances were introduced in the flow as wave trains and not as continuous waves. Blocks of only 20 images were collected per wave train at a constant frame rate of 40 Hz. Thereby, the acquired images would appear as a continuous movie if displayed in a sequence. The time elapsed between consecutive wave trains had to be long enough to enable a complete recovery of the base flow conditions. Preliminary tests have shown that 40 seconds after the slug initiation the base flow was completely recovered. For cases with no slug initiation, long lasting wave trains were introduced and blocks of 2000 images per camera position were acquired continuously.

Prior to the measurements, it was necessary to define the minimum number of blocks required for the convergence of wave statistics. For this test, a challenging measurement condition was selected. This corresponded to a regime with slug initiation close to the pipe outlet. At every repetition, a block containing 20 images was acquired. This test was important to observe whether variations in flow conditions during the tests would avoid convergence of the results. Mean liquid height and FFT amplitudes were analyzed for an increasing number of acquired blocks. The results are presented in Figure 38. For this test, the liquid

and gas velocities were set to 0.21 m/s and 1 m/s, respectively, and the excitation frequency was set to 4 Hz.

The statistics were evaluated with cameras positioned at the furthest position possible away from the perturbation site. The figures suggest a substantial variation of wave statistics for less than 50 repetitions. A satisfactory convergence of data is seen when more than 80 blocks were considered. All subsequent measurements were conducted with the slightly conservative number of 100 blocks, which corresponded to 2000 images per camera position.

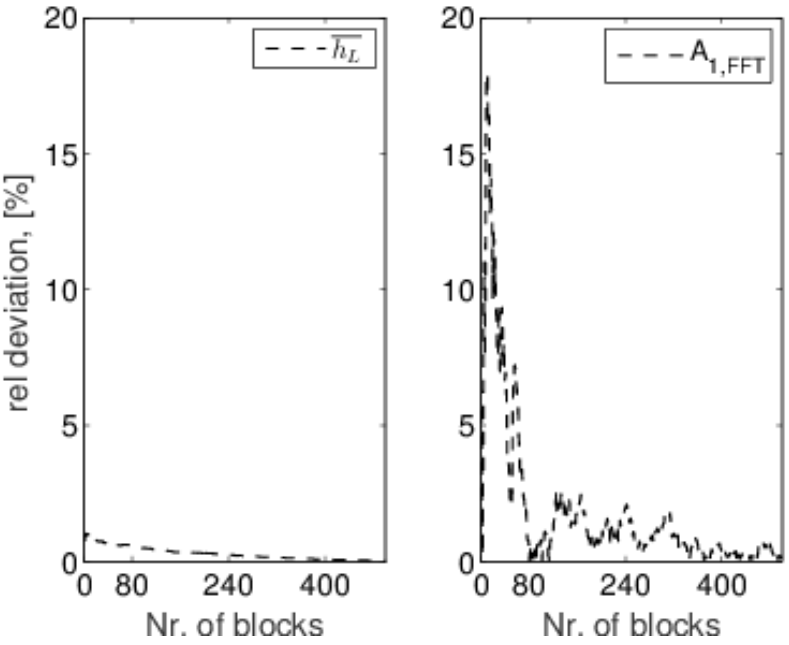

Figure 38 – Convergence of wave amplitude and liquid height. Flow conditions: U_{sg} = 1.0 m/s and U_{sl}= 0.21 m/s. Wave frequency of 4 Hz.

6.3.1.3

Reproducibility

It was also necessary to verify the reproducibility of amplification curves for different ambient conditions. This was tested by comparing experiments performed in different days. The results of the evolution of the waves are presented in Figure 39 for three different runs under fixed gas and liquid superficial velocities of 1 m/s and 0.16 m/s, respectively. The figure illustrates that all three amplification curves display similar behavior, thus demonstrating that the experiment is reproducible to a satisfactory degree.

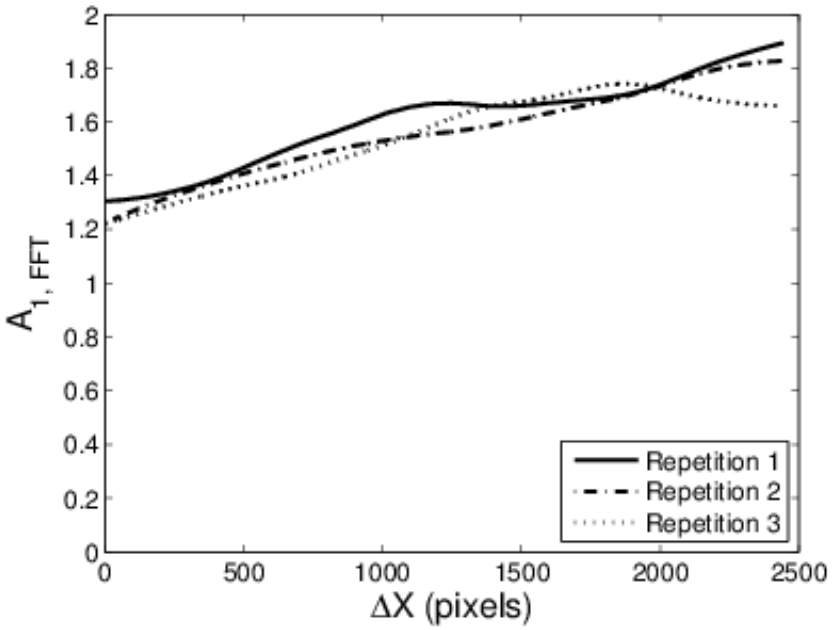

Figure 39 – Example of reproducibility. Measurements of wave height evolution performed at fixed frequency and flowrates in different days. Flow conditions: U_{sg} = 1.0 m/s and U_{sl} = 0.16 m/s.

6.3.1.4

Experimental determination of linear wave regime

The linear approach for any system is typically restricted by the amplitude of the disturbances. Unfortunately, the authors were not able to find in the literature an ubiquitous amplitude threshold to define a linear range for the evolution of interfacial waves in a stratified gas-liquid pipe flow. Thus, prior to the characterization of interfacial waves, a set of preliminary experiments were performed to ensure that excited disturbances were within the linear regime in the measurement domain.

At first, it was necessary to define an amplitude threshold for waves to be considered as linear. For this test, the driving voltage of the oscillating paddle was varied and the resulting change in amplitude of interfacial waves was monitored at the farthest measurement station downstream from the paddle (x/D = 30). The idea is to find a range of wave amplitudes where a linear scaling is observed between excitations and waves measured at the last streamwise station.

A similar procedure was previously used in the work of de Paula et al. (2013) to describe linear stages of instability waves in boundary layers. Here, the waves at frequencies of 4 and 6 Hz were analyzed. It is relevant to mention that the waves excited at frequencies higher than 6 Hz were also measured, but their

behavior was more complex and a linear regime of evolution was not clearly identified. The analysis of these waves demands a different approach from the one proposed here, and a description of two different methodologies would excessively extend the manuscript. Thus, nonlinear evolution of interfacial waves is intended to be addressed further in a continuation of the current study.

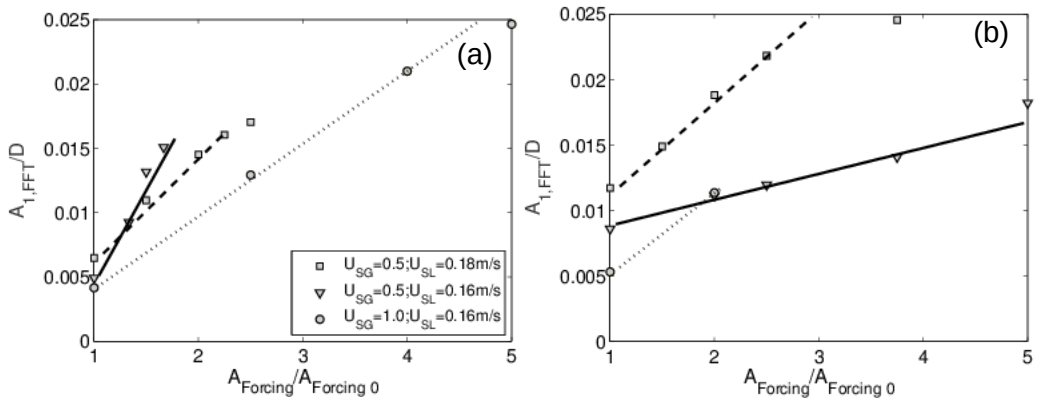

Figure 40–Variation of wave amplitude at the last measurement station according to the forcing amplitude. Forcing frequency: (a) 4 Hz, (b) 6 Hz

According to the results of Figure 40(a) and (b), no evident amplitude threshold was observed. However, waves having amplitudes below 0.015D seem to scale linearly with the excitations for all cases shown in the figure. Apparently, this is a conservative threshold, but it was assumed as an amplitude limit for the present work in order to avoid the influence of nonlinear effects on the experimental results.

The spectral evolution of interfacial waves having amplitudes lower than the threshold defined in the first set of tests was analyzed for different gas and liquid velocities. Results are depicted in Figure 41 and Figure 42, for excitation frequencies of 4 and 6 Hz, respectively. The amplitudes in the spectra are normalized by the excited wave amplitude at the first measurement location, namely, X = 0D, located 38 D from the pipe inlet. Although the spectral information is available at a much higher resolution, only discrete stations are shown in Figure 41 and Figure 42. All these features facilitate a direct comparison of the results obtained for different test conditions.

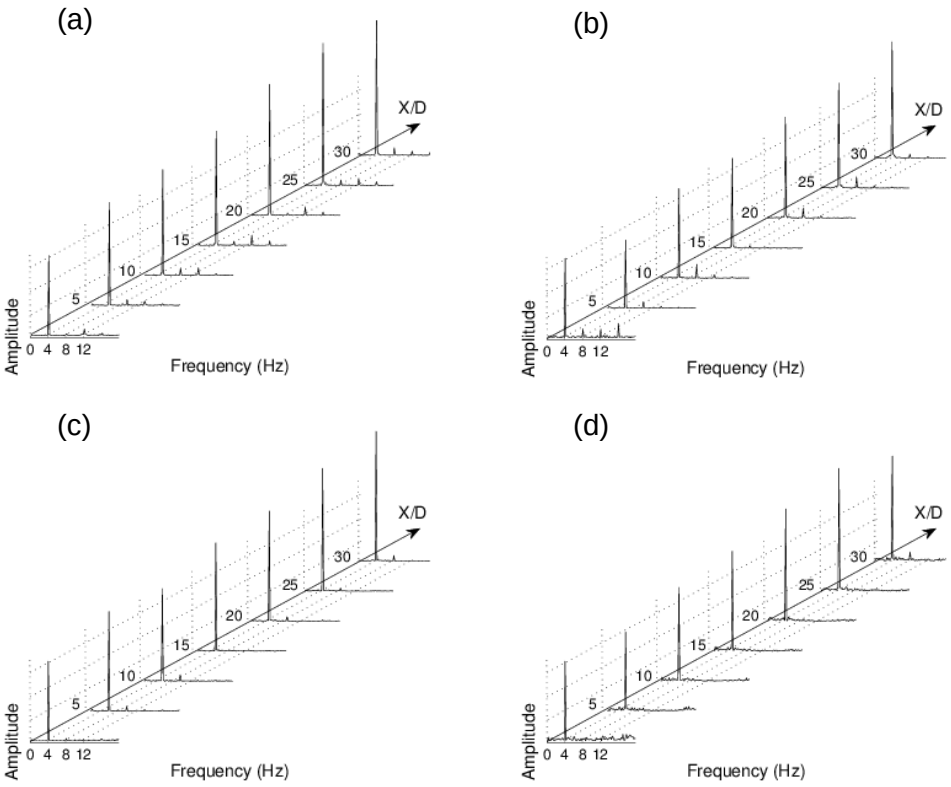

Figure 41 – Spectral evolution of interfacial disturbances for different superficial liquid and gas velocities. Excitation frequency, 4 Hz. (a) Usg = 0.50 m/s, Usl = 0.16 m/s. (b) Usg = 0.50 m/s, Usl = 0.18 m/s. (c) Usg = 1.00 m/s, Usl = 0.16 m/s. (d) Usg = 1.00 m/s, Usl= 0.18 m/s.

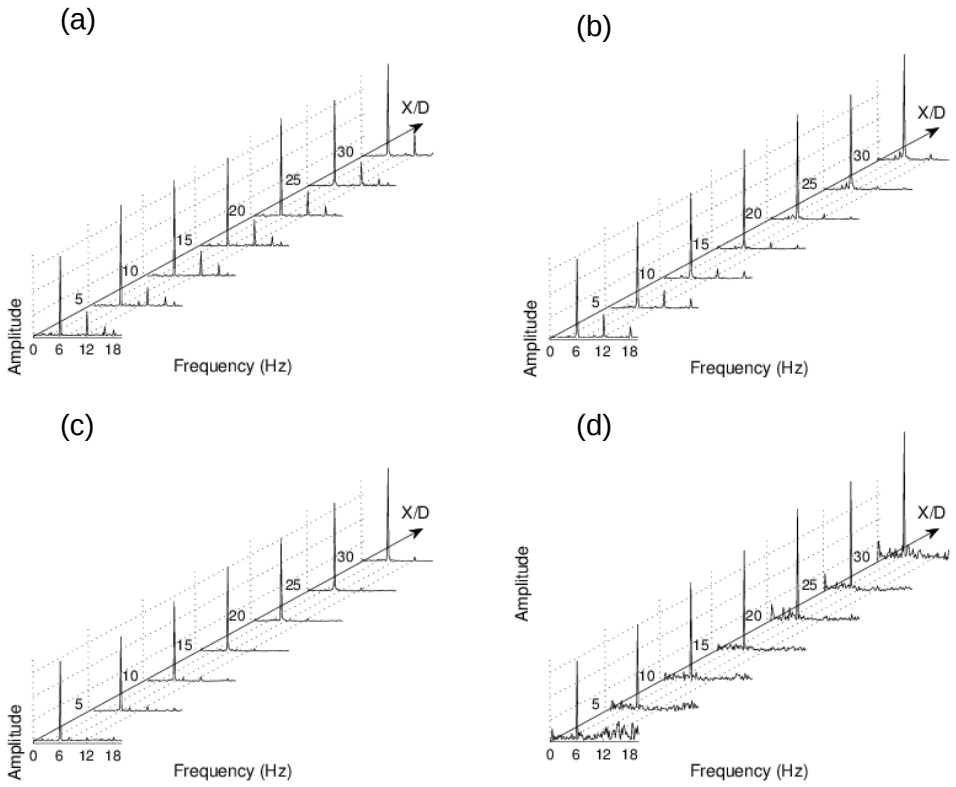

Figure 42 – Spectral evolution of interfacial disturbances for different superficial liquid and gas velocities. Excitation frequency, 6 Hz. (a) Usg = 0.50 m/s, Usl = 0.16 m/s. (b) Usg = 0.50 m/s, Usl = 0.18 m/s. (c) Usg = 1.00 m/s, Usl = 0.16 m/s. (d) Usg = 1.00 m/s, Usl= 0.18 m/s.

The spectra of Figure 41 show no evidence of any strong influence from subharmonics or harmonics of the excited wave on oscillations at the liquid interface. The results are somehow similar to those reported in the work of Bar-Cohen et al. (2016) for interfacial waves in micro channels. In that work, waves did not exhibit substantial variation of wavelength even after entering the non-linear wave regime. In Figure 41(a) and (b), which correspond to cases with a fixed superficial gas velocity of 0.5 m/s, harmonics having low amplitudes could be found at initial stations. Further downstream such high frequencies decay, or simply do not grow as the waves develop. The level of noise in the spectra of Figure 41(d) is higher in comparison to other cases. This might be linked to the instability of base flow, since this case is closer to the transition from a smooth stratified to a wavy flow regime.

For waves excited with a frequency of 6 Hz, the presence of harmonics is more evident as shown in the spectra of Figure 42. Nevertheless, the amplitude of the harmonics was significantly smaller in comparison to the excited disturbances. Overall, the spectra presented in Figure 42 display qualitatively the

same behavior as those from Figure 41. Thus, it can be stated that no evidence of strong wave-wave interactions could be found in these preliminary experiments.

It is well known from hydrodynamic instability studies that nonlinear disturbances can affect the base flow, see Schmid et al. (2002) for a review. In a linear regime, such an effect is not observed and the base flow is not modified when disturbances are present. In order to assess whether the waves investigated were, indeed, within the linear regime, the mean liquid height was monitored for different forcing amplitudes. Results are depicted in Figure 43. Measurements performed for different wave frequencies are combined in the same plot.

According to the results, a small decrement in the mean liquid height was observed for wave amplitudes higher than 0.015D. Amplitudes smaller than 0.015D induced no change in mean liquid height. This is in line with the amplitude threshold defined in the linearity test of Figure 40. The current findings strongly suggest that interfacial waves with amplitudes smaller than 0.015D are linear within the flow rates analyzed. Thus, the characteristics of these waves are detailed in the following section.

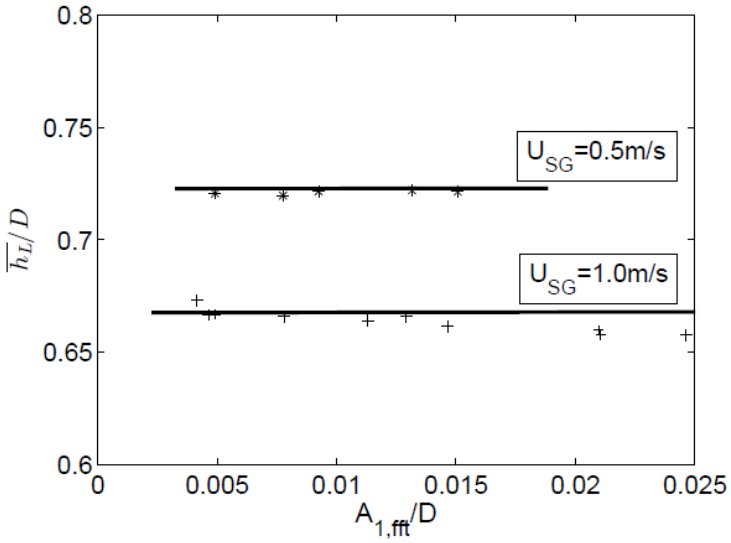

Figure 43 – Variation of mean liquid height with the wave amplitude for U_{sl} = 0.16 m/s

6.3.2

Characterization of waves

According to Kaffel and Riaz (2015), detailed characterization of the interfacial waves has been carried out mostly for two-phase boundary layer and shear flow problems. Channel and pipe flows are rather less explored. Up to date,

most of theoretical works address the problem when both phases are laminar. Indeed, turbulent two-phase flow modeling is challenging due to the interactions between the turbulence and the interface which can be coupled and lead to a modification of the flow. Recently, Ayati et al. (2015) used PIV measurements to observe the interaction between turbulence in the gas and interfacial waves. In the reported scenario, accurate stability predictions are rather difficult because turbulence can actively modify the wave development.

An experimental characterization of interfacial waves is important for validation of models. In the current study, some features of small amplitude interfacial waves were measured using shadowgraphy and phase-locked acquisitions. Characteristics such as wave number, celerity, and wave growth are obtained and reported. Similar data for waves composed by a single Fourier mode were not found in the literature. The results can shed some additional light on how the two-phase boundary layer problem compares with the two-phase channel and pipe flows.

The measured phase evolution of the waves is shown in Figure 44. Phases were extracted from the spectra of interfacial oscillations. The spatial resolution of the measurement was rather high, i.e., one time series per camera pixel. In order to avoid excessive amount of data in the graph, only phases from every 120 pixel are shown. It is worth to mention that no averaging or smoothing was applied to the data. Only phase corrections of 2π and its multiples were employed to account for complete wave cycles.

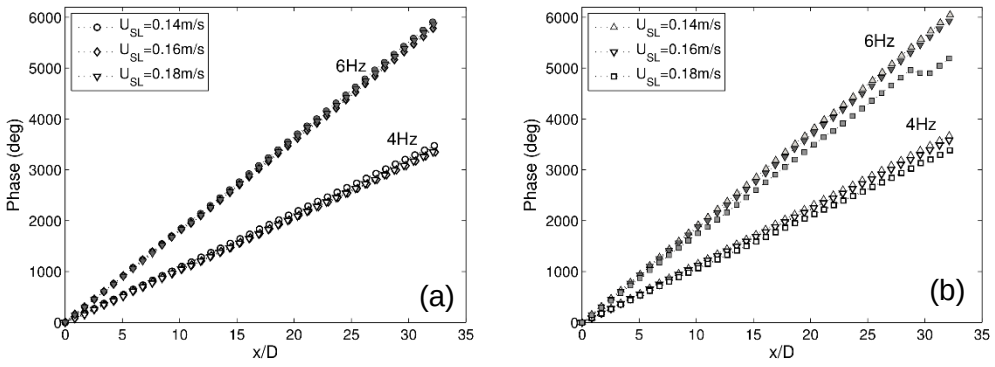

Figure 44 – Phase evolution of waves for different superficial velocities and wave frequencies. Open and filled symbols correspond to waves with frequencies of 4 Hz and 6 Hz respectively. (a) U_{sg}=0.5m/s (b) U_{sg} =1.0m/s.

The results show a linear phase variation of the waves for almost the whole measurement region. The only exception was the case with a wave frequency of 6 Hz at the highest mixture velocity. In this case, there was a phase variation

close to the end of the measurement region. This is apparently linked to the initial stages of non linear wave evolution. A detailed analysis of these stages is out of scope from this work, but the topic should be addressed in future works.

According to Figure 44 , phase increment of the waves was slightly modified by liquid and gas velocities. For increasing liquid velocity, it was expected to observe longer wavelengths. This tendency is qualitatively confirmed in the plots. On the other hand, higher superficial gas velocities induced a small shortening of the waves. Wave numbers were obtained from the phase evolution curves using linear curve fit. The same information could also be obtained using auto-correlation of the liquid film interface. However, this procedure was more expensive and less accurate than curve fitting. A compilation of the information extracted from these measurements is given in Table 1. It also includes the mean level of liquid in the pipe.

The measured wave celerity was compared with different linear wave dispersion relations. Johnson et al. (2009) and Sanchis et al. (2011) observed that the dominant phase velocity of interfacial waves propagating on a thin liquid layer can be matched with linear shallow water wave theory. However, shallow water wave theory is valid only when the wavelength is much higher than the water depth and this condition is not necessarily satisfied in the current experiment. Thus, the measured celerity was compared with other classical dispersion relations derived for linear waves at a finite depth.

Table 1 - Wave properties and mean liquid height for different flow rates and wave frequencies.

U_{SL} (m/s)	U_{SG} (m/s)	F (Hz)	k (m^{-1})	c (m/s)	$\overline{h_L}/D$
0.14	0.5	4	6.0	0.67	0.704
0.16	0.5	4	5.8	0.69	0.726
0.18	0.5	4	5.8	0.69	0.768
0.14	1.0	4	6.4	0.63	0.647
0.16	1.0	4	6.2	0.65	0.660
0.18	1.0	4	5.9	0.68	0.705
0.14	0.5	6	10.2	0.59	0.695
0.16	0.5	6	10.0	0.6	0.729
0.18	0.5	6	10.1	0.59	0.771
0.14	1.0	6	10.4	0.58	0.657
0.16	1.0	6	10.2	0.59	0.663
0.18	1.0	6	9.6	0.63	0.709

A list of dispersion relations used in this comparison are given in Table 2 (for reference, see Landau and Lifshitz 1987). In order to account for the Doppler-shift introduced by the mean flow, the liquid velocity was subtracted from the measured wave velocities.

Table 2 – Wave celerity given by different linear models.

Linear theory	Wave celerity
Shallow water	$c_{sw} = \sqrt{gh_L}$
Finite depth	$c_{fd} = \sqrt{\frac{g}{k}\tanh(kh_L)}$
Capillary-gravity	$c_{cg} = \sqrt{\left(\frac{g}{k} + \frac{\sigma}{\rho}k\right)\tanh(kh_L)}$
Interfacial waves	$c_{iw} = \sqrt{\frac{g(\rho_L - \rho_G)}{k(\rho_L \coth(kh_L) + \rho_G \coth(kh_G))}}$

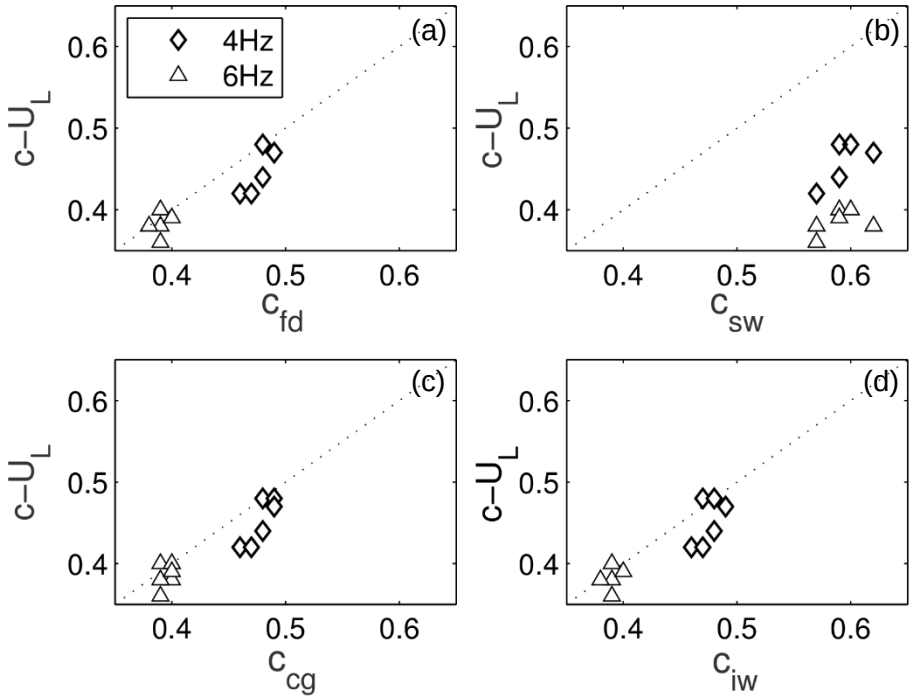

Figure 45 – Measured wave celerity. (a) Finite depth model. (b) Shallow water model. (c) Capillary-gravity model. (d) Interfacial waves model.

According to Figure 45, theories based on finite depth are in better agreement with the experimental findings. Furthermore, corrections introduced by different finite depth theories are not significant. Thus, within the range of parameters analyzed, there was no evident contribution from the surface tension and gas density to the wave celerity. The only dispersion relation in complete disagreement with the experiments was the shallow water equation. Although the experiments are only in qualitative agreement with the other theories, the results

strongly suggest that the shallow water relation is not appropriate to model interfacial waves in pipe flows. Similar observations are reported in the work of Ayati et al. (2014) for wavy flows.

The amplitude growth of interfacial waves was also observed for different test conditions. Results obtained for disturbances with a frequency of 4 Hz are depicted in Figure 46. Similar to the phase analysis, only points at every 120 pixels are shown in the figure. Curves were normalized by amplitudes at the first measurement station (x/D = 0). Amplitude growth predicted by a linear, 1-D viscous Kelvin-Helmholtz model, as proposed in the work of Barnea and Taitel (1993), was also included in the figure for a comparative analysis. Temporal growth rates predicted by that model were converted into spatial ones using Gaster's transformation (see Schmid et al., 2002 for a review).

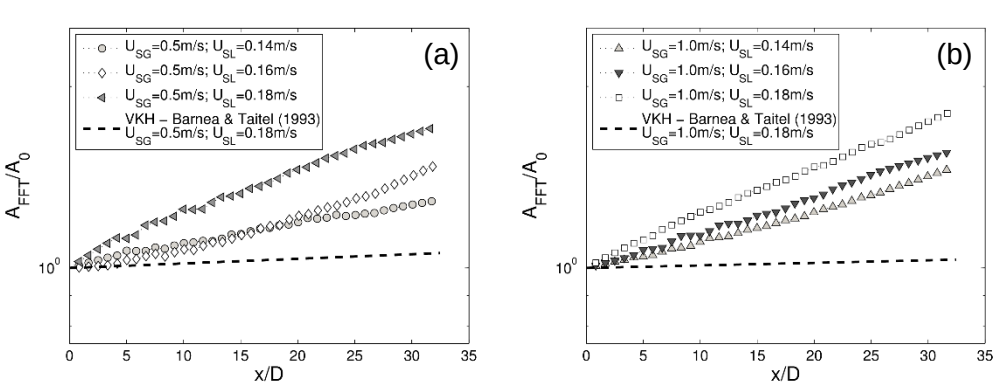

Figure 46 – Wave growth along pipe axis for three different flow rate combinations. Perturbation frequency 4 Hz. (a) U_{sg} =0.5 m/s. (b)U_{sg}=1.0 m/s.

According to these figures, amplification is stronger for increasingly higher liquid flow rates. Apparently, variations in the gas flow rate had minor influence on the wave growth. This is consistent with the picture drawn from flow regime maps, such as those from the works of Barnea (1987), Mandhane et al. (1974), Taitel and Dukler (1976), and many others. In general, those maps point towards higher influence of the liquid velocity on the stability of smooth stratified flow. This is, however, valid only for gas velocities remarkably lower than the transition limit to wavy or to annular flow regimes. Indeed, this is the condition of present experiments.

The curves in Figure 46 show linear amplification in a log scale. To the authors' knowledge, this is the first time that such a behavior is captured experimentally for a gas-liquid pipe flow. No evidence of other mechanisms than the instability of the interfacial waves was observed within the streamwise domain analyzed. For a linear regime, results suggest that wind shearing effects and gas

turbulence are not strong enough to influence the growth of waves with a frequency of 4 Hz. In addition, curves related to the Viscous Kelvin-Helmholtz (VKH) model proposed in the work of Barnea and Taitel (1993) displayed a significant deviation from the measurements. Further work it is necessary to investigate whether simple 1-D models can be properly tuned for a reasonable estimation of wave growth in turbulent flows. However, this is out of scope of present work and is therefore not addressed here.

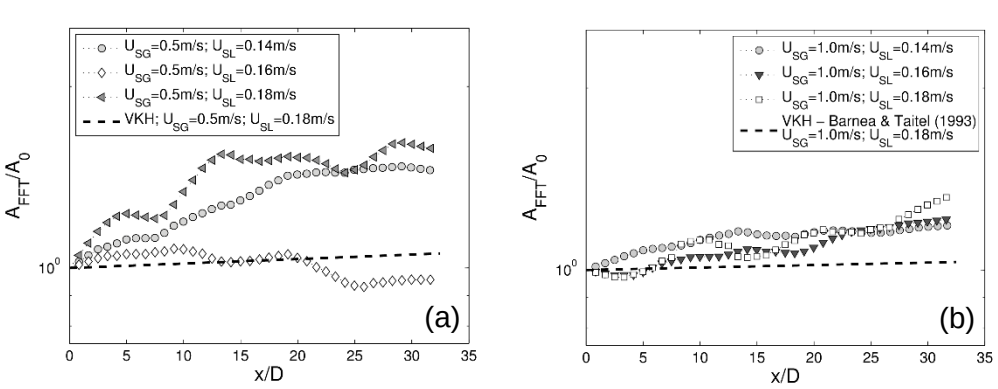

Figure 47 – Wave growth along pipe axis for three different flow rate combinations. Perturbation frequency 6 Hz. (a) U_{sg}=0.5 m/s. (b) U_{sg} = 1.0 m/s.

Amplitude evolution of waves excited with a higher frequency of 6 Hz does not exhibit a monotonic growth as illustrated in in Figure 47. According to Figure 47(a), no coherent tendency of amplification or decay was identified for different flow rates. Although in some cases the waves did apparently grow, the amplification exhibited was far from a linear trend. In Figure 47(b), the amplitude oscillation along the pipe was less pronounced, but again no tendency was observed. The result is quite interesting because it shows that small variation in the wavelength scale could substantially modify the dynamic of the waves. Due to the constant phase increment observed in Figure 44(a) and Figure 44(b), this change in the wave dynamics might be related to weak nonlinear mechanisms. A weak nonlinear wave interaction, such as the one proposed by Sanchis et al. (2011), might not explain the current findings because here amplitudes of disturbances are very low. In the viewpoint of the authors, the influence of gas turbulence has more potential for destabilization of the interfacial waves with high frequencies and short wavelengths, i.e., higher steepness. The conjectured mechanism is somehow similar to the one observed by Buckley and Veron (2016) in a wind-wave-tank and by Ayati et al. (2015) in a pipe. In this case, boundary layer separation of gas flow at the wave crest can couple with the wave and cause

the effect observed. However, the conjecture raised lacks of support and therefore it requires further investigations.

6.4
Analysis of velocity fields in the liquid layer — standard planar PIV

In this section, the mean flow and wave induced fluctuations profiles of interfacial waves are measured in the liquid layer using planar PIV.

The recent works of Kaffel and Riaz (2015) and Barmak et al. (2016) investigated the coalescence of shear and interfacial modes in a channel flow. According to Kaffel and Riaz (2015), wave induced fluctuation profiles are not well investigated for channel flows. For pipe flows, the experimental evidence of fluctuations related to interfacial waves is nearly absent. Thus, wave induced fluctuations corresponding to interfacial instability modes were carefully measured in the liquid layer. Prior to measuring, it is important to characterize the mean flow and the turbulence intensity. The corresponding profiles for streamwise mean flow velocity as well as streamwise and wall normal fluctuations are shown in Figure 48. The interrogation process of the recorded PIV realizations was carried out with TSI's commercial software, Insight 4G, using 64 x 64 pixels interrogation windows and 50% overlap. Hence, the final sub-window size was 32 x 32 pixels, resulting in 63 displacement vectors in each spatial direction (x and y). Note that in this figure, the y-axis is normalized with the interfacial position, y_i.

Profiles of mean flow velocity in Figure 48(a) display a small increment in the velocity close to the interface. This is typical for liquid layers in smooth stratified flows, as observed previously in the works of Ayati et al. (2014) and Birvalski et al. (2014). According to Ayati et al. (2014) and Birvalski et al. (2014), mean flow velocity profiles of wavy flows typically exhibit a small velocity decrement close to the interface. This was not observed here, under low disturbance conditions.

Streamwise and wall normal velocity fluctuations, depicted in Figure 48(b) and (c), respectively, do also show qualitative similarities with results reported in the literature for a smooth stratified flow (Ayati et al., 2014 and Birvalski et al., 2014). Profiles of streamwise velocity fluctuations display higher turbulence intensities near the wall and close to the interface. Apparently, the intensity peak close to the wall is related to wall shear disturbances of turbulent flows, whereas higher intensity at the interface is linked to interfacial disturbances. To date, it is not yet clear if these two disturbances are coupled in turbulent flows due to the

high intensity of fluctuations close to the wall, which cannot be regarded as infinitesimal for linearization of the problem. Wall normal fluctuations illustrated in Figure 48(c) display high intensities in the bulk of the liquid layer. Thus, no evident separation between the inner and interfacial disturbances could be extracted from this figure. In order to shed additional light on the physics of this problem, the inner disturbances and the interfacial ones were analyzed separately.

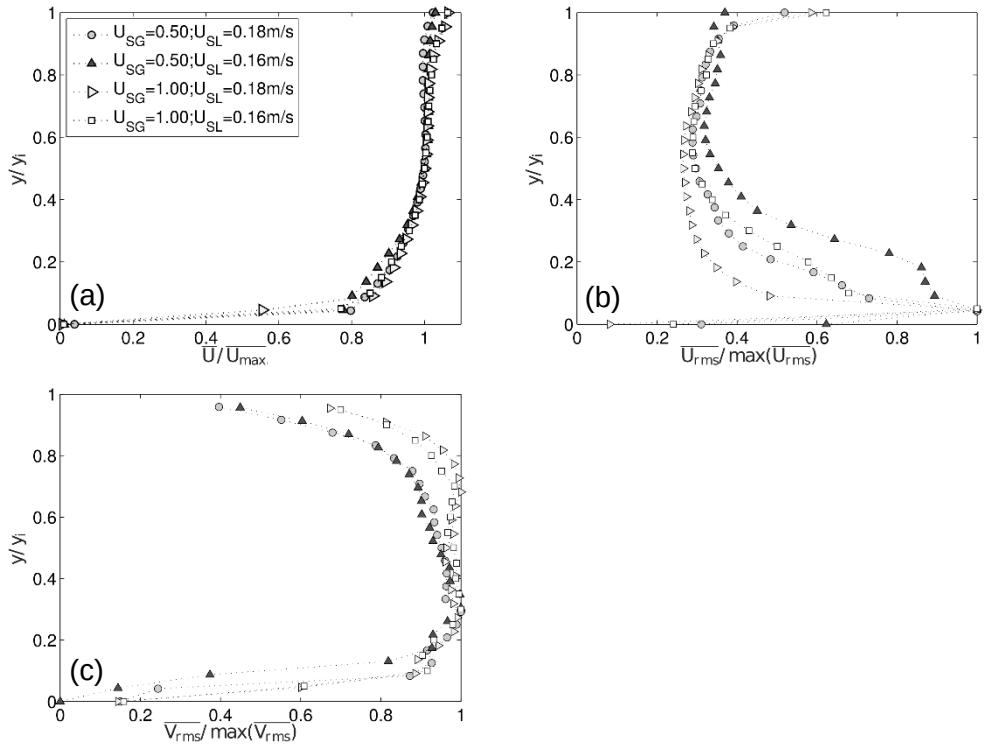

Figure 48 – Mean liquid velocity and RMS of fluctuations at low disturbance condition, i.e. A_{rms}/D below 0.01. (a) Mean velocity. (b) Streamwise fluctuations. (c) Wall normal fluctuations.

One of the main advantages of phase-locked measurements combined with controlled excitation of disturbances is the capability of extraction of coherent oscillations from the noisy signals. To this end, simple spectral decomposition is enough to enable extraction of coherent part of the signal. Thereby, portions of the turbulence intensity profiles related to the wave frequency were analyzed separately. These fluctuations corresponded to the wave induced fluctuations of the interfacial waves.

The eigenfunctions of streamwise and wall normal fluctuations are shown in Figure 49(a) and (b) for waves with a frequency of 4 Hz. The waves reached amplitudes of around 0.025D at the measurement station due to the growth of disturbances along the pipe. Although amplitudes were higher than the threshold suggested in Figure 40, the measured mean flow velocity profiles were

approximately similar to those shown in Figure 48(a). Therefore, nonlinear effects would be weak, if they were present, and hence the measured wave induced fluctuations would closely represent those related to linear interfacial waves. In general, the shapes of the wave induced fluctuations profile of Figure 49 were not modified for the tested conditions.

The profiles of ϕ_u, display a peak at the interface, but their amplitude nearly vanishes at the bottom wall. The current findings support the explanation aforementioned on the nature of the two peaks in the profile of streamwise fluctuations. According to Figure 49(a), the lower peak is, indeed, not related to the interfacial mode. In Figure 49(b), the wave induced fluctuations profile of ϕ_v, displays a peak slightly below the interface.

In Figure 50(a) and (b), waves with an oscillation frequency of 6 Hz show wave induced fluctuations profiles, qualitatively, similar to those obtained for an excitation frequency of 4 Hz. However, in the case of Figure 50 the profiles are rather noisy, possibly due to the low amplitude of the disturbances and to the interactions with turbulence. Interestingly, the near-wall peak in the streamwise fluctuation profile is more pronounced. This can be related to a lower signal to noise ratio. Thus, the contribution from near wall turbulence might not be completely removed from phase averaged signals. Another plausible argument is the coupling between interfacial waves and near wall disturbances via a mechanism analogue to that described in the work of Kaffel and Riaz (2015). However, this conjecture demands further investigation before any conclusion can be drawn.

For complete description of the wave induced fluctuations it is necessary to measure the velocity field in both phases. This is challenging task and only few works in the literature could perform such type measurements. In addition, application of PIV techniques to measure velocities in single and two phases combined with phase locked excitations of disturbances have no precedent in the literature. Results obtained with this framework are reported in Chapter 8.

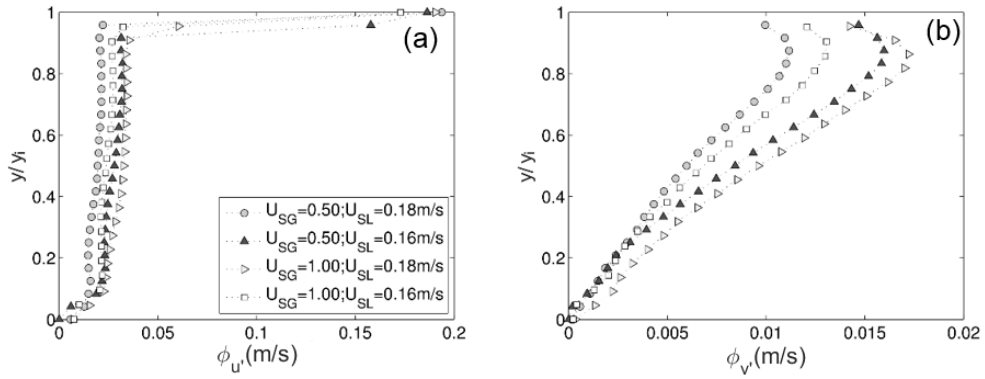

Figure 49 – Wave induced profiles at the excitation frequency 4 Hz.
(a) Streamwise direction. (b) Wall normal direction.

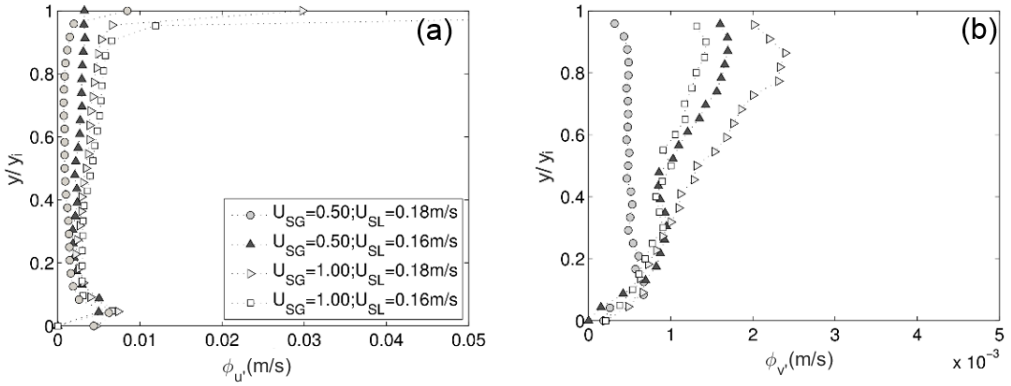

Figure 50 – Wave induced profiles at the excitation frequency 6 Hz.
(a) Streamwise direction. (b) Wall normal direction.

7
Experimental determination of a threshold for linear wave regime

The focus of this work is on linear stages of wave evolution. Unfortunately, there is no universal amplitude threshold for validity of linear wave regime in stratified flows. In Chapter 6, a rather conservative criteria was adopted to prescribe an amplitude limit for the excited disturbances. However, for PIV measurements in two phase flows, it is necessary to resolve, simultaneously, high velocities in the gas and low velocities in the liquid layer. Therefore, the conditions are not optimal for measurements of extremely small disturbances. Thus, in order to capture the wave induced disturbances it is important to have waves with amplitudes as high as possible.

In order to improve the criteria for nonlinearity adopted in Chapter 6, a set of experiments was performed for a range of wave parameters where related nonlinear effects in the liquid layer were monitored.

7.1
Comments about some nonlinear parameters of surface waves

In the literature related to ocean waves, dimensionless parameters are often proposed (Ursell 1953, Beiji 1995 and Kirby 1998) to establish a criteria for validity of linear theory of surface waves. Some simplified water wave models are restricted to a limited range of parameters. Most of these parameters depend on the water depth ($\overline{h_L}$). Typically, the dimensionless parameters are provided by a combination of water depth, wave amplitude (h_w), wavenumber (k) and wavelength (λ). However, a unique parameter to describe a threshold for appearance of nonlinear effects is not yet found.

The work of Ursell (1953) proposes a nonlinearity parameter for long surface waves ($k\overline{h_L} \ll 1$). The parameter is known as Ursell number and the corresponding relation is given in Equation (7.1). According to this parameter, second-order terms in water wave equations can be neglected for nondimensional values well below the unity ($U_r \ll 1$).

$$U_r = \frac{h_w \lambda^2}{\bar{h}_L{}^3} \tag{7.1}$$

According to Beji (1995) the wave steepness, given by Equation (7.2), often shows a good scaling with nonlinearity of surface waves.

$$e = kh_w \tag{7.2}$$

The work of Beji (1995) attempts to consolidate into an unique relation a nonlinear scaling parameter for shallow and deep water waves. However, the study indicates that this parameter offers a good scaling only for shallow and intermediate surface waves.

$$B = \frac{kh_w}{tanh^3(k\bar{h}_L)} \tag{7.3}$$

In the work of Kirby (1998) another nondimensional parameter is proposed for waves in water layers of arbitrary depth. This relation is named here as Kirby parameter, which is given by Equation (7.4).

$$K = \frac{kh_w}{\tanh(k\bar{h}_L)} \tag{7.4}$$

Variations of these parameters with respect to nonlinear effects induced by excited interfacial waves are observed in this section. The objective is to find a proper scaling relation and a threshold for validity of the linear wave regime.

7.2
Linear wave regime experimental results

Measurements were carried out for two different flow rate combinations (U_{sg}=0.8 m/s and U_{sl}=0.14 m/s; U_{sg}=0.6 m/s and U_{sl}=0.16 m/s) and for four different waves frequencies (4 to 7 Hz). For this test, the driving voltage of the oscillating paddle was varied. Corresponding changes in liquid layer were analyzed in terms of mean flow distortion and generation of wave harmonics. Next subsections report the results from this analysis.

7.2.1

Wave response to the forcing disturbance

The relation between wave forcing and wave amplitude was observed for different paddle driving voltages. The analysis is similar to that of section 6.3.1.4. The idea is to find the range where a linear scaling between forcing and measured wave amplitude still holds. Measurements were performed at 3.1 m downstream from the paddle (approximately 62 D).

In Figure 51 relative wave amplitude variation with respect to the relative wave forcing is depicted. In the linear wave regime this relation should also be linear. The reference wave (h_{w0}) and forcing ($A_{Forcing\ 0}$) amplitudes correspond to the case of lowest measured amplitude. A reference was found for each disturbance frequency and flow condition. Indeed, some cases depicted in Figure 51 show a clear linear trend between forcing and wave amplitude. This is the case for 4 and 7 Hz. However, for other cases this linear trend was not clearly observable. Therefore, the results do not allow to trace a coherent threshold for nonlinearity and additional tests were necessary.

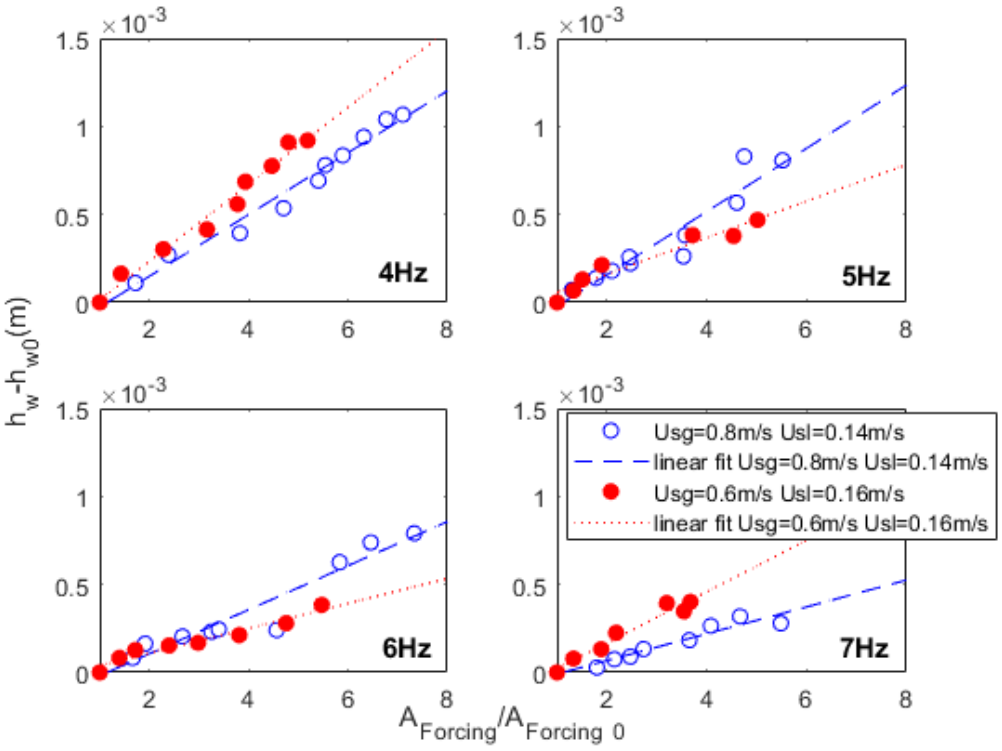

Figure 51 – Variation of wave amplitude at the last measurement station (X/D = 62) according to the forcing amplitude for U_{sg} = 0.8 m/s and U_{sl} = 0.14 m/s and U_{sg}=0.6 m/s and U_{sl}=0.16 m/s at 4, 5, 6 and 7 Hz.

7.2.2

Mean flow distortion in the liquid layer

It is well known from hydrodynamic instability studies that flow disturbances within a nonlinear regime can distort the base flow (Schmid et al. 2002). This effect is not observable in linear regimes. In order to analyze whether the excited waves were within the linear regime or not, measurements of mean flow velocity were performed in the liquid layer using the PIV technique.

Figure 52 illustrates typical mean velocity profiles measured with and without excitation of waves. In the figure, the normalized radial position (r/R) is -1, at the top wall, and 1, at the bottom one. Cases with two distinct excitation amplitudes are shown. In both cases the excitation frequency was equal to 6 Hz. Superficial gas and liquid velocities were kept constant and equal to U_{sg} = 0.8 m/s and U_{sl} = 0.14 m/s, respectively. The shaded area in the graph represents a region influenced by the laser light reflection. Within this region the velocity vectors were influenced by this reflection and therefore discarded.

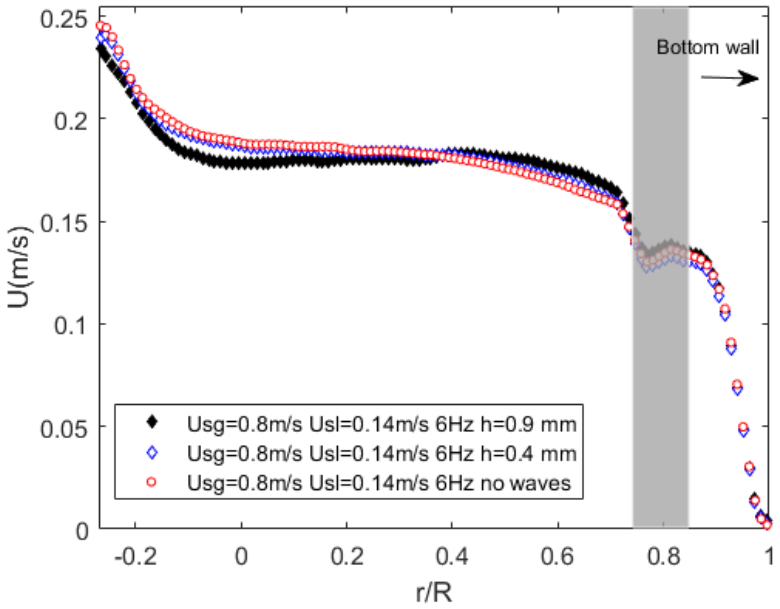

Figure 52 – Liquid layer velocity profile for U_{sg} = 0.8 m/s and U_{sl}= 0.14 m/s generated by a 6 Hz wave with two different amplitudes.

According to Figure 52 a significant distortion of the mean flow profile can be observed for the case with wave amplitude of 0.9 mm. In order to quantify the flow distortions, root mean square deviations from the case without excitation of waves were calculated. These distortions are represented here by the parameter S, which is given by equation (7.5). In the equation, U_{ref} represents the mean velocity profile of the case without wave. U_w, is the mean velocity profile

measured in the presence of excited waves, and N, is the number of valid measured points within the water layer. The mean velocity profile is calculated in one axial position of the image. According to the equation (7.5), higher values of S are related with higher wave nonlinearity.

$$S_{rms} = \frac{1}{N}\sum\sqrt{\left(\frac{U_w}{U_{ref}} - 1\right)^2} \tag{7.5}$$

The parameter S was calculated for the measured profiles and plotted in Figure 53 to Figure 55 against the nonlinearity parameters described in the beginning this chapter.

According to Figure 53, the mean flow distortions observed at different wave amplitudes and water depths show a remarkable scattering when plotted against the Ursell number. This suggests that Ursell number is a not good scaling for wave nonlinearity. This was somehow expected because the ratio between wavelength to water depth in the present pipe experiments were not within the range of shallow water waves (Dean R. and Dalrymple R, 1991).

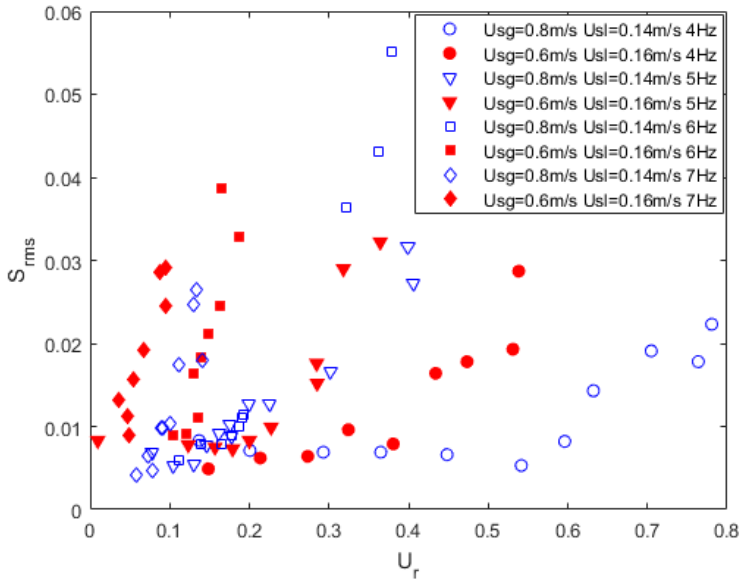

Figure 53 – Variation of mean flow distortion with Ursell number.

Figure 54 show less data scattering when compared to Figure 53. This suggest a better scaling with wave nonlinearity effects when employing the Beiji parameter. Results show that higher distortions are observed for higher values of the parameter B.

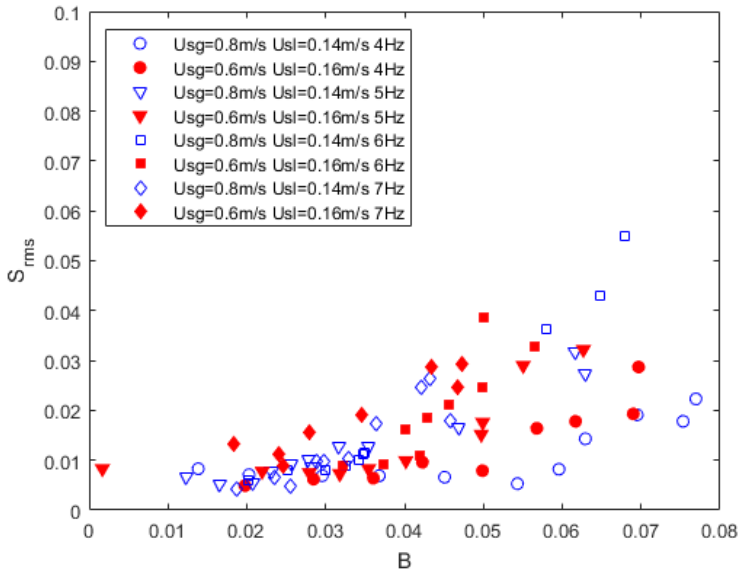

Figure 54 – Variation of mean flow distortion with Beji parameter

The variation of the mean flow distortion with Kirby dimensionless number, is depicted in Figure 55. Results show considerably less scattering in comparison to U_r and B. This suggest a better scaling of K parameter with wave induced nonlinearity. According to Figure 55 the parameter S, is rather weak for a range of K numbers lower than approximately 0.03. The area limited by $K < 0.03$ is shaded in the figure for reference. For values of K higher than 0.03 there is a clear tendency of stronger mean flow distortions for increasingly higher K values.

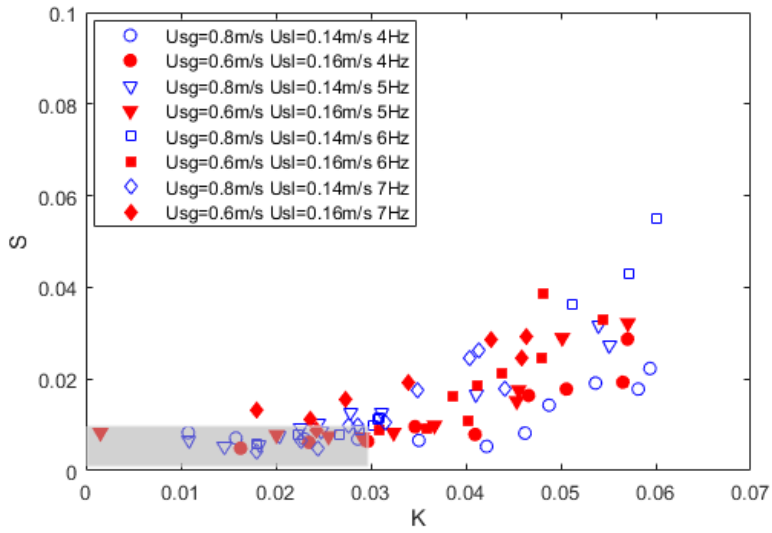

Figure 55 – Variation of mean flow distortion with Kirby parameter.

7.2.3

Generation of wave harmonics

The spectra content of interfacial disturbances was also analyzed. The idea here is to observe any evidence of wave-wave interaction, which are typical from nonlinear regimes. Figure 56 illustrates a typical wave spectra observed for the lowest and the higher amplitude of excited waves.

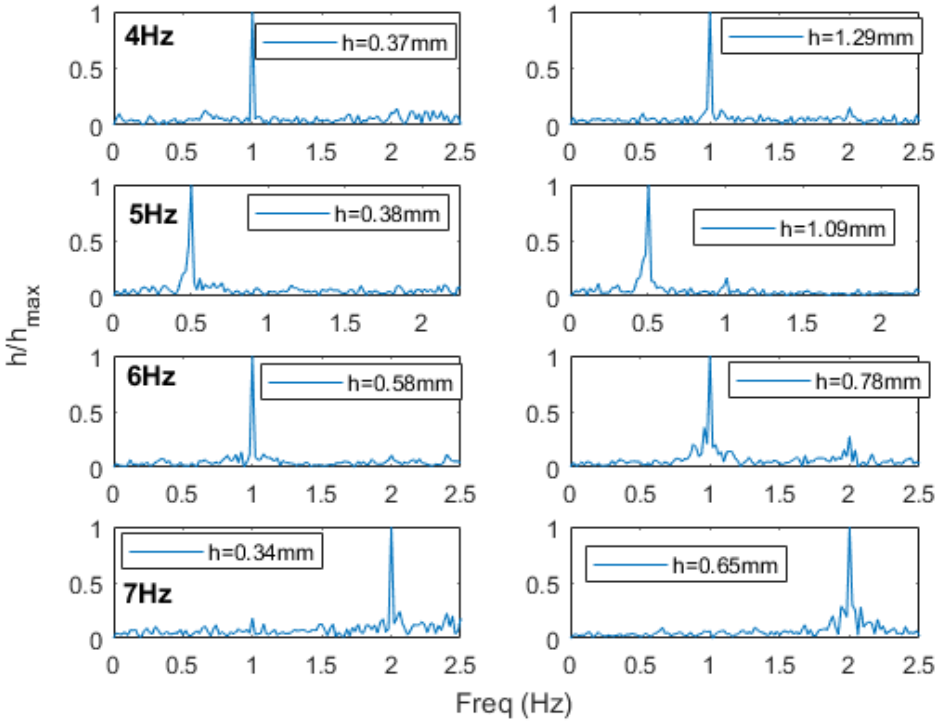

Figure 56 - Wave spectra for two different wave amplitudes. Lower amplitude (left). Higher amplitude (right). Waves generated at 4, 5, 6 and 7 Hz for U_{sg} = 0.6 m/s and U_{sl} = 0.16 m/s.

In case of waves excited with high amplitude, the appearance of harmonics or subharmonics can be observed in the spectra of Figure 56. The amplitude ratio between excited waves (h) and its harmonics (h_{h0}) was analyzed in Figure 57, for different values of K. The reference case (h_{h0}/h_0) corresponds to the case with lowest Kirby number. Thus, the curves of Figure 57 represent the variation of the amplitude ratio with respect to this reference case. Amplitudes of harmonic and fundamental waves were taken directly from measured spectra of interfacial oscillations. The figure resumes, into a single plot, the results obtained for all investigated cases.

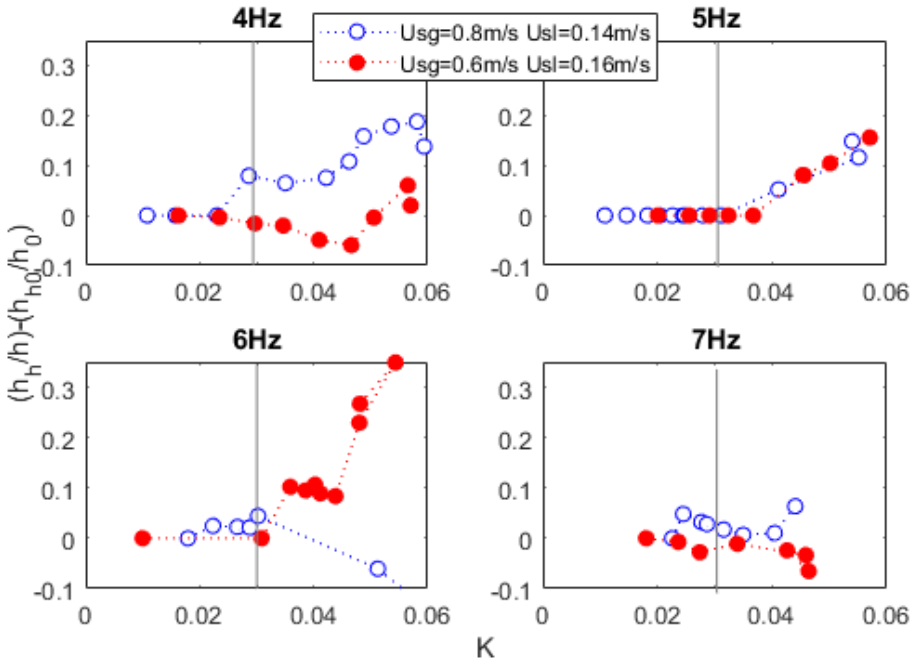

Figure 57 - Ratio between harmonic and fundamental wave amplitudes for different disturbance conditions.

According to Figure 57 the ratio of harmonic to fundamental wave do not show a remarkable difference for Kirby numbers lower than, approximately, 0.03. Some cases present a low level of harmonics even at Kirby numbers above the threshold. Nevertheless, in all cases no abrupt appearance of harmonics is observed for Kirby numbers below, approximately, 0.03. The results corroborate the conclusions drawn from the analysis of mean flow distortions.

The analysis presented in this chapter suggests that the parameter proposed in the work of Kirby (1998), within the framework of ocean waves, might be useful to define a nonlinearity threshold criterion for the evolution of waves in stratified flows. Based on these findings, this amplitude threshold was estimated to be around Kirby numbers of 0.03, as suggested by Equation (7.6). Further support for this threshold of nonlinearity is provided in Chapter 9.

$$h_w < 0.03 \frac{\tanh(k\bar{h}_L)}{k} \tag{7.6}$$

In the present work, the condition of Equation (7.6) was always satisfied in experiments related to linear wave regime. This was important because the parameters can change significantly with wave frequency and liquid level. In addition, it is important to excite waves with amplitudes as high as possible in order to improve the quality of measured velocity fields with PIV.

8
Velocity measurements in gas and liquid layers

The synchronization of all devices enabled phase locked measurements of velocity fields, simultaneously, in liquid and gas layers. However, before the analysis of velocity fields it was necessary to assess the methodology adopted. This validation is important to ensure the high quality of the data obtained for further comparison with theoretical models and numerical simulations. Afterwards, a detailed characterization of velocity fields in the gas and liquid layers is provided for different flow and disturbance conditions.

8.1
Assessment of experimental methodology

This section reports on the validation of the methodologies employed. To this end, experimental results were compared against a benchmark from the literature. Details about these validation tests are given in the next sections.

8.1.1
Validation experiments – Single phase flow

Particle Image Velocimetry (PIV) measurements were performed using an off-axis arrangement that was previously described in Section 3.3.3. To validate the methodology, a few measurements were carried out in single phase flow and the results were compared against a benchmark from the literature. The numerical results from the DNS simulations provided by Wu X. and Moin P. (2008) were used as a benchmark. Tests were performed in fully turbulent gas and liquid single phase flows with Re = 7000 and Re = 15000, respectively.

Polyamide particles of 50 μm in diameter were selected as tracers for PIV measurements in water. For the PIV measurements in air, a fog machine was employed (Luz de Prata®, model LP400). This fog machine vaporizes a solution of glycol and water to produce an aerosol of small particles (1-3 microns). For this test, the ultrasonic humidifiers were not used because they did not provide enough amount of particles to seed the gas flow at the desired high speeds. Due to the unsteady particle generation of the fog machine, it was necessary to fill a

reservoir with particles before the measurements. This reservoir consisted of an air-tight gallon with a capacity of 50 liters. The manometric pressure inside the gallon was adjusted to less than one bar using a pressure regulation valve. The flow rate of compressed air injected into the reservoir was adjusted with a valve and measured with a rotameter Omega® (model D6563).

PIV measurements in liquid and gas were performed and velocity statistics were estimated according to a dataset of 1000 image pairs. The sampling frequency adopted for image acquisitions was equal to 5 Hz. The time delay between two consecutive image acquisitions were 2500 μs and 300 μs, respectively for measurements in liquid and gas cases. These time delays provided particle displacements of approximately 10 pixels. The velocity field was estimated with a multi-pass PIV algorithm. The initial interrogation window size was 64 X 64 pixels and the final one was 32 X 32 pixels. The overlap was constant and equal to 75%.

The initial field of view was 2.5 D in length and 1.1 D in height. However, due to strong light reflections in images of the gas phase, it was necessary to reduce this field of view to about 0.5 D. Nevertheless, this was enough to allow for comparisons of experimental results against DNS calculations.

Figure 58(a) and Figure 58(d) present mean velocity profiles normalized by the maximum velocity, (U_b) for the gas and liquid phases, respectively. The normalized radial position (r/R) is -1, at the top wall, and 1, at the bottom one. The streamwise and wall normal RMS profiles, u' and v', are normalized by their maximum absolute values. Figure 58(b) and Figure 58(c) display the turbulence profiles of the gas-phase, whilst Figure 58(e) and Figure 58(f) show the turbulence profiles for the liquid-phase.

All results of Figure 58 were plotted against results from Direct Numerical Simulation (DNS) of the Navier-Stokes equations at Reynolds number equal to 2.4 x 10^4. The simulations are reported in the work of Wu X. and Moin P. (2008) and the corresponding data is available online.

According to Figure 58, first and second statistical moments were in good agreement with DNS simulations for both, liquid and gas experiments. According to Figure 58(f), the intensity of v' in the central region of the pipe exceeded the DNS prediction. These small discrepancies are believed to be related to the PIV uncertainty, since the fluctuations in the wall normal direction are considerably smaller than those in the streamwise direction. Nevertheless, results presented in Figure 58 were considered satisfactory for validation of the methodology employed in the present work.

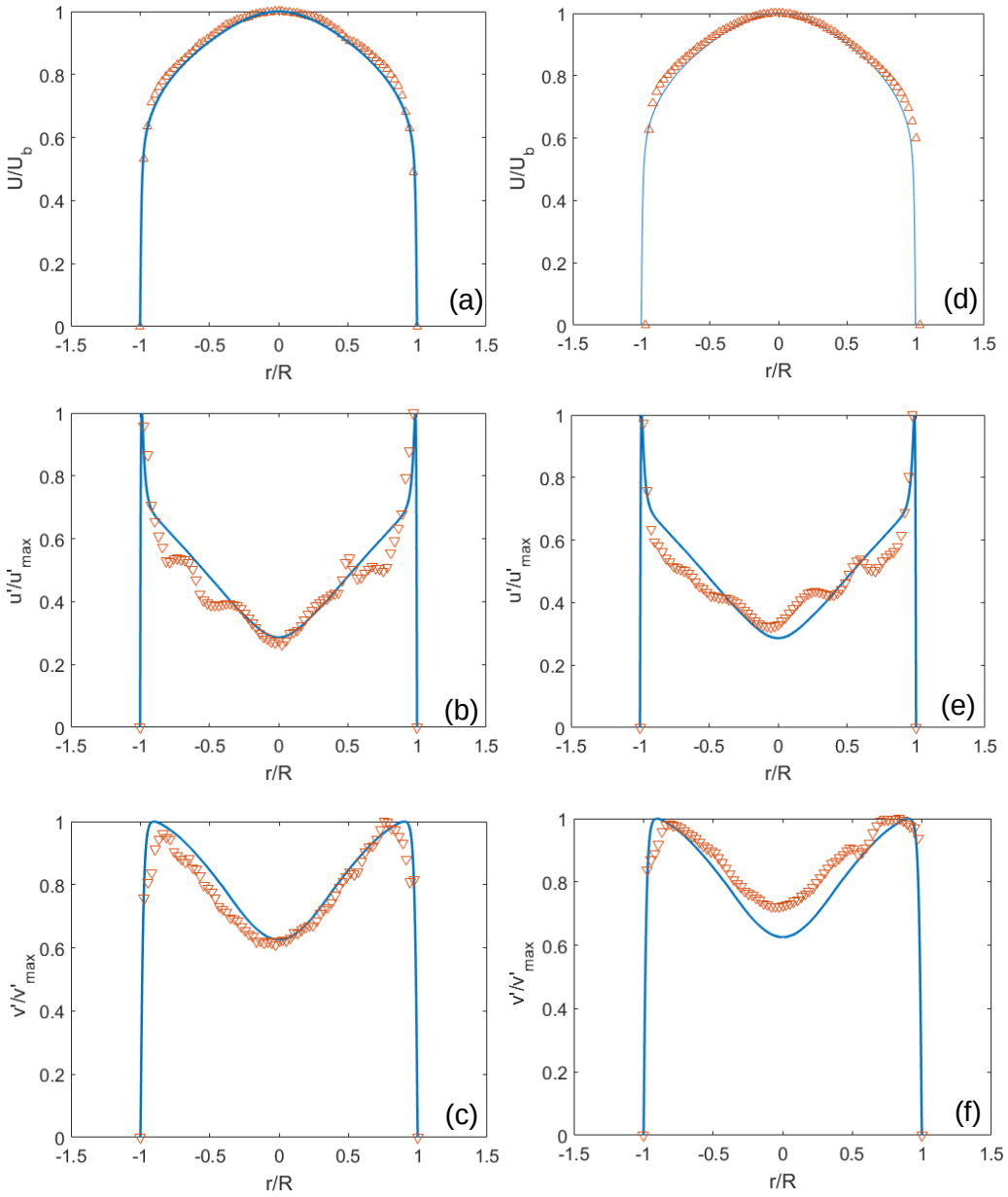

Figure 58 –Velocity profiles measured for single phase flows. Comparison of PIV data against DNS from Wu and Moin (2008). Gas flow at Re = 7000: (a) Mean velocity profile (b) Streamwise turbulence profile.(c) Wall normal turbulence profile. Liquid flow at Re=15000: (d) Mean velocity profile (e) Streamwise turbulence profile (f) Wall normal turbulence profile.

8.1.2

Optimization of PIV parameters for measurements in two-phase flow

The accuracy of PIV measurements is affected by several parameters such as particle displacement and gradients, sub-pixel peak fitting algorithm, particle diameter, concentration, illumination intensity, window interrogation size, background noise, out-of-plane particle displacement, among others. According to Raffel et al. (2007), the time lapse between successive light pulses affect many

of those parameters and therefore is one of most relevant settings to be optimized in PIV measurements. The time lapse should allow the particle displacement to be as large as possible in order to minimize the influence of noise inherent to the image correlation procedure. Conversely, long time lapses imply in large displacements that can exceed by far the extension of the interrogation windows. In this case a weak image correlation is expected. Thus, it is clear that the time lapse must be chosen to provide a good compromise between two sources of error.

There is an additional constraint for simultaneous PIV measurements in gas and liquid with a single illumination source. In this case, the optimization should allow a suitable resolution of the displacement in both phases. Depending on the liquid and gas superficial velocities, a proper time lapse for capturing particle displacements within an acceptable accuracy might not exist. Therefore, it was necessary to verify the feasibility of using a single light source for the proposed measurements.

For testing the PIV conditions, the time lapse was varied from 150 to 350 μs and measured velocity statistics were analyzed. For this test, the liquid and the gas velocities were set to 0.14 m/s and 0.8 m/s, respectively. This corresponds to the case with highest difference of superficial velocities and represent the most challenging condition for the PIV measurements, within the range of flow rates covered in this work.

The PIV processing of gas images were performed with a multipass algorithm. Initial interrogation window size was set to 64 x 64 pixels with 75% overlap, and final window size was 32 x 32 pixels. For measurements in the liquid layer, a single pass algorithm was employed and the interrogation window size was set to 16 x 16 pixels, with an overlap of 75%. The resulting particle displacements and the number of vector outliers are summarized in Table 3 for different time lapses.

Table 3 – Mean particle displacement and number of vector outliers detected in the time delay optimization analysis.

Dt (µs)		% outliers	Dx (px)
150		No corrrelations	
200		12.4%	0.58
250	Liquid	8.7%	0.88
300		5.1%	0.96
350		3.6%	1.00
200		3.3%	5.38
250	Gas	4.0%	6.19
300		4.0%	6.55
350		No corrrelations	

Figure 59 depicts the measured profiles of mean velocity and turbulence intensity in the liquid phase for different values of the time delay between consecutive PIV images. Both quantities are normalized by the value at the liquid layer mid-height. According to these figures, similar profiles were obtained for pulse delays of 300 and 350 µs. In addition, the level of vector outliers was within an acceptable level.

Profiles measured in gas phase are shown in Figure 60. They present no correlation for time a lapse of 350 µs, but for a time lapse of 300µs the number of outliers was acceptable. Thus, acceptable results were obtained only within a narrow range of time lapses centered around 300µs. Nevertheless, the test showed that it is possible to use a single light source for simultaneous PIV measurements in gas and liquid layers. This is valid only for the range of flow conditions covered in this work. For higher velocity differences an acceptable condition for PIV measurements in both phases might not exist.

It is important to mention that a small region in images in the gas phase did always show strong wall reflections. This region was masked for PIV analysis and, from here on, a gray colored rectangle is superposed to the graphics in order to represent this mask. The location of the reflection changes with the mean liquid height. Therefore, the mask is not located at the same wall normal distance in all figures.

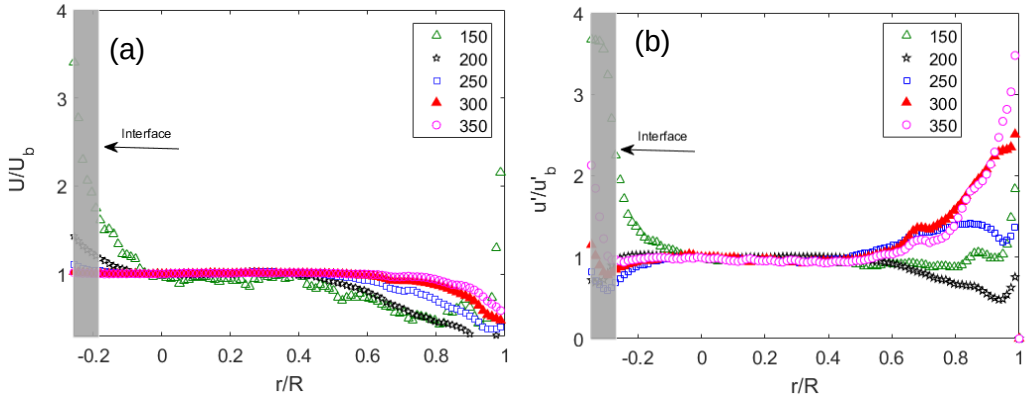

Figure 59 – Influence of the time delay between PIV images on velocity profiles in the liquid layer. Velocities normalized by the value at the liquid layer mid-height. (a) Mean velocity profiles. (b) Intensity of streamwise velocity fluctuations. Flow conditions: U_{sg} = 0.8 m/s and U_{sl} = 0.14 m/s. X/D = 62.

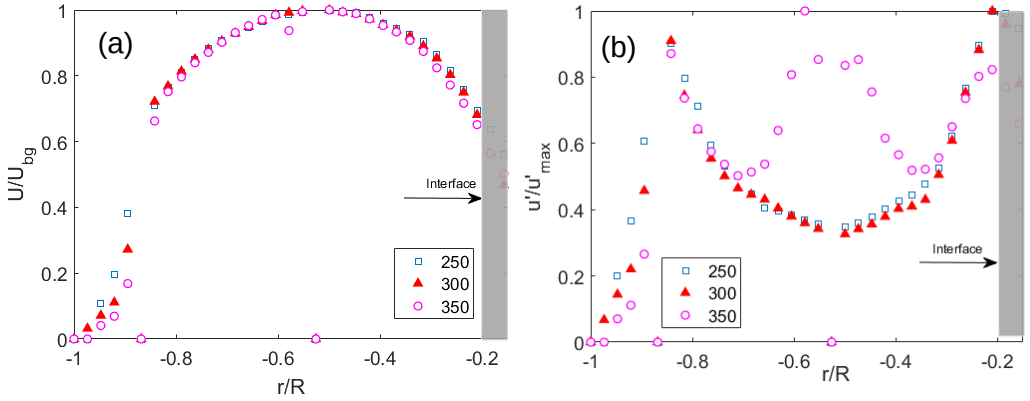

Figure 60 – Influence of time delay between PIV images on velocity profiles in the gas layer. Velocities normalized by the value at the gas layer mid-height. (a) Mean velocity profiles. (b) Intensity of streamwise velocity fluctuations. Flow conditions: U_{sg} = 0.8 m/s and U_{sl} = 0.14 m/s. X/D = 62.

8.1.3

Data convergence

An optimization of the number of acquisitions is important to shorten the time of experimental campaigns and the amount of stored data. For instance, 1000 image pairs in gas and liquid demand more than 60 Gbytes of memory and require about 1h and 30min of measurements. In addition, an optimization of datasets might contribute to improve the results, due to the expected variations in flow conditions during long test campaigns. This is especially important for a quantitative comparison between experiments performed under different test conditions.

For this test, a large set of image pairs was acquired, and the data convergence within the series of image pairs was analyzed. The same flow condition used in the previous section was kept for this analysis (U_{sg} = 0.8 m/s

and U_{sl} = 0.14 m/s). The cameras were also kept at the furthest downstream measured station (X/D = 62). Linear waves ($K < 0.03$) with a frequency of 4 Hz were introduced at the interface. Mean flow, turbulence and wave induced fluctuation profiles were analyzed and results obtained for 500 to 3000 image pairs were compared in Figure 61.

The profiles presented in Figure 61(a), (b) and (c) show a rapid convergence with the number of image pairs. According to these figures, only 500 image pairs would be enough for data convergence. However, wave induced disturbances, which are depicted in Figure 61(d) and (e), apparently require a higher number of samples for convergence. The most critical one is the wave induced wall normal fluctuation. For this component, the amplitude of the peak near the interface seems to converge only for a dataset of 1500 samples. Thus, all subsequent results presented in this thesis were obtained from datasets formed from 1500 image pairs.

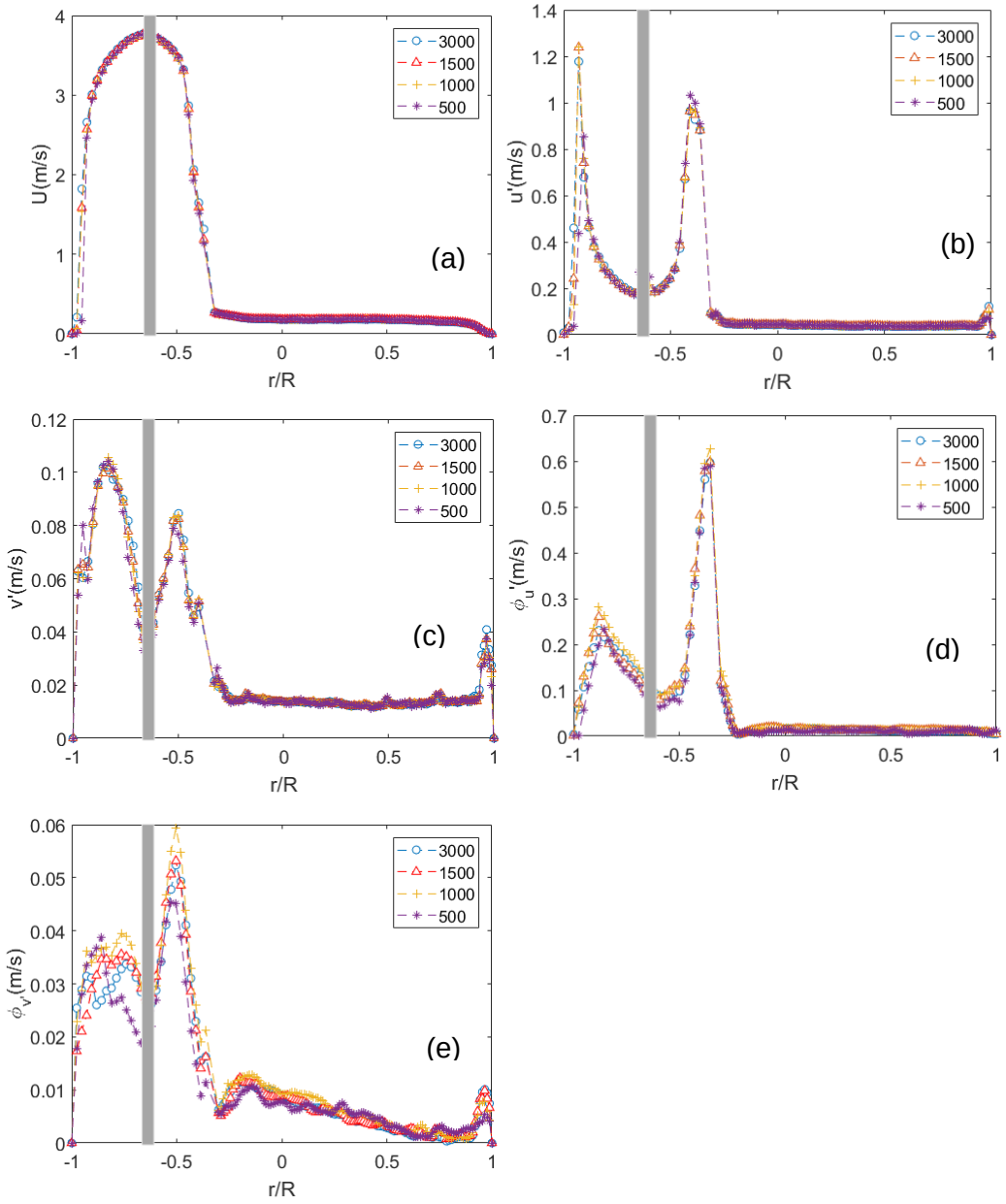

Figure 61 – Data convergence test. (a) Mean velocity profile. (b) Intensity of streamwise velocity fluctuation (c) Intensity of wall normall velocity fluctuation (d) Wave induced streamwise fluctuations. (e) Wave induced wall normal fluctuations. Flow conditions: U_{sg} = 0.8 m/s and U_{sl} = 0.14 m/s.
Wave frequency = 4 Hz. X/D = 62.

8.2

Analysis of velocity fields in gas and liquid — Linear wave regime

In this section, measured mean flow, turbulence and wave coherent velocity components are reported for different flow conditions. An overview of all cases investigated is summarized in Table 4. This table contains also the Reynolds number based on the hydraulic diameter of each phase and the corresponding superficial velocities. The liquid depth and hold up are also displayed. For a quick

reference in this manuscript, the flow conditions are named as cases 1 to 4, according to the Table 4.

Table 4 - Experimental flow conditions

	U_{SG} (m/s)	U_{SL} (m/s)	h_L (mm)	Re_L	Re_g	α_L
Case 1	0.6	0.14	35.48	10978	3068	0.76
Case 2	0.6	0.16	37.62	11974	3297	0.81
Case 3	0.8	0.14	34.56	11162	4021	0.74
Case 4	0.8	0.16	35.74	12469	4127	0.77

8.2.1

Mean velocity profile analysis

According to the review presented in Chapter 2, the stability analysis of two phase flows is usually performed using 1-D models. These models demand geometrical and closure relations for solvability of the conservation equations. However, for a 1-D instability analysis based on Orr-Sommerfeld equations a base flow profile is required. The analytical solution for a laminar and steady stratified flow in a 2-D channel can be easily obtained (Kaffel and Riaz, 2015 and Barmak et al., 2016). However, there is no consensus in the literature about a model for turbulent flows, which can be used to predict the base flow profile for a variety of conditions.

The work of Biberg (2007) proposed an algebraic-logarithmic model for a stratified turbulent flow. The model is based on two layers of wall bounded single phase flows. Interfacial boundary conditions are used to couple solutions obtained for each phase. Thereby, it can provide the cross sectional velocity distribution of the flow and yields mechanistic expressions for wall and interfacial shear stresses. However, this model still demands an extensive validation against experimental results.

More recently, Chinello et al. (2018) used CFD simulations to compare numerical simulations against experimental results from the works of Ayati et al. (2015 and 2016) and Birvalski et al. (2016). Chinello et al. (2018) reported that numerical simulations were not in agreement with the experimental data. They concluded that turbulence models adopted in the simulations were not capable to reproduce the flow dynamics of wavy stratified gas-liquid flows, and highlighted the importance of turbulence modelling to resolve the interface. According to those authors, the quantification of pressure drop induced by waves might be useful to improve existing models.

In order to address this problem, mean flow velocity profiles in the liquid and gas layers were measured and results from experiments are reported here for cases with and without excitation of linear waves.

8.2.1.1

Adherence to base flow models

First, it was analyzed the adherence of measured velocity profiles to standard base flow models developed for turbulent flows in pipes.

8.2.1.1.1

Velocity profiles in the liquid phase

Mean velocity profiles were analyzed within the liquid layer for test conditions listed in Table 4. Experimental results are depicted in Figure 62(a) and (b). In Figure 62(a) values are shown in m/s whereas in Figure 62(b) the profiles are normalized by the velocity at half of the liquid height. These figures show profiles with a S-shaped velocity distribution. This S-shaped profiles within the liquid layer of stratified two-phase flow have been reported in many works from the literature using different techniques, such as LDV, PIV and conductance probes (Fernandino and Ytrehus 2008, Ayati et al. 2015, Birvalski et al. 2016). Those findings are qualitatively in agreement with the current observations. This typical feature of velocity distribution results from the shear at the interface due to high velocities.

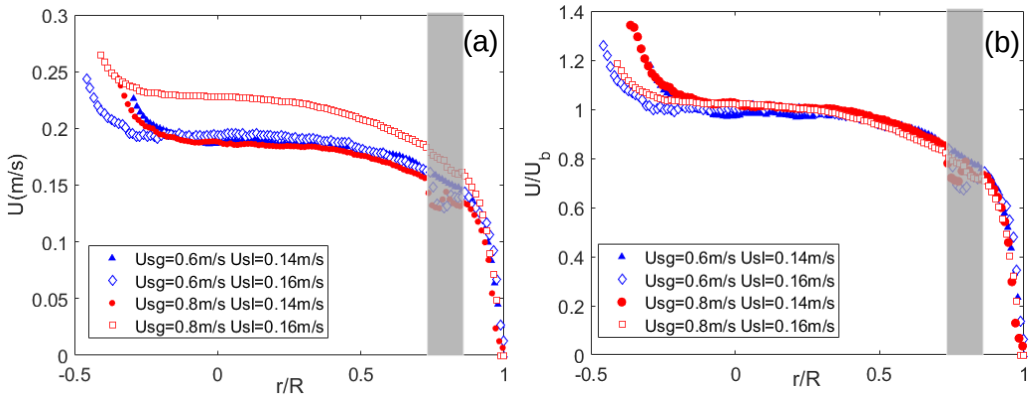

Figure 62 – (a) Mean velocity profile of the liquid phase. (b) Mean velocity profile of the liquid phase normalized by the bulk velocity.

According to Figure 62(b) the mean flow profiles have a similar distribution near the wall. This suggest a weak influence of interfacial effects on the wall

region. Thus, it might be interesting to evaluate the adherence of experimental data near the wall with models developed for single phase flows.

Birvalski et al. (2015) investigated the velocity profile within the liquid layer using the classical log-law (see Hinze, 1975). Thus, one profile from Figure 62(a) was selected to be rescaled using wall shear velocity, U_τ, and plotted in terms of inner coordinates, $y^+$and U^+ (equations (8.1) and (8.2)). The profile selected corresponds to Case 3.

$$y^+ = \frac{yU_\tau}{\nu} \tag{8.1}$$

$$U^+ = \frac{U}{U_\tau} \tag{8.2}$$

The wall shear velocity was estimated from the measured pressure drop using the following relations:

$$U_\tau = \sqrt{\frac{\tau_w}{\rho}} \tag{8.3}$$

$$\tau_w = \frac{\Delta PD}{4L} \tag{8.4}$$

The mean flow profile measured within the liquid layer is shown in Figure 63, using inner coordinates. Results are compared against the log-law profile. Standard von Kármán coefficients for turbulent pipe flows with smooth walls were used to compute the log-law profile. The coefficients used to plot this log-law were, k = 0.41 and C = 5. According to Figure 63, excellent agreement can be found near the wall up to y^+ values around 150. Above this value, the flow deviates significantly from the logarithmic profile due to influence of interfacial effects.

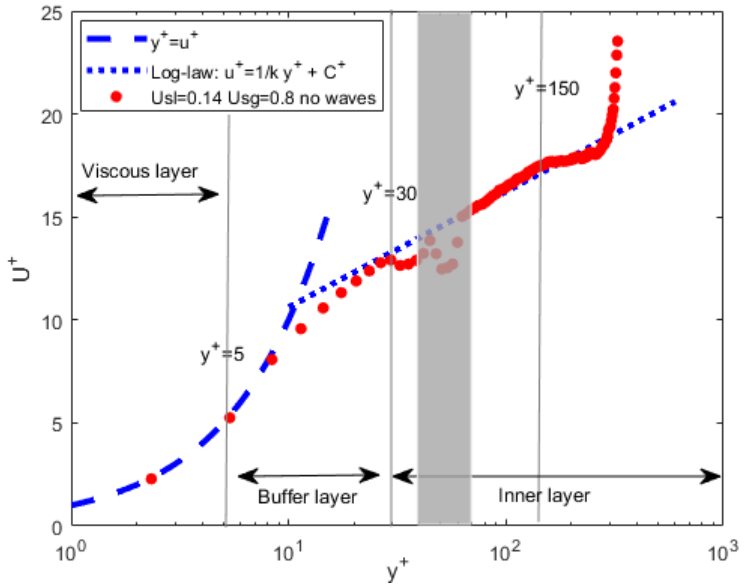

Figure 63 – Mean streamwise velocity profiles in inner coordinates. Von Karman´s constant k = 0.41 and C = 5. Measurements conditions of Case 3 (U_{sg} = 0.8 m/s and U_{sl} = 0.14 m/s).

8.2.1.1.2

Velocity profile in the gas phase

Mean velocity profiles in the gas phase are shown in Figure 64(a), for all cases of Table 4. The profiles were normalized by their maxima. All results presented in this figure were measured without excitation of waves. A dimensionless coordinate (h_g/H_g) was used to plot the results, using as a reference the positions of the top wall and of the gas-liquid interface. This is interesting for a proper comparison of results, because the liquid heights change according to the case investigated. The variable H_g represents half of the total height of the gas layer ($2 * H_g = D - \overline{h_L}$). The coordinate h_g varies from -H_g, at the top wall, to H_g, at the interface. The interface location was detected experimentally by digital image processing (for a complete description, see Chapter 5). To enhance the clarity of Figure 64(a), it was chosen not to display the gray colored rectangles, which represent the image mask at the reflection area.

The curves in Figure 64(a) are coincident close to the top wall ($h_g/H_g = -1$). This suggests a weak influence of interfacial phenomena on the near wall turbulence. Close to the interface the profiles display remarkable differences. In the work of Birvalski et al. (2016) similar observations are reported. Thus, it might be interesting to verify the adherence of profiles at the top wall to base flow models.

Figure 64(b) illustrates only the velocity profile of Case 3, for sake of clearness, because it was already observed that all cases perform similarly close to the wall. In this figure the log-law with k = 0.41 and C_2= 2.7 is also shown. Results show a fair agreement between experimental data and the log-law profile at the top wall region. Thus, the boundary layer near the top wall does not differ substantially from a single-phase flow boundary layer. Birvalski et al. (2016) also report a reasonable agreement between the mean velocity profiles in the gas-phase with a log-law profile. Near the interface significant discrepancies are found and standard models do not capture the characteristics of the mean flow in this region. This subject demands additional studies.

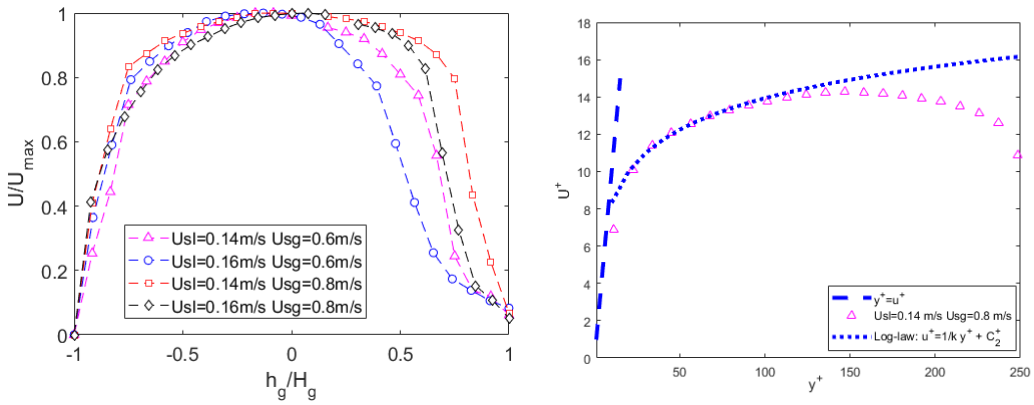

Figure 64 – (a) Mean velocity profiles with the radial coordinate scaled by height of the gas layer. (b) Mean streamwise velocity profiles in inner coordinates. Von Karman´s constant k = 0.41 and C_2 = 2.7. Measurements conditions of Case 3 (U_{sg} = 0.8 m/s and U_{sl} = 0.14 m/s).

8.2.1.2

Simultaneous two phase measurements – velocity profiles at the interface

The velocity profiles in the liquid and gas phases just presented were obtained in distinct experiments for each phase. This was done to obtain the best quality profiles that our setup could provide for each phase, resulting from an optimization of the experimental parameters for liquid and gas phases. However, simultaneous measurements of the velocity profiles in both phases can provide valuable information on the behavior of the velocity across the interface region.

Mean velocity profiles measured simultaneously in both phases are shown in Figure 65(a) and (b). These profiles were obtained without excitation of controlled waves. The figures represent the same data, but in Figure 65(a) velocities were displayed in m/s, while in Figure 65(b) velocities are normalized

by their maxima. Results are reported for all tested cases. The results indicate that gas velocities are rather sensitive to variations of superficial liquid velocities. This is clearly observable by comparing cases with the same gas velocity. This behavior is linked to variations of liquid hold up, which reduces the area occupied by the gas within the pipe cross section. The profiles do show qualitative similarities with results reported in the literature for a smooth stratified flow (Ayati et al., 2015). The normalized profiles show a clear discrepancy near the interface, which is not captured by standard engineering models.

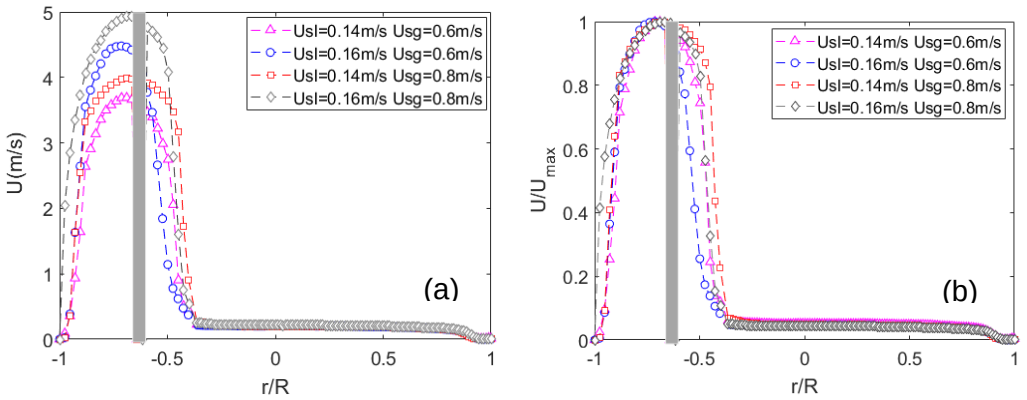

Figure 65 – Simultaneous measurements of velocity profile in the gas and liquid phases. (a) Mean velocity profile. (b) Normalized mean velocity profile.

8.2.1.3

Influence of linear waves

Mean velocity profiles were measured with and without excitation of controlled disturbances, and are shown in Figure 66. Waves of different frequencies were introduced, and measurements were compared for the same flow rates. The profiles of Figure 66 were normalized by their maximum velocities.

According to Figure 66 the introduction of disturbances did not modify the mean flow in gas and liquid phases. This behavior was expected since waves were excited with amplitudes lower than the threshold of Kirby numbers suggested in Chapter 7.

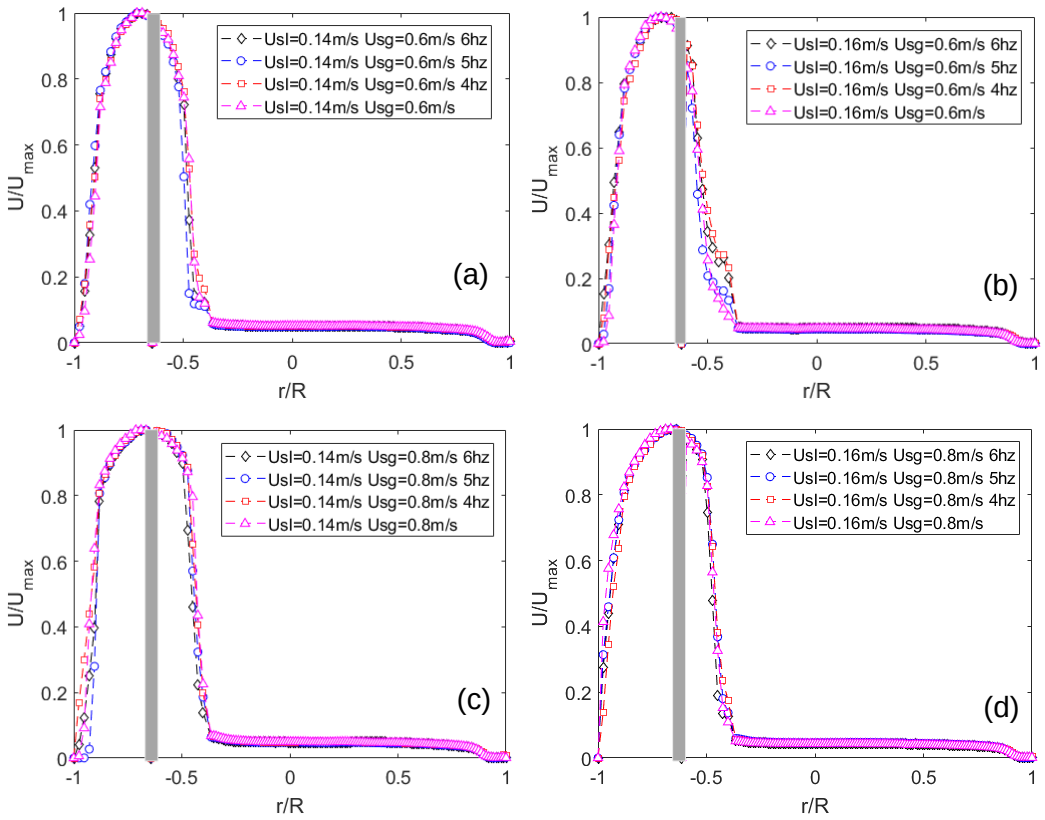

Figure 66 – Mean dimensionless streamwise velocity profiles, y measured in the presence of linear waves at 4, 5 and 6 Hz. (a) Case 1 (U_{sg} = 0.6 m/s and U_{sl} = 0.14 m/s). (b) Case 2 (U_{sg} = 0.6 m/s and U_{sl} = 0.16 m/s). (c) Case 3 (U_{sg} = 0.8 m/s and U_{sl} = 0.14 m/s). (d) Case 4 (U_{sg} = 0.8 m/s and U_{sl} = 0.16 m/s).

It is worth mentioning that a quantitative comparison between cases was performed for campaigns carried out within the same day. This procedure was adopted to reduce data scattering due to small variations of test conditions. Therefore, many tests were replicated in order to provide the best conditions for a comparative analysis. Even so, small variations might have occurred since a single test condition, corresponding to one flow rate and one wave frequency, lasted for about two hours. Within the period of a campaign composed of several tests, particles could accumulate in the liquid reservoir and/or tracer water droplets could condensate at the pipe wall. This is conjectured as a plausible explanation for the variations observed near the interface in Figure 66(b).

8.2.2

Turbulence intensity

The distribution of turbulence intensity in the pipe cross section provides an important information regarding the transport of momentum between the phases in stratified two-phase flows. However, detailed measurements of turbulence

distribution near the interface of two phase flows is a challenging task due to optical constrains. Therefore, successful measurements of this quantity were only recently reported in the literature (Ayati et. al. 2014, 2015, 2017; Birvalski et al. 2016). In those works, the turbulence was modified spontaneously by modifications of flow conditions. The present work does also contribute for a characterization of turbulence distribution in stratified flows, but in a scenario of controlled flow disturbances.

Figure 67 illustrates dimensional and dimensionless profiles of streamwise turbulence intensity. All cases represented in Figure 67 were measured without the presence of excited waves. The profiles display higher intensities near the walls and close to the interface. Under conditions of Cases 1, 2 and 3, the intensity peak near the top wall is larger than that close to the interface. The profile obtained for Case 4 indicates the opposite behavior. This change was also noticed in the works of Ayati et al. (2014 and 2015) in a comparative analysis between smooth stratified and wavy flow regimes. It is interesting to note that for the present conditions, Cases 1 to 3 correspond to smooth stratified regime, however, Case 4 is close to the transition threshold for wavy flow. Figure 67(c) displays dimensionless profile of Figure 67(a) in the liquid phase only, to have a clearer gasp of the liquid turbulence profile shape with the flow conditions variation.

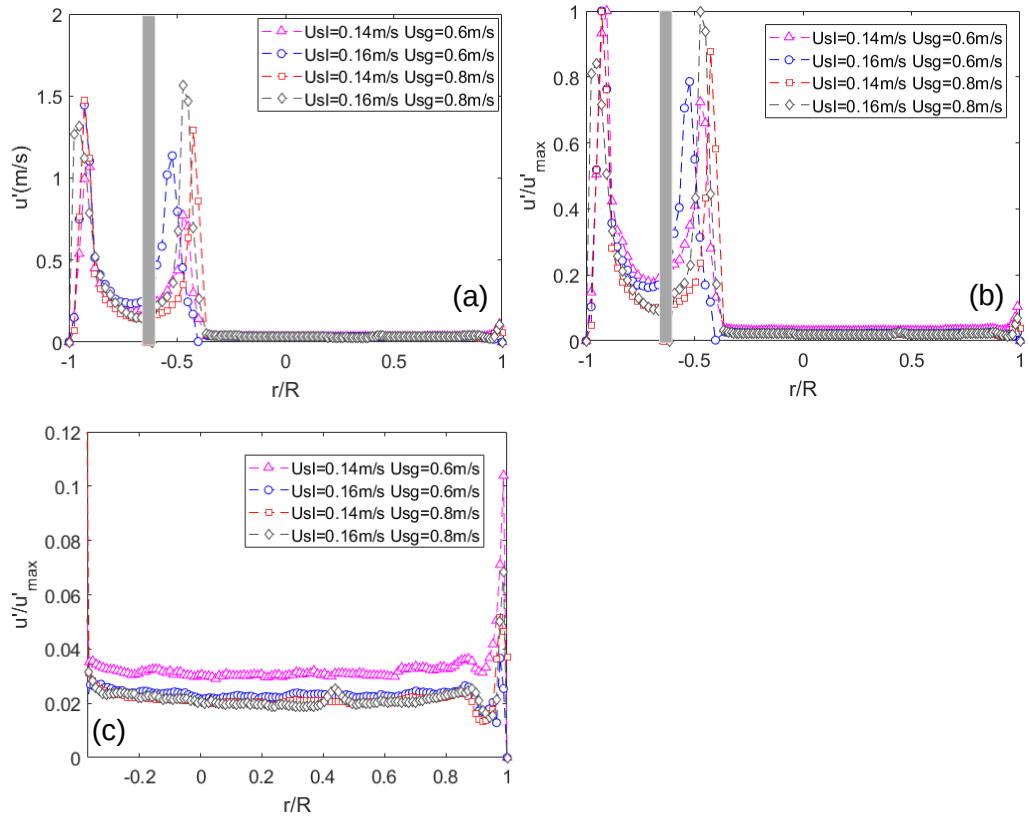

Figure 67 – (a) Streamwise velocity fluctuations profiles for all test cases. Streamwise velocity fluctuations profiles normalized by its maximum value: (b) for all test cases. (c) for all test cases (in liquid phase only).

Velocity fluctuations in the wall normal direction were considerably lower than those observed for the streamwise direction. Due to this fact, the profiles of wall normal turbulence display some scattering, especially close to the wall. For this reason, the velocity fluctuations in the wall normal direction were post processed by using a moving average filter with a width of 3 points. This procedure performs similarly to a low pass spatial filtering. The low-pass filtered profiles are depicted in Figure 68(a) and (b). According to the experimental results, the intensities of the wall normal fluctuations were highly sensitive to variations of gas flow Reynolds Number (Re_G). For a qualitative comparison of profile shapes, the fluctuations were normalized by its maximum and results are shown in Figure 68(b). According to this figure, the profiles in the gas phase resemble those measured for single phase flows. The works of Ayati et al. (2015) and Birvaslki et al. (2016) report similar results. This agreement with the literature provides additional validation of present methodology.

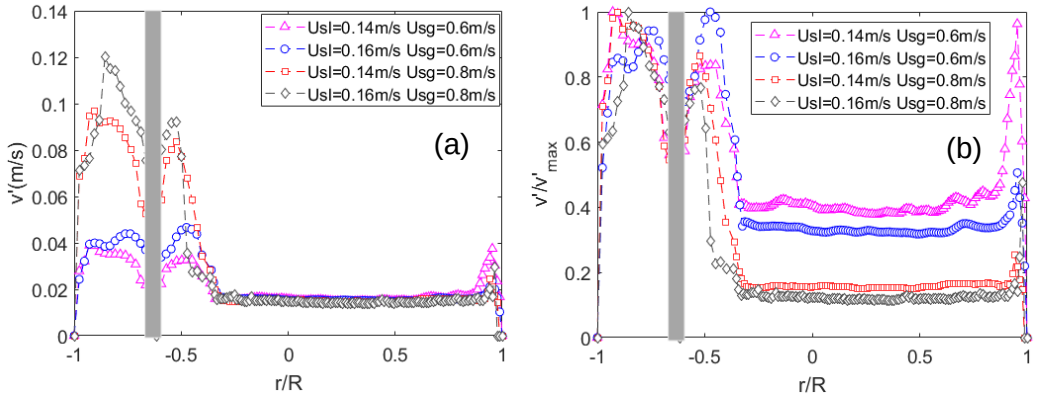

Figure 68 – (a) Wall velocity fluctuations profiles of all test cases. (b) Wall velocity fluctuations profiles normalized by its maximum value.

Turbulence intensity profiles were also measured in the presence of excited interfacial waves. Figure 69(a) displays dimensionless streamwise turbulence intensity profiles measured with the paddle oscillating at a constant frequency of 6 Hz. Results can be compared against those from Figure 67. No remarkable differences can be found in the profiles measured with and without excited waves. However, a quantitative comparison between results from Figure 67(b) and Figure 69(a) is difficult because the tests were not performed in the same day. Therefore, small discrepancies related to differences of the mean flow could be presented.

For a direct comparison of profiles, a test campaign was carried out for a fixed flow rate and for different excitation frequencies. Results are shown in Figure 69(b). Wave amplitudes were adjusted in order to keep K values lower than 0.03. . Figure 69(c) and (d) displays respectively the dimensionless profiles of Figure 69(a) and (b) in the liquid phase only, to have a clearer gasp of the liquid turbulence profile shape with the parameters variation.

Measured profiles emphasize that turbulence intensity was not changed by the presence of linear waves. Indeed, the waves were too small to interfere with the main flow structure. For instance, amplitudes of wave with 6 Hz were smaller than 0.7 mm at the measurement station.

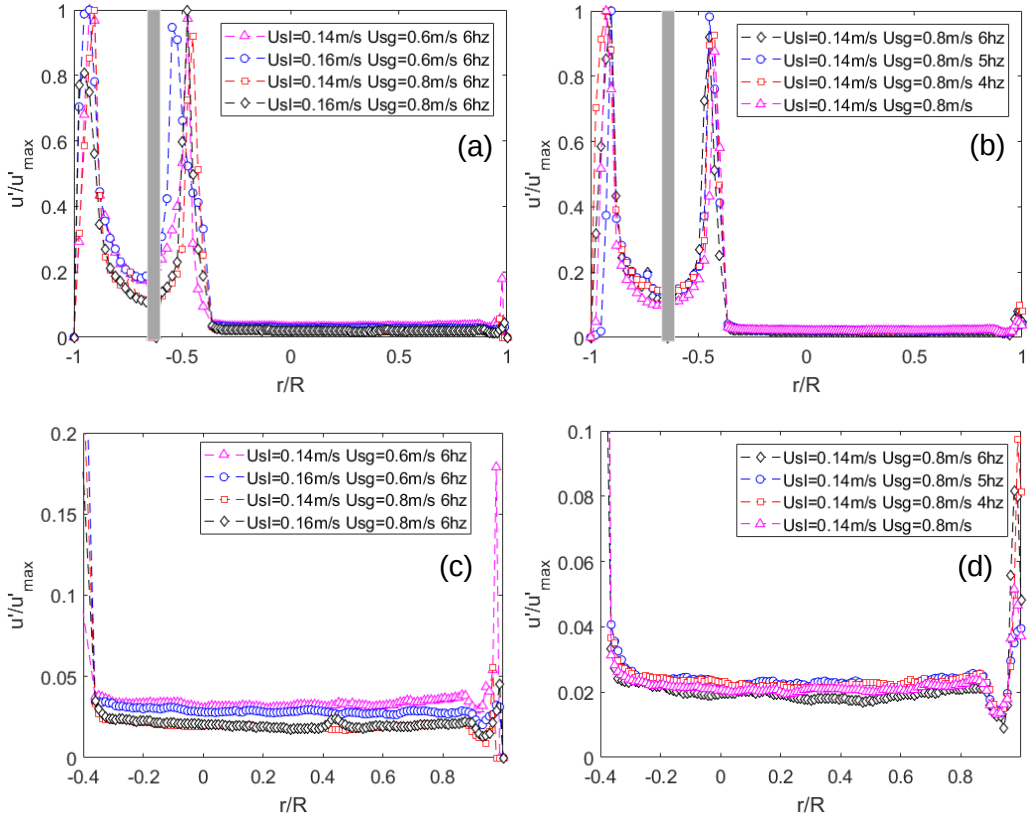

Figure 69 – Streamwise velocity fluctuations profiles adimensionalized by its maximum velocity measured in presence of linear waves at: (a) 6 Hz for all test cases. (b) 4, 5 and 6 Hz for Case 3 (U_{sg} = 0.8 m/s and $U_{s\,l}$= 0.14 m/s). (c) 6 Hz for all test cases (in liquid phase only). (d) 4, 5 and 6 Hz for Case 3 (in liquid phase only).

The wall normal velocity fluctuations are analyzed in Figure 70(a) and Figure 70(b). Profiles show a noticeable variation for different flow conditions (Figure 70a). However, profiles of cases with and without controlled waves were alike and display essentially the same picture for similar flow conditions (Figure 68b). However, for a quantitative evaluation of wave influence on the profiles, a test campaign was carried out with a fixed flow rate. Results presented in Figure 70(b) for different wave frequencies, show a very weak influence of excited waves on the turbulence intensities. This gives further support to the idea that waves were indeed within a linear regime.

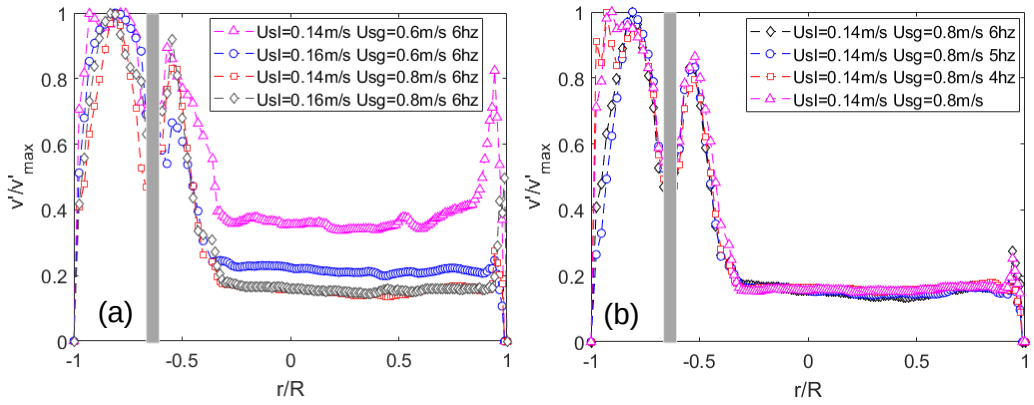

Figure 70 – (a) Wall normal velocity fluctuations profiles adimensionalized by its maximum velocity measured in presence of linear waves at 6 Hz for all test cases. (b) Wall normal velocity fluctuations profiles adimensionalized by its maximum velocity measured in presence of linear waves at 4, 5 and 6 Hz for Case 3 (U_{sg} = 0.8 m/s and U_{sl} = 0.14 m/s).

Some works in the literature associate the interface waviness with an equivalent roughness height to justify the higher turbulence intensities in this region. Fulgosi et al. (2003) performed DNS simulations to investigate the influence of interfacial waviness on the turbulence of stratified flows. That work attempted to model the wavy interface as a flexible solid surface. They observed a systematically higher turbulence intensity near wavy interfaces. Based on the simulations, Fulgosi et al. (2003) suggested that waves promote reduction of dissipation at the interface and do not affect, significantly, the production. However, no clear distinction between wave induced disturbances and turbulence was made. Next subsection is devoted to study wave induced disturbances and can contribute to this discussion.

8.2.3

Wave induced velocity fluctuations

One advantage of having phase-locked measurements with controlled excitation, is the capability to extract coherent information from apparently random signals. Thus, wave coherent parts of turbulence were analyzed separately in the present study. These results can contribute to clarify the relation between shear at the wall and the shear at the gas-liquid interface in the transition from stratified to slug flow. In addition, they might be useful for validation of models and simulation tools employed in engineering applications.

A comparison between profiles of wave induced streamwise velocity fluctuation against flow-induced velocity fluctuations is shown in Figure 71. Results were obtained for the test conditions described in Table 4. For this set of

measurements, the wave frequency was kept constant and equal to 6 Hz. As can be seen, the profiles of wave induced disturbances display a peak near the interface and small amplitudes at the top (r/R = -1) and bottom walls (r/R = 1). These findings suggest that the high turbulence intensity is mostly related to wall turbulence, whereas higher intensity at the interface is linked to interfacial disturbances. This complements the observations reported in Chapter 6 for the liquid layer.

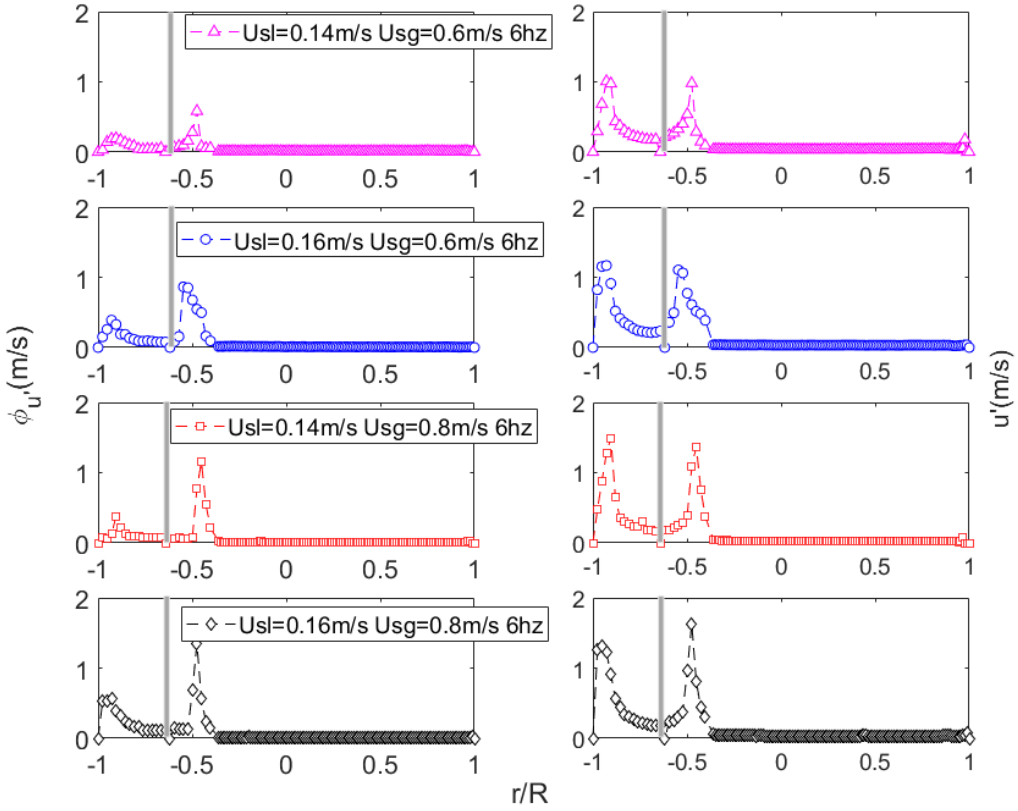

Figure 71 – Velocity fluctuations profiles (right) and wave induced velocity fluctuations profiles (left) for streamwise direction from Case 1 (top) to Case 4 (bottom) in presence of linear waves excited at 6 Hz.

Figure 72 displays the turbulence intensity profiles after subtracting the wave induced fluctuation. This corresponds to the random turbulence component (u^*) displayed in Equation (5.2). It is observed a high peak close to the top wall, which increases with the Reynolds number. At the interface the velocity fluctuations have nearly the same magnitude. This might be linked to the shear induced fluctuations. Close to the top wall, all profiles in the gas phase resemble those observed for single phase flows.

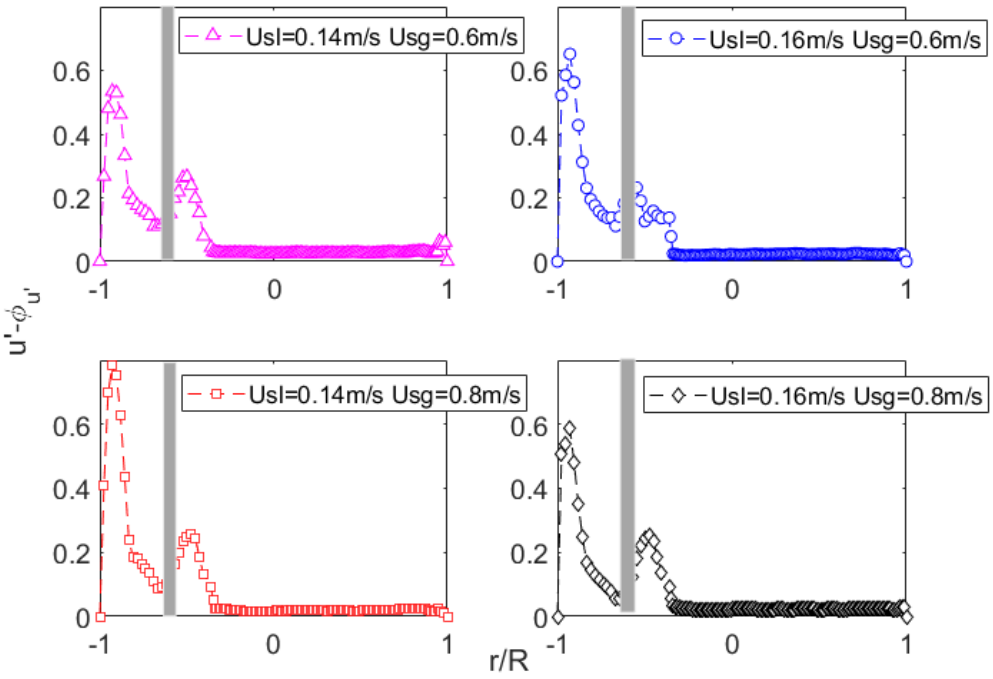

Figure 72 – Streamwise random turbulence for al test cases in presence of linear waves exited at 6 Hz. Case 1 (top left). Case 2(top right). Case 3 (bottom left). Case 3 (bottom right)

The influence of the waves on the turbulence of wavy flows was studied in the experimental work of Birvalski et al. (2014 and 2015). In that work, a planar conditional sampling technique was employed to extract the wave coherent fluctuation from the measured turbulent flow field. The analysis was applied to velocity fields measured in the liquid layer. A similar technique was employed recently in the works of Vollestad et al. (2019a, 2019b) to study coherent structures using PIV. The conditional sampling technique relies on a threshold criterion for detection of a given wave phase. Thereby, the velocity field could be decomposed into average, wave induced fluctuations and turbulence. The main drawback of this approach is the absence of control of the disturbance content. Thus, waves with different amplitudes and spectral content might be considered in the same estimation of wave coherent fluctuations.

Results reported in Birvalski et al. (2014 and 2015) indicate that the turbulence close to the wall has nearly no phase dependency on the turbulence. Observations reported in present thesis are in close agreement with their findings, even though wave amplitudes were considerably different. It is worth to mention that in the work of Birvalski the waves are rather nonlinear, according to the criteria proposed in Chapter 7.

Results for wall normal velocity fluctuations are illustrated in Figure 73. Profiles show a slightly higher amplitude of wave coherent fluctuations near the

interface. However, in this case the fluctuations are distributed towards the center of the gas layer. Near the top wall (r/R = -1), the wave coherent profile tends to zero. Again, this suggests a weak influence of waves on the disturbances near the wall. At the bottom wall, there is a peak in both coherent and RMS profiles. It is important to mention that in the liquid layer the fluctuations of v' are within the same order of magnitude as the resolution of the PIV technique. Therefore, even a weak light scattering can significantly reduce the signal to noise ratio, hence affecting the results. Thus, these peaks are considered as spurious noise.

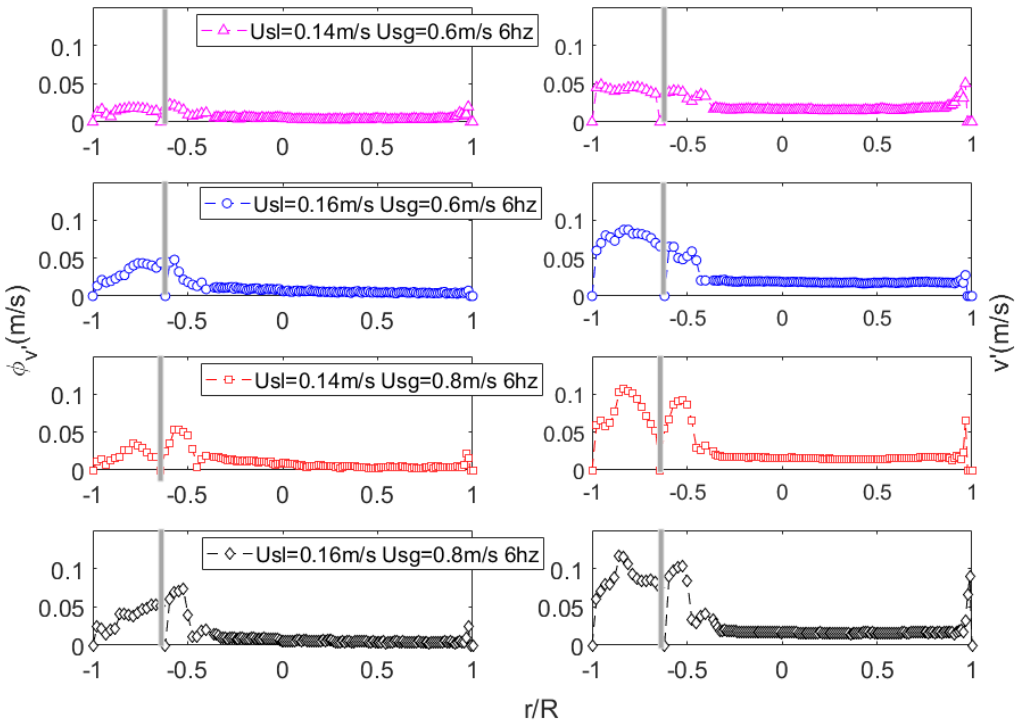

Figure 73 – Velocity fluctuations profiles (right) and wave induced velocity fluctuations profiles (left) for wall normal direction from Case 1 (top) to Case 4 (bottom) in presence of linear waves exited at 6 Hz.

Figure 74 displays profiles of random turbulence component in wall normal direction (v^*). Cases 2, 3 and 4 display a similar distribution, whilst Case 1 show a significant lower intensity. This case corresponds to the smallest Reynolds number. Thus it might be possible that v' and $\varphi_{v'}$ were estimated with a low signal to noise ratio and the remaining turbulence after subtraction was not well resolved. Nevertheless, most profiles resemble those observed near the wall for single phase flows.

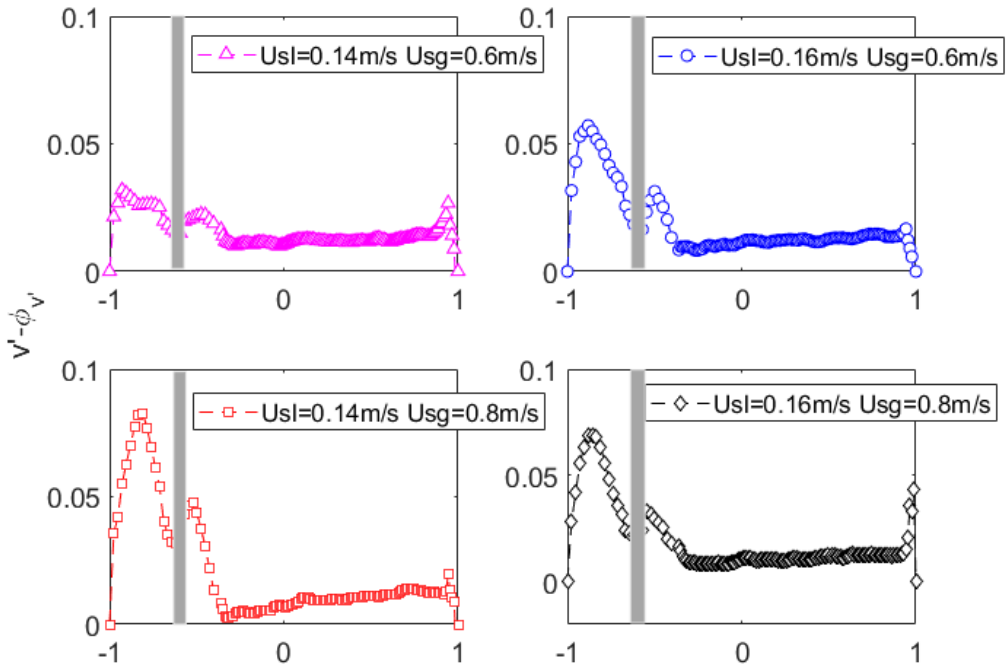

Figure 74 – Wall normal random turbulence for al test cases in presence of linear waves exited at 6 Hz. Case 1 (top left). Case 2 (top right). Case 3 (bottom left). Case 3 (bottom right)

Dimensionless profiles of wave induced disturbances are displayed in Figure 75 to Figure 78. Different flow velocities and wave frequencies are analyzed. For all cases tested, the waves were associated with streamwise velocity fluctuations very near the interface. The wave induced fluctuations of wall normal velocities were higher at the region close to the interface. However, the intensity was somehow spread into this region.

In general, the profiles of streamwise wave coherent fluctuations do not display remarkable differences within the conditions analyzed. In this case, wave frequencies have a weak influence on the general distribution of streamwise fluctuations. For wall normal disturbances the picture is somewhat different. Wave coherent fluctuations measured with different oscillation frequencies show some noticeable modifications. Thus, wall normal fluctuations would be more interesting for a proper validation of numerical simulations and models against experiments. In addition, the growth rates reported in Chapter 6 are even more sensitive to wave parameters and therefore would be used together with the wave induced velocity fluctuations profiles for accurate validation of models

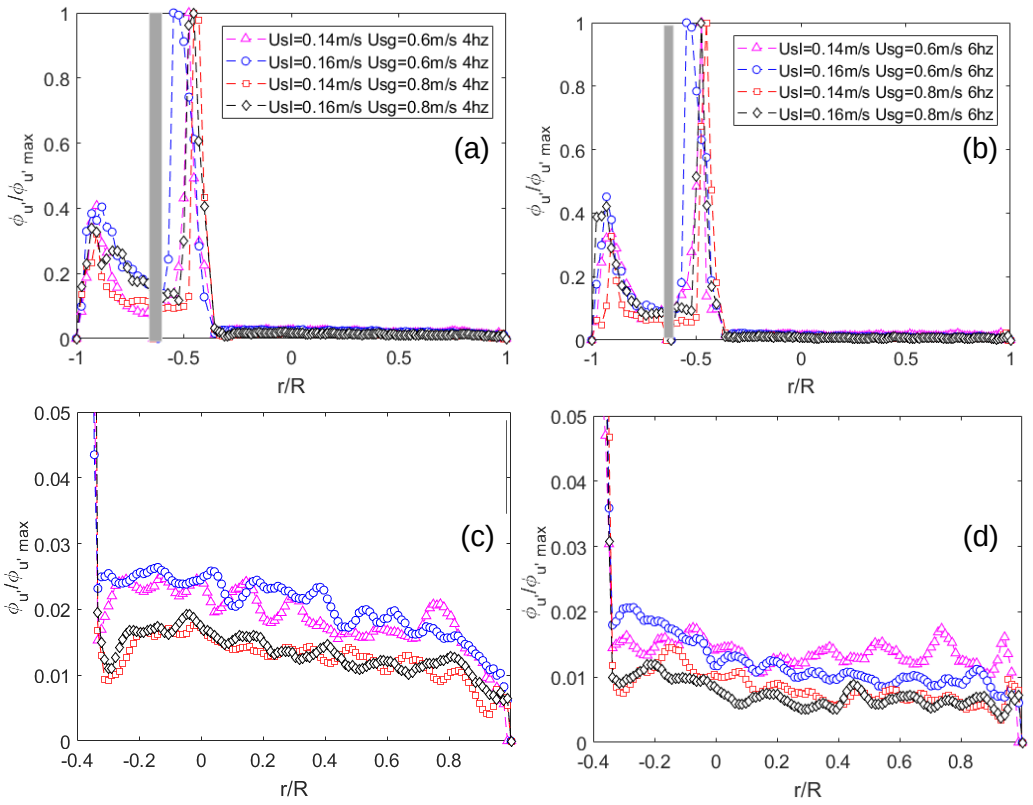

Figure 75 – Dimensionless profiles of wave induced streamwise velocity fluctuations for different flow rates in presence of linear waves at: (a) 4 Hz. (b) 6 Hz. (c) 4 Hz (in liquid phase only). (d) 6 Hz (in liquid phase only).

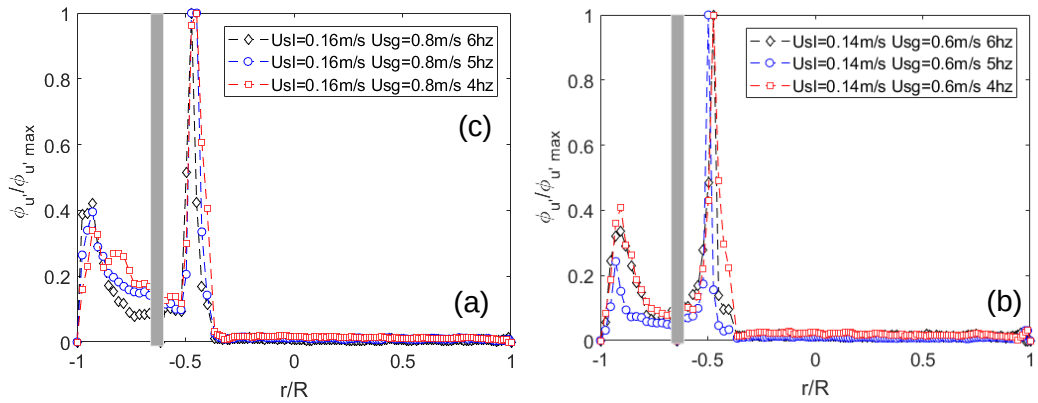

Figure 76 – Dimensionless profiles of wave induced streamwise velocity fluctuations in presence of linear waves excited at 4, 5 and 6 Hz (a) Case 4 (U_{sg} = 0.16 m/s and U_{sl} = 0.8 m/s). (b) Case 1 (U_{sg} = 0.6 m/s and U_{sl} = 0.14 m/s).

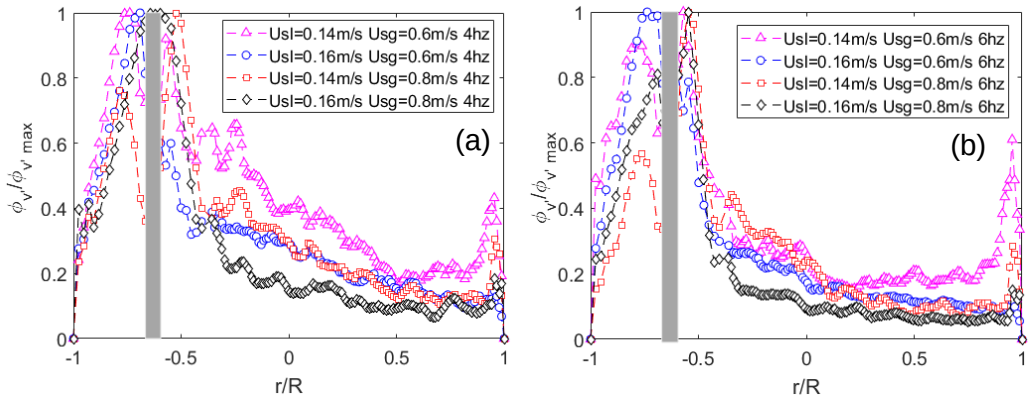

Figure 77 – Dimensionless profiles of wave induced wall normal velocity fluctuations for diferent flow rates in presence of linear waves at: (a) 4 Hz. (b) 6 Hz.

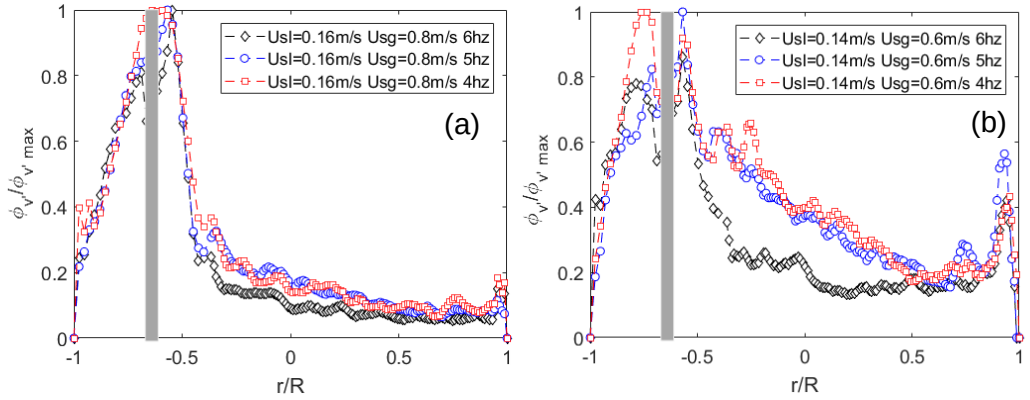

Figure 78 – Dimensionless profiles of wave induced streamwise velocity fluctuations in presence of linear waves excited at 4, 5 and 6 Hz: (a) Case 4 (U_{sg} = 0.16 m/s and U_{sl} = 0.8 m/s). (b) Case 1 (U_{sg} = 0.6 m/s and U_{sl} = 0.14 m/s).

Figure 79 shows a color plot of wave induced velocity obtained for Case 4 with an excited frequency wave of 4Hz. The velocity fields were reconstructed from measured flow fluctuations at the excited wave frequency. The oscilation of the interface was superimposed to the color plot as a continuous line. Thus, its phase relation with the disturbances can be clearly seen. The velocity fluctuations in Figure 79(a) and (b) show a characteristic phase relation of Kelvin-Helmholtz modes. These modes are ±45 deg phase shifted with the wave crest or valley. In addition, streamwise and wall normal fluctuations have a phase shift of 90 deg. All these features are typical for Kelvin Helmholtz waves. Thus, the results suggests that waves observed in this work correspond to K-H waves.

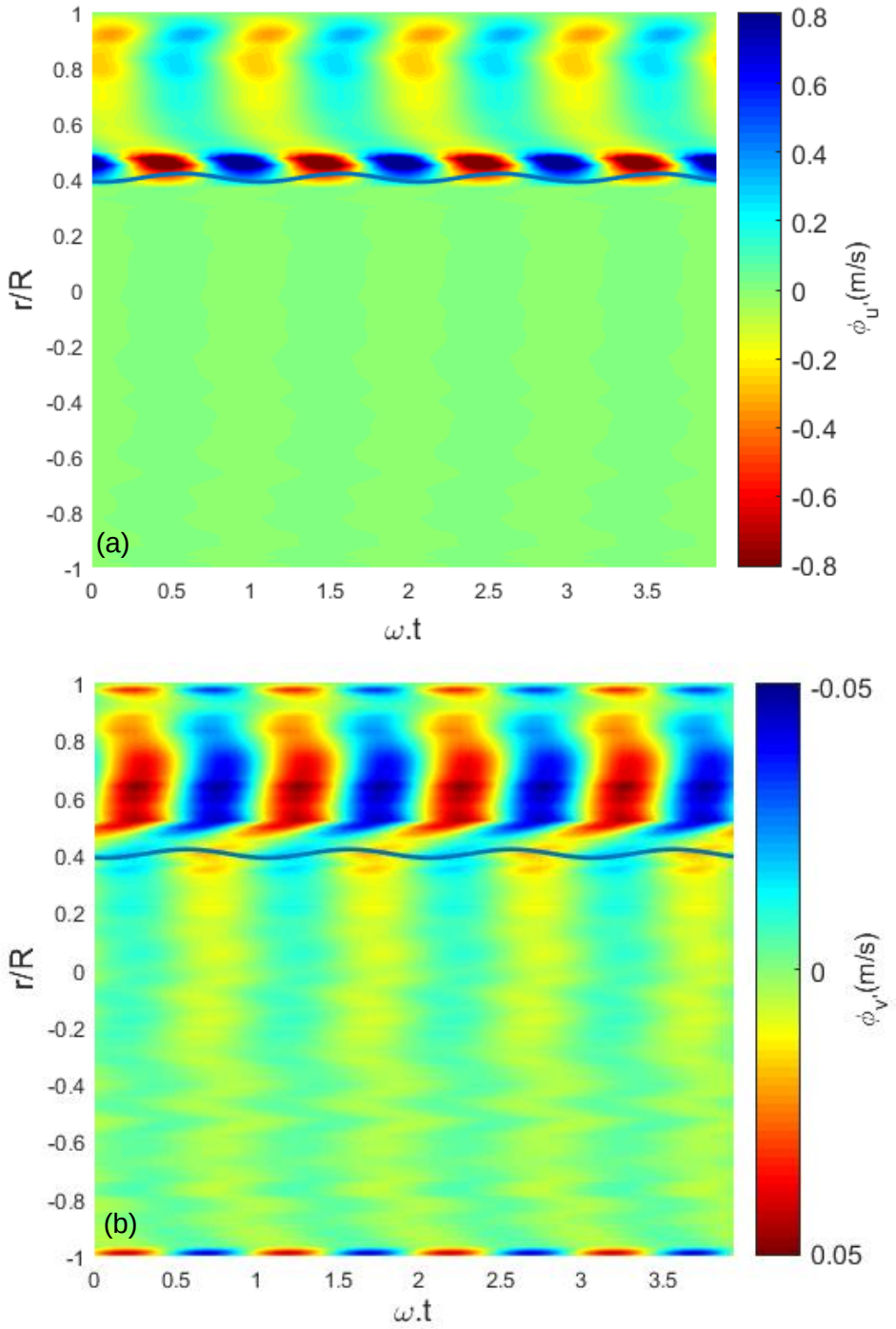

Figure 79 – 2D contours plot of wave induced velocity components obtained for Case 4 (U_{sg} = 0.16 m/s and U_{sl} = 0.8 m/s). with an excited wave of 4 Hz. (a) Streamwise direction (b) Wall normal.

Based on the present findings, it might be interesting to compare the experimental results against LST calculations of the Kelvin-Helmholtz instability problem of a stratified flow in a 2-D channel. Thus, a speculative comparison with the work of Barmak (2016) is provided in Figure 80. It is important to emphasize that the Reynolds numbers, mean flow profiles and wave frequencies adopted in the work of Barmak (2016) are different from those of the present study.

Nevertheless, the experimental profiles have shown some similarities for a range of velocities and frequencies. It can provide at least an idea whether the results from pipe flows can be captured by methods based on 2-D channel flows. Similarities can be found in streamwise wave induced profiles. Model and experiments show a clear peak near the interface. Evident discrepancies are found for wall normal velocities. This was somehow expected, because this profile is more sensitive to flow and wave parameters. Overall, the comparison show in Figure 80 show promising results, but no conclusion can be drawn before a quantitative comparison is performed with exactly the same flow and wave conditions.

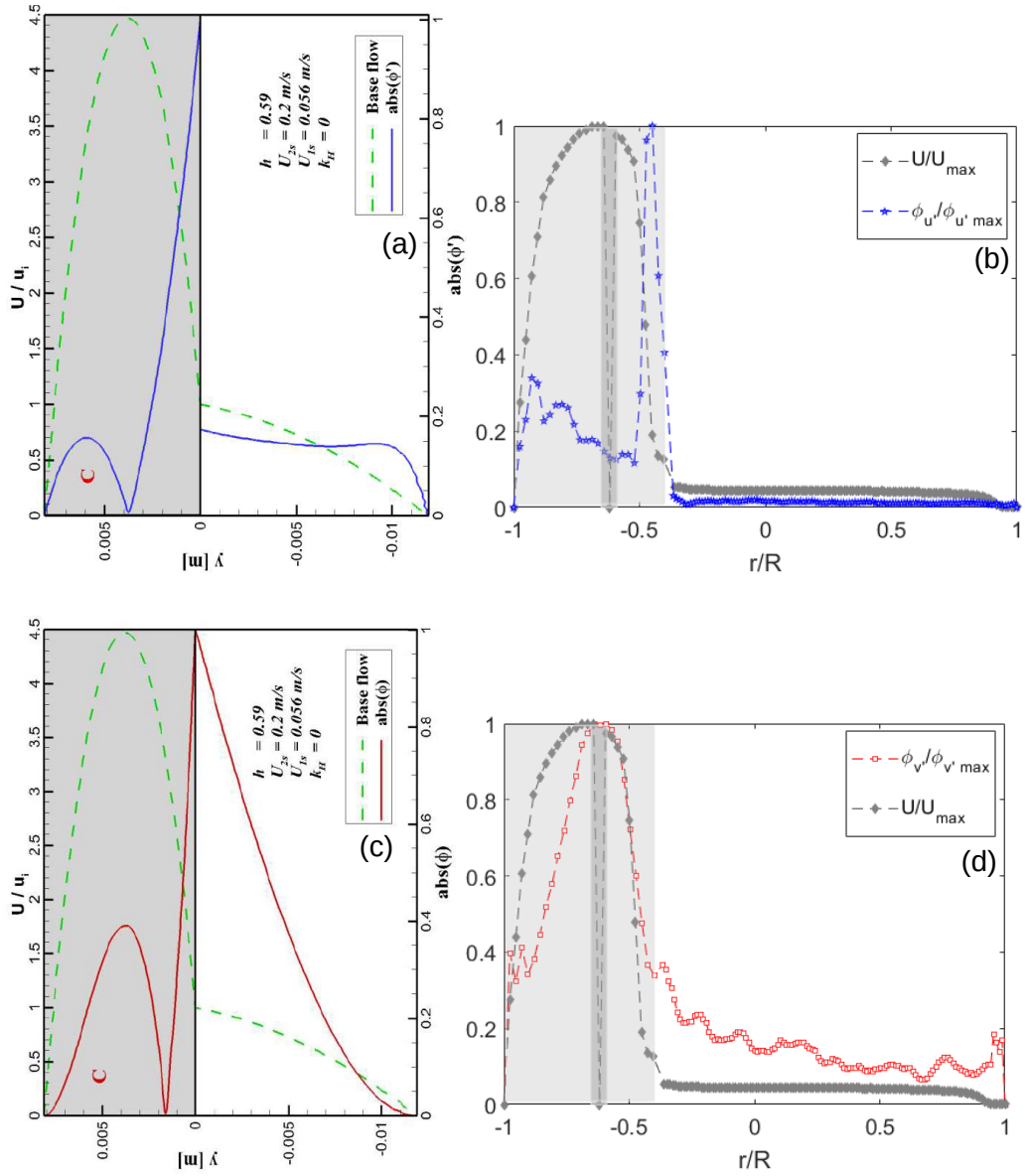

Figure 80 – Orr-Sommerfeld eigenfunctions for stratified flow (extracted from Barmark al., 2016): (a) Streamwise direction (b) Wall normal direction. Experimental profile of wave induced elocity fluctuation of Case 4 (U_{sl}=0.16m/s U_{sg}=0.8m/s 4 Hz) for exitation frequency of 4 Hz: (c) Streamwise direction (d) Wall normal direction.

8.3
Velocity fields in nonlinear wave regime

Slug predicting models, based on linear stability, include empirical correlations for interfacial friction factors that might implicitly incorporate non-linearities of the interfacial region (Tzotzi and Anidritsos, 2013). However, it is not clear to which extend these nonlinear effects are confined at the interface and how they affect the mean flow, the flow turbulence and the wave induced velocity fluctuations. Moreover, is also unclear if there is a weakly nonlinear regime, where disturbances can interact nonlinearly without severe modifications of wave nature and of flow conditions. In attempt to analyze the effect of non-linear interfacial waves in flow structure, a set of measurements were performed and the results are reported in this section.

8.3.1
Effect of nonlinear waves on velocity fluctuations

The effect of nonlinear waves in the distribution of velocity fluctuations is addressed in this section. The flow conditions selected for this test correspond to those of Case 3 (U_{sg} = 0.8 m/s and U_{sl} = 0.14 m/s). A monochromatic wave was introduced with a frequency of 6 Hz. The selected amplitudes correspond to Kirby values of approximately 0.03 and 0.08. This last amplitude is far higher than the threshold of 0.03, which was suggested in Chapter 8. The other amplitude was exactly at this threshold. In terms of wave amplitude, the case with K equals to 0.03 corresponds to a wave height of 0.65 mm (0 to peak). The nonlinear wave, with K=0.8, corresponds to a wave height of 1.5 mm. It can be noticed that such a wave was not extremely high.

Figure 81(a) display profiles of normalized streamwise velocity fluctuation without a superposed wave ($K = 0$), with a linear wave ($K < 0.03$) and with a high amplitude nonlinear wave ($K = 0.08$). According to the results in the figure, the turbulence intensity shows a high intensity near the interface also in the nonlinear regime. However, in nonlinear regime the fluctuations near the interface become more prominent than those close to the wall.

According to the numerical simulations reported in works of Fulgosi et al. (2003) and of Chinello et al. (2017), this effect might be linked with a redistribution of the energy in the flow. Fulgosi et al. (2003) suggest that, since no external kinetic energy was added into the system, the effect caused by the introduction

of a “rough interface” causes a redistribution of energy from viscous boundary layer near the wall to the interface region.

Figure 82(a) displays some profiles of normalized wall normal turbulence for different wave conditions. The nonlinear case shows a higher turbulence intensity near the interface in comparison to cases with linear waves and smooth interface. Ayati et al. (2015) and Birvalski (2016) also observed the enhancement of wall normal turbulence near the interface in wavy regimes. However, in their work this change was observed for different flow conditions. According to present findings it becomes clear that such a change is a wave related feature.

The wave induced profile of the streamwise and wall normal velocity components are displayed in Figure 81(b) and Figure 82(b). Some minor differences of near wall and near interface fluctuations were observed. Overall, the profiles show essentially a similar shape. These results indicate that even within the nonlinear regime, the disturbances near the wall and close to the interface are weakly correlated. In addition, apparently in the nonlinear regime, the modal behavior of the disturbances seems to be preserved. This suggest that weakly nonlinear models, like the one from the work of Campbell and Liu (2016), might be useful to predict the wave behavior under the range of Kirby numbers analyzed here.

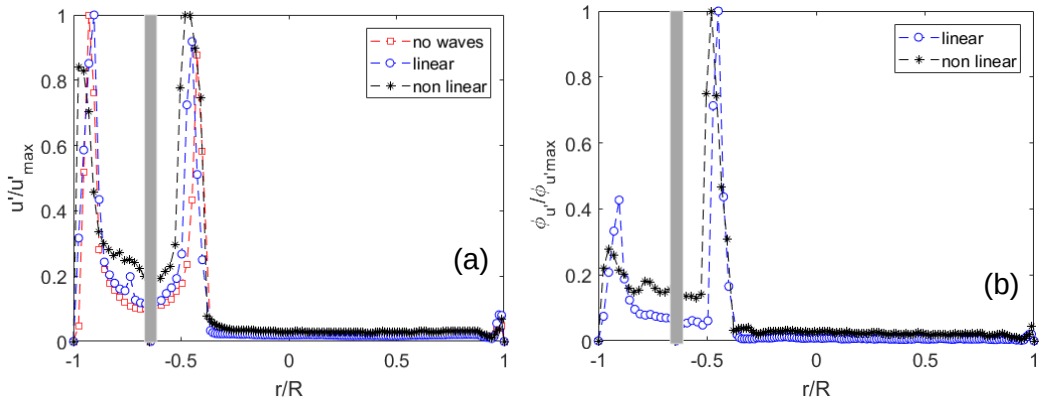

Figure 81 – (a) Normalized streamwise velocity profile. (b) Normalized streamwise wave induced profile of velocity fluctuations. Results for Case 3 (U_{sg} = 0.8 m/s and U_{sl} = 0.14 m/s) flow condition, without a superposed wave ($K = 0$), with a linear wave ($K < 0.03$) and with a high amplitude nonlinear wave ($K = 0.08$).

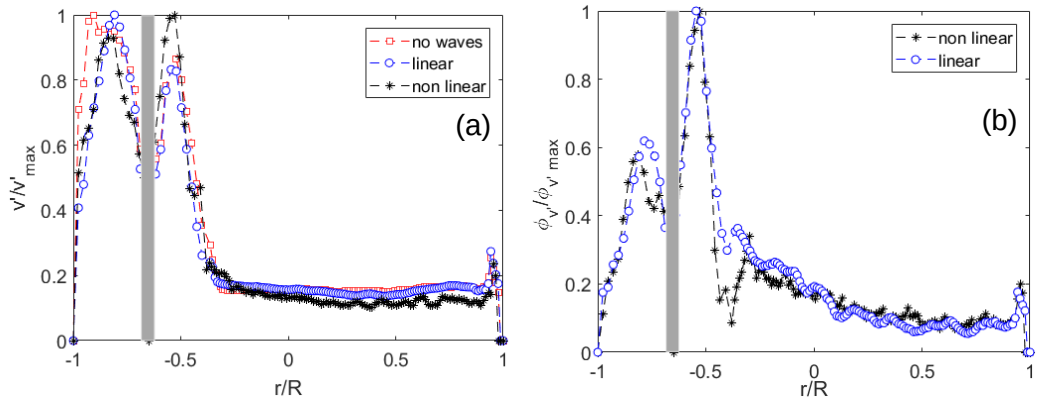

Figure 82 – (a) Normalized wall normal velocity profile. (b) Normalized wall normal wave induced profile of velocity fluctuations. Results for Case 3 (U_{sg} = 0.8 m/s and U_{sl} = 0.14 m/s) flow condition, without a superposed wave ($K = 0$), with a linear wave ($K < 0.03$) and with a high amplitude nonlinear wave ($K = 0.08$).

Spectra of streamwise turbulence, in the presence of nonlinear waves, are shown in Figure 83 for two regions, one near the interface and other close to the top wall. Side peaks around the disturbance frequency, which is centered in 1Hz, were found. This suggest a redistribution of energy towards sideband modes. Close to the interface some energy is found on harmonic (or subharmonic) frequencies. It is important to mention that due to signal aliasing it is not possible to distinguish between harmonic and subharmonic frequencies because both appear around the frequency of 2 Hz.

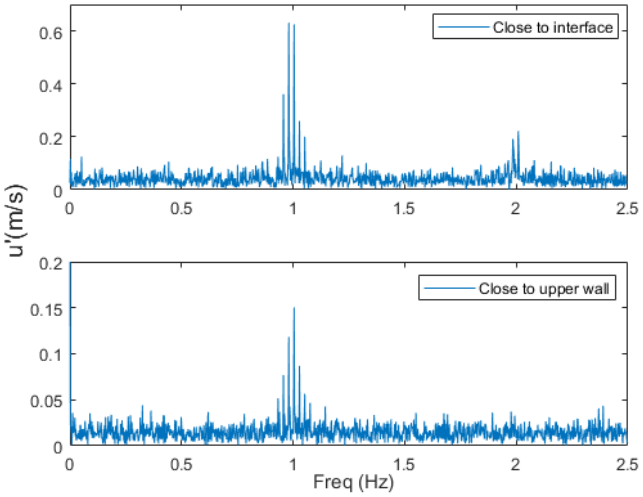

Figure 83 – Streamwise turbulence spectra signal in a region close to interface and close to top wall in gas-phase.

The resonant interaction between waves of different frequency is a well-studied phenomenon (Jurman et al. 1992, Valluri et al. 2008, Campbell and Liu 2014, Ayati 2018). This mechanism is characterized by fast energy transfer from

the fundamental to the sub-harmonic mode. Campbell and Liu (2014) derived weakly nonlinear formulation to account for nonlinear resonant interaction. They have shown that resonant coupling can induce wave growth faster than exponential. Ayati (2018) explored the spectra content of measured interfacial waves in stratified turbulent gas-liquid flow in horizontal pipe with conductance probes. The author reported that for higher gas velocities the fundamental modes can excite the subharmonics. The period doubling associated with this subharmonic resonance was also observed in the experiments performed by Jurman et al. (1992). For substantiation of nonlinear mechanisms proposed in the literature for wave interaction, a time resolved measurement system would be necessary. Therefore, this topic is not addressed in the present thesis.

According to present results, the wave induced velocity fluctuations measured in the presence of nonlinear waves are weakly correlated with wall disturbances. Moreover, evidences of harmonics or subharmonics modes were found only near the interface. These observations are interesting from the viewpoint of problem modeling. They suggest that interfacial effects might be modeled independently from those at the wall, even in weakly nonlinear regimes ($K<0.08$). This supports the conjecture that weakly nonlinear strategies might be an interesting solution to model the evolution of interfacial waves in stratified flows. To this end, it is necessary to model the influence of nonlinear waves on the mean flow. This is addressed in next section and in Chapter 9.

8.3.2
Influence of nonlinear waves on mean velocity profiles

This section is devoted to investigate the effect of nonlinear interfacial waves on the structure of the mean velocity profiles of all same cases listed in Table 4.

8.3.2.1
Liquid phase mean velocity profiles

The presence of interfacial waves on mean velocities of stratified flow has been extensively addressed in the literature. Rashid at al. (1992) used a wave maker in a water channel to show that, the waves can increase the mean velocity at intermediate distances from the wall, whilst creates a deficit near the interface. In this case the waves produce an S-shaped mean velocity profile. They related this effect to the finite depth of water layer.

In the present work the effect of waves on the mean velocity profile was investigated for two wave amplitudes and two frequencies, according to Table 5. Wave amplitudes were adjusted to two levels, corresponding to Kirby numbers within linear and nonlinear regimes. Table 5 summarizes the main characteristics of excited disturbances.

Table 5 – Characteristics of excited waves

U_{sg} (m/s)	U_{sl} (m/s)	f (Hz)	λ(mm)	K	h_w (mm)	Condition
0.8	0.14	4	155	0.03	0.67	Linear
0.8	0.14	4	155	0.06	1.31	Non-linear
0.8	0.14	6	120	0.03	0.51	Linear
0.8	0.14	6	120	0.06	1.13	Non-linear

The influence of nonlinear waves on mean liquid velocity is depicted in Figure 84. Mean flow profiles in the presence of waves of with 4 Hz and 6 Hz, are shown in Figure 84(a) and Figure 84(b), respectively. The profiles show that nonlinear waves can promote noticeable changes in the mean flow. These waves modify the flow in the center of the liquid layer to form an S-shaped profile. Close to the wall, the mean flow is nearly unaffected. The characteristic S-shaped profile with strong distortions near the interface are in accordance to most experimental studies reported in the literature (Rashid at al. 1992, Ayati et al. 2015, Sanjou & Nezu 2011, Birvalski et al. 2016 and Fernandino et al. 2008). However, in those works it was not possible to separate the wave effect from the modification of the Reynolds Numbers and of the mean liquid height. In present thesis, this can be clearly traced as a nonlinear wave effect.

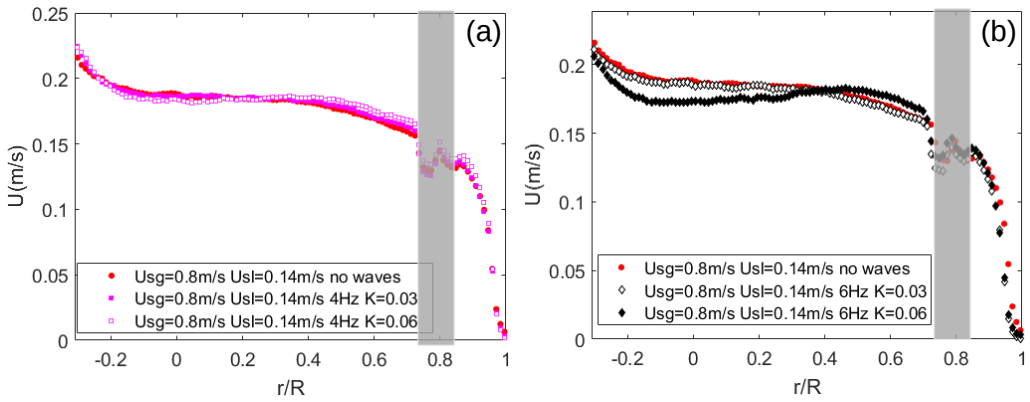

Figure 84 – Mean velocity profiles in the liquid layer for flow condition of Case 3 (U_{sg} = 0.8 m/s and U_{sl} = 0.14 m/s). Cases without and with exitated wave at: (a) 4 Hz. (b) 6 Hz.

Figure 85 shows the mean profile in terms of inner coordinates. Results suggest that nonlinear waves have, indeed, a weak influence of mean velocities near the wall. For intermediate heights $30 < y^+ < 150$ the trend follows the log-law even in the nonlinear case. For this nonlinear case, the values of U^+ and y^+ are slightly shifted with respect to the Von-Karman profile. This profile shifting is linked to variations in the pressure drop after the introduction of a nonlinear wave, hence wall shear velocity need to be revalued. Most pronounced deviations are confined to a region far from the wall, corresponding to $y^+ > 150$. This wall distance is equivalent to half of the water depth. The experimental results from Birvalski (2016) also show a good agreement with Von-Karman profile in the lower half depth of the liquid layer. In that case the flow was highly wavy. Thus, the distortion of the mean flow profile in wavy flow regimes seems to be mostly linked with interfacial waves. Fernadino and Ytrehus (2008) and Rashid et al. (1992) also reported a reasonable agreement with log-law profile in the near wall region but discrepancies were observed close to the interface. The work of Fernadino and Ytrehus (2008) suggests that the interface might be modeled as a flat surface with an imposed shear. This possibility is addressed in Chapter 9.

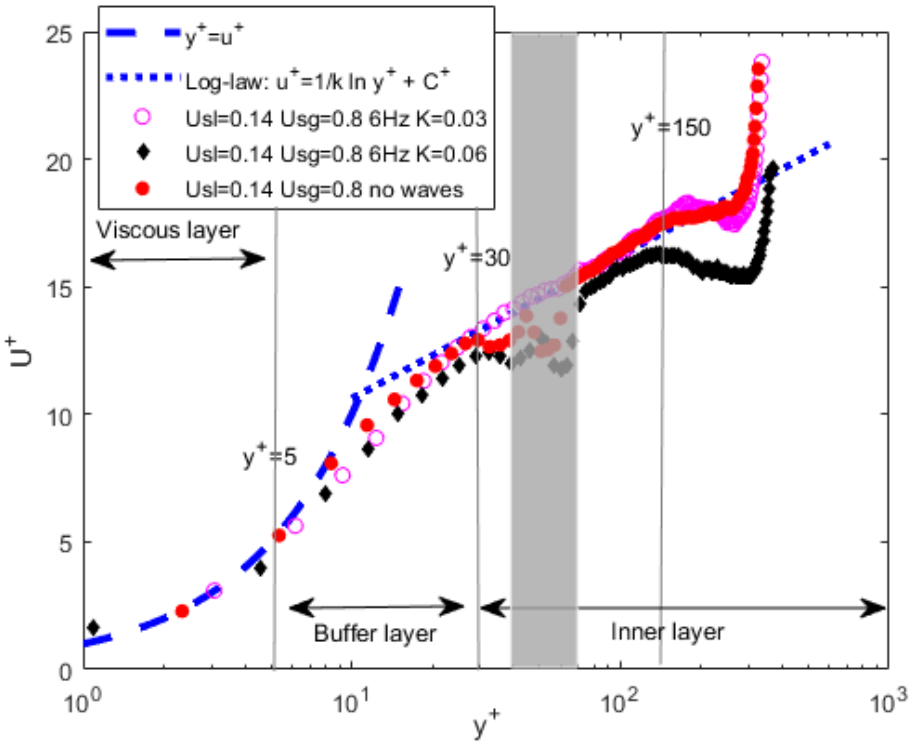

Figure 85 – Mean streamwise velocity profiles in inner coordinates. Von Karman´s constant k = 0.41 and C = 5. Measurements conditions of Case 3 (U_{sg} = 0.8 m/s and U_{sl} = 0.14 m/s).

8.3.2.2

Gas phase mean velocity profiles

The influence of a nonlinear wave in the mean velocity profile in the gas layer is addressed in Figure 86. In this test, the velocity profile was measured in the presence of a nonlinear wave with the Kirby number equal to 0.08. It is important to mention that the mean liquid height was also affected by the presence of this nonlinear wave. For instance, the mean liquid height decreased by approximately 1.5mm, due to the presence of a nonlinear wave with K=0.08.

The profile measured in the presence of nonlinear wave show a more pronounced asymmetry with the maximum velocity displaced towards the interface. A similar behavior was also reported in the work of Ayati et al. (2014, 2015) and Chinello et al. (2017). Numerical simulations reported in the work of Chinello et al. (2017) were not capable to capture this feature. They relate the discrepancies with inadequate turbulence modelling of the flow near the interface. In view of the current results, it seems that although weakly nonlinear models, such as the one proposed by (Campbell and Liu, 2016), look promising for simulation of wave interactions, the base flow modelling is still an issue for accurate predictions. Thus, it is evident that better turbulence models and

correlations for interfacial friction factors can contribute to account for the effects induced by nonlinear waves. The next chapter addresses this problem.

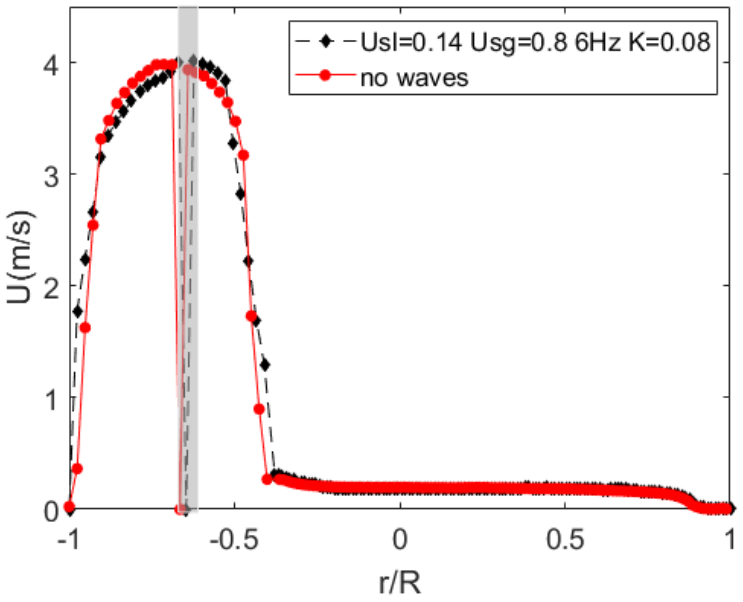

Figure 86 – Mean velocity profile of Case 3 (U_{sg} = 0.8 m/s and U_{sl} = 0.14 m/s) with and without a presence of a nonlinear wave (K=0.08).

9
Characterization of the wave-induced friction factor

Simplified one dimensional models are widely used in the oil and gas industry for prediction of transition between flow regimes in pipelines. For stratified pipe flow, Barnea and Taitel (1993) developed a one dimensional mechanistic approach that applies a local momentum balance equation for each phase and uses a simplified geometric representation of the pipe cross-section. This model, and many others in the literature, require some empirical closure relations to be solvable. Therefore, the development of correlations for different flow conditions are extensively investigated in the literature (Soleimani and Hanratty 2002, Andritsos and Hanratty 1987, Kadri et al. 2009). The interface friction factor, in many models is either a constant value or a function of gas friction factor. However, it is well-known that the pressure drop is larger in the presence of waves (Andritsos and Hanratty, 1987). Unfortunately, a detailed characterization of additional friction factors related with wave parameters are scarce in the literature. The reason might be the lack of test rigs with the capability to introduce interfacial waves in a controlled fashion.

Some recent studies investigate the relation of pressure drop with some flow features. Ayati et al. (2014) found a linear trend between the pressure drop and the gas flow rate. The intensity of the turbulence close to the interface region also followed a similar trend. This suggests a connection between turbulence and pressure drop, but they could not separate the wave-induced loss from the effect of change on the flow rate. In addition, wave amplitude could not be controlled, therefore this effect was not parametrically assessed in their study.

In the present study the turbulence and the wave-induced disturbances were detailed in Chapter 8. It was possible to show that interfacial waves mostly affect the flow near the interface. This is supported by experimental results for the range of parameters covered in this work. Thus, the wall shear is expected to be weakly affected by the presence of waves. These conclusions motivated a set of tests to determinate the wave induced friction factor. The idea is to contribute for improvement of interfacial shear stress correlations and hence for accuracy of models.

Measurements of the pressure drop for six different flow rates combinations were monitored for increasingly higher wave amplitudes. The paddle oscillation frequency was kept constant at a frequency of 4 Hz. The conditions were chosen in order to have a neutral growth of excited waves within the measurement region. Thus, disturbance amplitudes were nearly constant between the pressure taps used for measurement of pressure drop. During the tests, the paddle oscillated continuously.

A highly accurate differential pressure transmitter (GE STX2100) was employed in the measurements. The sensor has an accuracy of 0.04% of the full scale. Pressure taps were installed at 1.5 m and 7.5 m from the pipe inlet, which corresponds to approximately 30 D and 150 D, respectively.

The 1-D momentum balance equation for base flow was used to estimate the additional friction factor induced by the presence of the waves. To this end, it was assumed that all additional dissipation caused by the presence of the waves could be accounted into a wave related friction factor. In other words, it was assumed that the pressure drop is given by a stratified flow, with flat surface, and the waves produce an additional pressure loss. For stratified flow with flat surface, the momentum balance is given by Equation (9.1) with $F = 0$. Geometric parameters and equations presented in this chapter are described in the appendix, where the formulation proposed by Barnea and Taitel (1993) is outlined.

$$F = -\frac{\tau_L S_L}{A_L} + \frac{\tau_G S_G}{A_G} + \tau_i S_i \left(\frac{1}{A_L} + \frac{1}{A_G} \right) - (\rho_L - \rho_G) g \sin\beta \tag{9.1}$$

In the presence of waves, it is expected an additional condition to the friction factor of the interface, like:

$$\tau_{i+} = \tau_i + \tau_{wave}. \tag{9.2}$$

The increment on the momentum balance equation can be represented by:

$$\Delta F = \tau_{wave} S_i \left(\frac{1}{A_L} + \frac{1}{A_G} \right) \tag{9.3}$$

The momentum increment is directly related to the pressure drop, by the following relation:

$$\Delta F = \frac{\Delta P}{\Delta x}\Big|_{with\ wave} - \frac{\Delta P}{\Delta x}\Big|_{non\ disturbed} = \frac{\Delta P}{\Delta x}\Big|_{wave} \tag{9.4}$$

The wave induced friction factor was estimated directly from Equations (9.3) and (9.4), as shown in Equation (9.5).

$$f_{wave} = \frac{\left.\frac{\Delta P}{\Delta x}\right|_{wave}}{\frac{1}{2}\rho_g (U_g - U_l)\left|U_g - U_l\right| S_i \left(\frac{1}{A_l} + \frac{1}{A_g}\right)} \tag{9.5}$$

Here it was chosen to present the wave characteristics as a function of the Kirby parameter. Measured wave amplitudes and mean liquid heights were obtained by digital image processing. Only the amplitudes of the excited waves were considered. Therefore, the time series of the interfacial oscillations were transformed into a spectrum via Fourier transform and the corresponding amplitude at 0 (mean) and 4 Hz were extracted, according to the description given in Section 5.1.2.

Results shown in Figure 87 suggest a linear relation between the wave friction factor and Kirby parameter, for the range of parameters covered in this work. The experimental uncertainty of each measured point was calculated and represented by error bars in the figure. The correlation obtained for the friction facor inducd by the waves is given by Equation (9.6).

$$f_{wave} = 0.0176\,K - 0.00027 \tag{9.6}$$

It is interesting to observe that for Kirby numbers lower than approximately 0.03, the additional drag induced by waves is of the same order of experimental uncertainties. This corroborates the results from previous chapters about a threshold for linear wave in stratified flows. Thus, it seems that the threshold proposed in Chapter 7 is indeed appropriate.

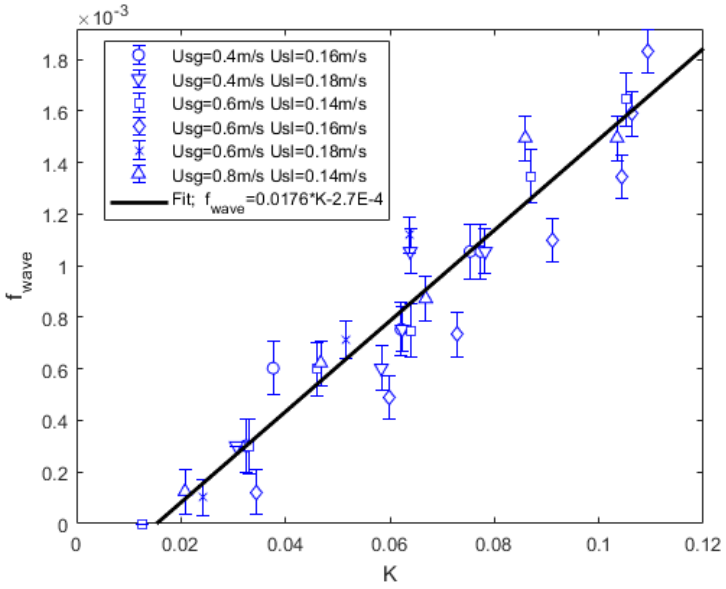

Figure 87 – Measured wave-induced friction factor as a function of the Kirby parameter.

The correlation obtained for the additional wave drag was added into the closure relations used for the balance of 1-D momentum equation of an undisturbed flow. This allows to observe the impact of the correlation on the estimation of the mean liquid height in the presence of waves. In this analysis the friction factors adopted in the works of Issa and Kempf (2003) and Carneiro et al. (2011) were used for dry and wet walls and for the interface. The friction factor correlation applied in that works is presented in Equation (9.7).

Figure 88 displays the comparison between the experimental liquid height obtained in the current work with the estimate provided by the 1-D momentum balance. Open symbols show the same model prediction for cases with different wave amplitudes. However, the experiments show a clear variation of the mean liquid height for cases for different wave amplitudes. The solid symbols present results obtained with the additional friction factor included in the closure relations. It can be seen that predictions do follow the experimental tendency. There is still a discrepancy in the measured heights and the predictions related to pressure drop prediction of the stratified flow with flat surface, hence this is not linked with the presence of waves.

$$f_{Issa\&Kempf} = 0.046\, Re_i^{-0.2} \tag{9.7}$$

Where Re_i is the interface Reynolds number.

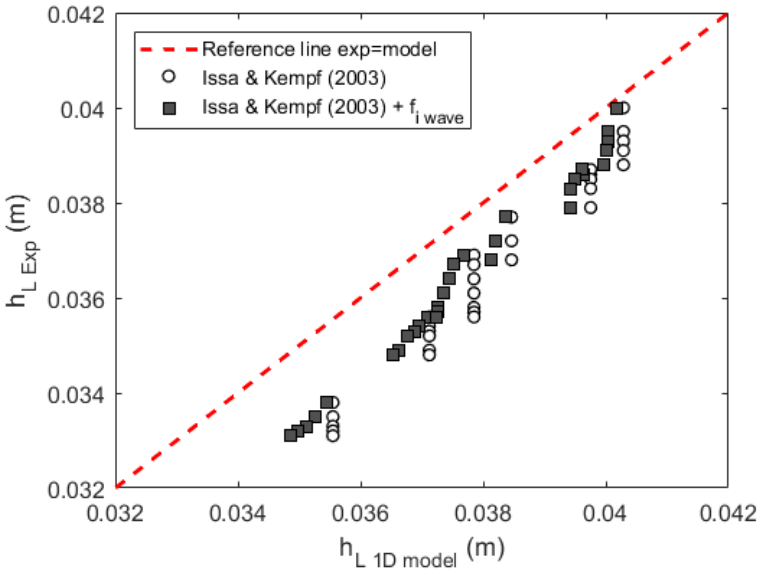

Figure 88 – Comparison between experimental and theoretical liquid height with the friction factor from Issa and Kempf (2003) with and without the combination with the wave friction factor estimative.

The influence of the change in the mean liquid height induced by higher friction factors at gas-liquid interface on the predictions of the transition from stratified to slug flow regimes, is illustrated in Figure 89. The transition limit was calculated using the 1D viscous K-H stability criteria proposed in the work of Barnea and Taitel (1993). This analysis is conceptually flawed because the correction of friction factor is related with nonlinear effects and the 1-D VKH stability analysis is linear. However, the idea here is just to conjecture about how the modifications of the mean flow induced by the waves would affect the linear stability of the flow. Hence the energy provided to the waves by linear stability mechanisms. In this analysis the friction factor of Issa and Kempf (2003) was applied combined with the wave friction factor estimated for different waves amplitudes. For the stability calculations is necessary to input a wavelength. This wavelength was used for the calculation of Kirby numbers and hence the additional wave drag.

The results displayed by in Figure 89 indicate that waves with high amplitudes tend to shift the transition towards higher liquid and gas velocities. The delay in the transition limits indicates a more stable flow. In fact, this was expected since the liquid height decreases for increasingly higher waves. However, this effect of wave amplitude and transition limits is not in agreement with the analysis presented in Section 6.2. Hence, the correlation for wave friction factor proposed could be used to improve liquid height and pipe head loss

estimation. However, for a proper prediction of the wave evolution it iseems necessary to have nonlinear or weakly nonlinear models.

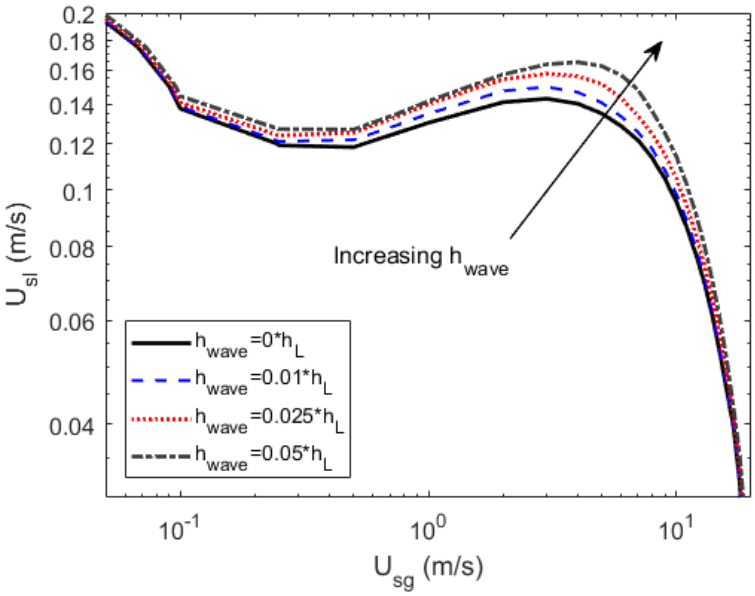

Figure 89 – Stratified to slug flow transition based on Issa and Kempf (2003) friction adapted with the wave friction factor estimative.

10
Conclusions

The present study aimed to provide accurate characterization of interfacial waves in stratified gas liquid flow in horizontal pipes. Concepts of shadow technique, particle image velocimetry, controlled disturbances, and phase-locked image acquisitions were applied to investigate the evolution of interfacial waves in a turbulent gas-liquid stratified flow. Measurements were carried out at flow rates close to the transition from smooth stratified to slug flow. The results show a high degree of reproducibility which enabled to track the evolution of excited disturbances along the pipe. The methodology adopted in the present work is an original contribution to two phase flow studies. Measurements of velocity profiles and wave coherent information such as, wave induced fluctuations and friction factor, can help to shed some additional light on how the two-phase stratified pipe flow compares with other two-phase shear flows such as, boundary layer and channel flows. Hence, the results reported here captured within well defined disturbances could provide a valuable experimental database for comparison with models and numerical simulations, which are based on modal stability analysis.

The work focused on the characterization of interfacial waves within the linear regime of their development. Unfortunately, there is no universal amplitude threshold for validity of linear wave regime in stratified flows. Measurements of mean flow velocity in the liquid layer using the PIV technique and of the spectra content of excited disturbances within the range of tested parameters, enable to experimentally determinate the amplitude threshold for assuming waves within the linear regime. The analysis presented suggests a wave induced nonlinearity threshold criterion for the evolution of waves in stratified flows scaled with the parameter proposed in the work of Kirby (1998). For the tested situations, significant harmonics and subharmonics and the distortion of the velocity profile of the liquid layer flow were not noticed for waves characterized below than Kirby parameter of 0.03. Therefore, only waves with very small amplitudes were investigated.

Another interesting result observed in the experimental data was the rather linear phase evolution of the interfacial waves. According to the current

findings, no evident influence of turbulence in the evolution of the waves was observed. The results clearly showed that dispersion characteristics of the waves remained unaffected even in the presence of highly noisy environment. A comparison of measured wave celerities against different linear models showed that linear wave theories based on finite depth are in better agreement with the experiments. Furthermore, most finite depth models displayed similar results, suggesting a weak influence of surface tension and gas density on the wave speed. Amplification of the disturbances was measured and a monotonic exponential growth was observed for waves excited with a frequency of 4 Hz. Waves with a frequency of 6 Hz displayed a completely different behavior and no clear evidence of exponential growth or decay was traced. This result is rather interesting and suggests that small variation on the wave scale can induce severe modifications on the phenomenon.

Mean flow, streamwise and wall normal fluctuations were measured simultaneously in liquid and gas phases at a fixed streamwise location applying off-axis PIV technique. It was observed close to both pipe walls a fair adherence of experimental mean velocity profiles to standard engineering models developed for turbulent flows in pipes. For the gas layer, an excellent agreement between experimental mean velocity profiles and the power-law profile from the upper wall to the gas bulk velocity was detected. For liquid layer, a fair agreement with log-law profile was found near the wall, up to a wall distance equivalent to half of the water depth.

The phase-locked technique measurements were employed to extract the wave coherent fluctuations from the flow turbulence. To the best of the authors knowledge, this is the first time that linear interfacial modes are measured in gas-liquid pipe flow. The experimental results show that interfacial modes are nearly independent of inner modes for the range of the current investigation. In general, the profiles of streamwise wave coherent fluctuations do not display remarkable differences within the conditions analyzed. Thus, wave frequencies have a weak influence on the general distribution of streamwise fluctuations. For wall normal disturbances, wave coherent fluctuations measured with different oscillation frequencies show some noticeable modifications. Thus, wall normal fluctuations would be preferred for a proper validation of numerical simulations and models against experiments.

The nonlinear wave regime was superficially investigated but interesting conclusions could be found. Noticeable changes were observed in the mean velocity profiles and a higher wave coherent fluctuations close to the interface.

However, a weak coherence between wall and interfacial velocity fluctuations was still detected. Hence, the current work suggests that interfacial effects might be modeled independently from the flow at the wall, even in nonlinear regimes, for Kirby parameter up to 0.08. However, the base flow modelling is an obstacle for accurate model predictions.

Further, a correlation for friction factor increment induced by wave was obtained. This additional wave drag was added to the closure relations used for the balance of 1-D momentum equation. The correlation showed an improvement in the predictions of mean liquid height in the presence of waves. However, the effect of the additional drag on the transition prediction of slugs was analyzed. Results suggest a transition in the presence of waves with high amplitude. This is contrary to the experimental findings and the literature. Thus, it is suggested that although the predictions of base flow can be improved with corrections for the wave drag, the improvement of transition predictions might demand nonlinear and weakly nonlinear modelling.

In view of current state of affairs, the methodology proposed in this work contributed significantly to describe the phenomenon and to shed some light on the physical mechanisms involved in the initial stages of the transition from stratified to slug flows, more precisely, in linear and weakly nonlinear wave regime. The results presented here compose a valuable database for validation of theoretical models and numerical simulations.

As suggestion for the extension of experiments to address open questions in the literature, nonlinear physical mechanisms effects on turbulence structure such as, wave coupling and resonance deserve further investigations. In addition, effects of fluid properties, pipe diameter and inclination on flow stability should be definitively deeply studied using the developed methodology.

11
References

Andreussi, P., Asali, J. C., and Hanratty, T. J., Initiation of roll waves in gas-liquid flows. AIChE J. 31(1), 119–126 (1985).

Andritsos, N. and Hanratty, T. J., Interfacial instabilities for horizontal gasliquid flows in pipelines. Int. J. Multiphase Flow 13, 583–603 (1986).

Andritsos, N., Williams, L., Hanratty, T.J. Effect of liquid viscosity on the stratified-slug transition in horizontal pipe flow. International Journal of Multiphase Flow,Volume 15, Issue 6,(1989).

Andritsos, N., Effect of pipe diameter and liquid viscosity on horizontal stratified flow. Ph.D. Thesis, Univ. of Illinois, Urbana (1986)

Ansari, M. R. and Shokri, V. Numerical modeling of slug flow initiation in a horizontal channels using a two-fluid model, Int. J. Heat Fluid Flow 32(1), 145–155 (2011).

Ayati, A. A., Kolaas, J., Jensen, A., and Johnson, G. W. Combined simultaneous two-phase PIV and interface elevation measurements in stratified gas/liquid pipe flow. Int. J. Multiphase Flow 74, 45–58 (2015).

Ayati, A. A., Kolaas, J., Jensen, A., and Johnson, G. W. The effect of interfacial waves on the turbulence structure of stratified air/water pipe flow. Int. J. Multiphase Flow 78, 104–116 (2016).

Ayati, A., Kolaas, J., Jensen, A., and Johnsonvre, G. W. A PIV investigation of stratified gas-liquid flow in a horizontal pipe. Int. J. Multiphase Flow 61, 129–143 (2014).

Ayati, A. Experimental characterization of non-linear interfacial wave interaction in stratified gas-liquid pipe flow. Physics of Fluids. (2018).

Bai, Y. and Q. Bai, Q. Subsea Pipelines and Risers. Elsevier Ocean Engineering Book Series. Elsevier, Amsterdam, 2005, pp. 751-785.

Baker, O. Design of Pipe Line for the Simultaneous Flow of Oil and Gas. The Oil and Gas Journal. (1954).

Bar-Cohen, A., Holloway, C., Kaffel, A., and Riaz, A. Waves and instabilities in high quality adiabatic flow in a microgap channels. Int. J. Multiphase Flow 83, 62–76 (2016).

Barmak, I., Gelfgat, A.,Vitoshkin, H., Ullmann, A., and Brauner, N. Stability of stratified two-phase flows in horizontal channels. Phys. Fluids 28(4). (2016).

Barnea, D. A unified model for predicting flow-pattern transitions for the whole range of pipe inclinations. Int. J. Multiphase Flow 13(1), 1–12 (1987).

Barnea, D. and Taitel, Y. Transient-formulation modes and stability of steady-state annular flow. Chem. Eng. Sci. 44(2), 325–332 (1989).

Barnea, D. and Taitel, Y. Kelvin-Helmholtz stability criteria for stratified flow: Viscous versus non-viscous (inviscid) approaches. Int. J. Multiphase Flow 19(4), 639–649 (1993).

Beji, S. Note on a nonlinearity parameter of surface waves, Coastal Engineering, Volume 25, Issues 1–2, (1995).

Bendiksen, K. and Espedal, M. Onset of slugging in horizontal gas-liquid pipe flow. Int. J. Multiphase Flow 18(2), 237–247 (1992).

Bendiksen, K. H., Maines, D., Moe, R., and Nuland, SThe Dynamic Two-Fluid Model OLGA: Theory and Application. Society of Petroleum Engineers. . (1991).

Berthelsen, P.A. and Ytrehus, T. Calculations of stratified wavy two-phase flow in pipes. Int. J. Multiphase Flow, 31(5), 571-592 (2005).

Biberg, Dag. A mathematical model for two-phase stratified turbulent duct flow. Multiphase Science and Technology. (2007).

Birvalski, M. and Tummers, Mark and Delfos, R. and Henkes, R. A. W. M. Laminar–turbulent transition and wave–turbulence interaction in stratified horizontal two-phase pipe flow. Journal of Fluid Mechanics. 780. 439-456. (2015).

Birvalski, M. and Tummers, Mark and Henkes, R. A. W. M. Measurements of gravity and gravity-capillary waves in horizontal gas-liquid pipe flow using PIV in both phases. International Journal of Multiphase Flow. 87. 102-113. (2016).

Birvalski, M., Tummers, M. J., Delfos, R., and Henkes, R. A. W. M. PIV measurements of waves and turbulence in stratified horizontal two-phase pipe flow. Int. J. Multiphase Flow 62, 161–173 (2014).

Bontozoglou, V. Weakly nonlinear Kelvin-Helmholtz waves between fluids of finite depth. Int. J. Multiphase Flow 17(4), 509–518 (1991).

Boomkamp, P., Miesen, R. Classification of instabilities in parallel two-phase flow, International Journal of Multiphase Flow, Volume 22, Supplement, (1996).

Boomkamp, P., Boersma, B., Miesen, R., Beijnon G. A Chebyshev collocation method for solving two-phase flow stability problems. J. Comput. Phys., 132 (1997), pp. 191-200.

Brennen, C. Bibliography. In Fundamentals of Multiphase Flow (pp. 321-340). Cambridge: Cambridge University Press. (2005).

Buckley, M. P. and Veron, F. Structure of the airflow above surface waves. J. Phys. Oceanogr. 46(5), 1377–1397 (2016).

Campbell, B. K. and Liu, Y. Sub-harmonic resonant wave interactions in the presence of a linear interfacial instability. Massachusetts Institute of Technology, Cambridge, Massachusetts 02139, USA (2014)

Campbell, B. K. and Liu, Y. A nonlinear flow-transition criterion for the onset of slugging in horizontal channels and pipes. Phys. Fluids, 28 (8). (2016).

Campos, D. E. G. Estudo da instabilidade de ondas na interface do escoamento estratificado laminar-laminar em um canal. Tese de Doutorado, Pontifícia Universidade Católica (2018).

Carneiro, J. N. E.; Fonseca Jr, R.; Ortega, A. J.; Chucuya, R. C.; Niekele, A. O.; Azevedo, L. F. A. Statistical Characterization of Two-Phase Slug Flow in a Horizontal Pipe. Journal of the Brazilian Society of Mechanical Sciences and Engineering, 33, p. 251-258 (2011).

Chinello, Gabriele and Ayati, Anis and McGlinchey, Don and Ooms, Gijsbert and Henkes, R.A.W.M. Comparison of CFD simulations and experiments for stratified air-water flows in pipes. Journal of Fluids Engineering. (2018).

de Paula, I. B., W¨urz, W., K¨amer, E., Borodulin, V. I., and Kachanov, Y. S., “Weakly nonlinear stages of boundary-layer transition initiated by modulated Tollmien-Schlichting waves,” J. Fluid Mech. 732, 571–615 (2013).

Danielson, T., Bansal, K., Djoric, B., Larrey, D., Johansen, S., De Leebeeck, A., Kjølaas, J., 2012. Simulation of slug flow in oil and gas pipelines using a new transient simulator. In: Offshore Technology Conference 2012, Texas, USA .

Dean, R.G. and Dalrymple, R.A. Water Wave Mechanics for Engineers and Scientists. Advanced Series on Ocean Engineering, 2. (1991).

Drazin, P., and Reid, W. Bibliography and author index. In Hydrodynamic Stability (Cambridge Mathematical Library, pp. 559-594). Cambridge: Cambridge University Press. (2004).

Drazin, P. Introduction to Hydrodynamic Stability. Introduction to Hydrodynamic Stability, by P. G. Drazin, pp. 276. Cambridge, UK: Cambridge University Press. (2002).

Dvora Barnea, On the effect of viscosity on stability of stratified gas—liquid flow—application to flow pattern transition at various pipe inclinations, Chemical Engineering Science, Volume 46, Issue 8,(1991).

Fan, Z., Lusseyran, F., and Hanratty, T. J. Initiation of slugs in horizontal gas-liquid flows. AIChE J. 39(11), 1741–1753 (1993).

Fernandino, Maria and Ytrehus, T. Effect of Interfacial Waves on Turbulence Structure in Stratified Duct Flows. Journal of Fluids Engineering-transactions of The Asme - J FLUID ENG. (2008).

Fernandino, Maria and Ytrehus, T. Determination of flow sub-regimes in stratified air–water channel flow using LDV spectra. International Journal of Multiphase Flow - INT J MULTIPHASE FLOW. 32. 436-446. (2006).

Fulgosi, M., Lakehal, D., Banerjee, S., and De Angelis, V. Direct Numerical Simulation of Turbulence in a Sheared Air-Water Flow With eformable Interface," J. Fluid Mech., 482, p. 319319 (2003),

Funada, T. and Joseph, D. D., "Viscous potential flow analysis of Kelvin-Helmholtz instability in a channel," J. Fluid Mech. 445, 263–283 (2001).

Gonzales, R. C., Woods, R. E., and Eddis, S. L. Digital Image Processing Using Matlab. 2nd ed. (Gatesmark Publishing, 2009), p. 1.

Groth, J., and Johansson, A. Turbulence reduction by screens. Journal of Fluid Mechanics, 197, 139-155. (1988).

Hanratty, T.J., Interfacial instabilities caused by air flow over a thin liquid layer, Waves on Fluid Interfaces, Academic Press, New York (1983).

Havre, K., Stornes, K. O., and Stray, H. Taming slug flow in pipelines. ABB Rev. 4, 55–63 (2000).

Hewitt, G. F., Jayanti, S., and Hope, C. B. Structure of thin liquid films in gas-liquid horizontal flow. Int. J. Multiphase Flow 16(6), 951–957 (1990).

Hewitt, G.F. and Roberts, D.N.. Studies of Two-Phase Flow Patterns by Simultaneous X-ray and Flash Photography. (1969).

Hinze, J. O., Turbulence, 2nd ed. New York: McGraw-Hill (1975).

Holmås, H. and Biberg, Dag and Johnson, G. and Schulkes, R. and Sira, T. Stability analysis of the Biberg pre-integrated stratified two-phase flow model including profile factors. BHR Group - 6th North American Conference on Multiphase Technology. 127-141. (2008).

Ishii, M. and Mishima, K. Study of Two-Fluid Model and Interfacial Area. NUREG/CR-1873 (ANL-80-111). (1980).

Issa, R. I. and Kempf, M. H. W. Simulation of slug flow in horizontal and nearly horizontal pipes with the two-fluid model. Int. J. Multiphase Flow 29(1), 69–95 (2003).

James T. Kirby, Discussion of `Note on a nonlinearity parameter of surface waves' by S. Beji, Coastal Engineering, Volume 34, Issues 1–2, (1998).

Johnson, G. W., Bertelsen, A. F., and Nossen, J. An experimental investigation of roll waves in high pressure two-phase inclined pipe flows. Int. J.Multiphase Flow 35(10), 924–932 (2009).

Jurman, L. A., Deutsch, S. E., and MacCready, M. J. Interfacial mode interactions in horizontal gas–liquid flows. J. Fluid Mech. 238, 187–219 (1992).

Kadri, U., Mudde, R. F., Oliemans, R. V. A., Bonizzi, M., and Andreussi, P. Prediction of the transition from stratified to slug flow or roll-waves in gas–liquid horizontal pipes. Int. J. Multiphase Flow 35, 1001–1010 (2009).

Kaffel, A. and Riaz, A. Eigenspectra and mode coalescence of temporal instability in two-phase channel flow. Phys. Fluids 27(4), 042101 (2015).

Kahraman Albayrak, Design of a low-speed axisymmetric wind tunnel contraction, Journal of Wind Engineering and Industrial Aerodynamics, Volume 37, Issue 1 (1991).

Kao, T.W. and Park, C. Experimental investigations of the stability of channel flows.J. Fluid Mech. 52 (1972) 401 – 424

Kjell H. Bendiksen, An experimental investigation of the motion of long bubbles in inclined tubes, International Journal of Multiphase Flow, Volume 10, Issue 4, (1984).

Kjølaas, Jørn and Leebeeck, A. and Johansen, Stein. Simulation of hydrodynamic slug flow using the LedaFlow slug capturing model. BHR Group - 16th International Conference on Multiphase Production Technology 2013. 365-383. (2013).

Klebanoff, P., Tidstrom, K., and Sargent, L. The three-dimensional nature of boundary-layer instability. Journal of Fluid Mechanics, 12(1), 1-34. (1962).

Kordyban, E. S. and Ranov, T., Mechanism of slug formation in horizontal two-phase flow. J. Basic Eng. 92(4), 857–864 (1970).

Kundu, P. K.; Cohen, I. M.; Dowling, D. R. Fluid Mechanics. Fifth Edition. Elsevier Inc. (2012).

Landau, L. D. and Lifshitz, E. M., Fluid Mechanics, Course of Theoretical Physics. Elsevier (1987).

Landau, L.D. and Lifshitz, E.M. Theory of Elasticity. Addison-Wesley Publishing Co., Boston. (1959).

Lin, P. Y. and Hanratty, T. J., “Prediction of the initiation of slugs with linear stability theory,” Int. J. Multiphase Flow 12(1), 79–98 (1986).

Lumley, J. L., and McMahon, J. F. Reducing Water Tunnel Turbulence by Means of a Honeycomb. ASME. J. Basic Eng. December 1967; 89(4): 764–770. (1967).

Mandhane, J. M., Gregory, G. A., and Aziz, K., A flow pattern map for gasliquid flow in horizontal pipes, Int. J. Multiphase Flow 1(4), 537–553 (1974).

Mccready, Mark and D. Uphold, D. Formation of large disturbances in separated fluid-fluid flows. American Society of Mechanical Engineers, Fluids Engineering Division (Publication) FED. 244. (1997).

Mendonça M. T., 2000. Laminar Flow Stability: Linear Theory. . 2ª Escola de Primavera de Transição e Turbulência EPTT (2000). Universidade Federal de Uberlândia.

Mendonça M. T., de Medeiros M. A. F. Instabilidade Hidrodinâmica e transição para turbulência com aplicações em engenharia e meteorologia. ENCIT (2002).

Mihe-Thomson, L. M., Theoretical Hydrodynamics, The Mac-Millan Co., New York (1960).

Nogueira, S., Sousa, R. G., Pinto, A. M. F. R., Riethmuller, M. L., and Campos, J. B. L. M., Simultaneous PIV and pulsed shadow technique in slug flow: A solution for optical problems," Exp. Fluids 35 (6), 598–609 (2003).

Ocana, L. M. P. Medições do Escoamento Turbulento em Tubos na Presença de Polímeros Redutores de Atrito. Dissertação (Mestrado em Engenharia Mecânica) – Pontifícia Universidade Católica do Rio de Janeiro, PUC-Rio, 2011. Orientador: Prof. Luis Fernando Alzuguir Azevedo.

Orr, W. The Stability or Instability of the Steady Motions of a Perfect Liquid and of a Viscous Liquid. Part II: A Viscous Liquid. Proceedings of the Royal Irish Academy. Section A: Mathematical and Physical Sciences, 27, 69-138. (1907).

Raffel et al., 2007 M. Raffel, C. Willert, S. Wereley, J. Kompenhans Particle Image Velocimetry – A practical guide (second ed.), Springer (2007)

Raffel, M and Willert, Christian and Kompenhans, Juergen. Particle Image Velocimetry: A Practical Guide. 10.1007/978-3-662-03637-2. (1998).

Raimondi, L. Stratified gas-liquid flow–An analysis of steady state and dynamic simulation for gas-condensate systems. Petroleum. (2017).

Rashidi, M., Hetsroni, G., and Banerjee, S. Wave-Turbulence Interaction in Free-Surface Channel Flows. Phys. Fluids A. (1992).

Rodríguez, D. A combination of parabolized Navier–Stokes equations and level-set method for stratified two-phase internal flow International Journal of Multiphase Flow 88, p. 50-62 (2017).

Rodríguez, D. A novel modeling method for the interfacial instability of immiscible fluids along ducts. COBEM 2015, 23 ABCM International Congressof Mechanical Engineering. Rio de Janeiro, RJ, Brazil (2015).

Rodriguez, O. M. H., 2008. Estabilidade hidrodinâmica e Escoamento bifásico Paralelo. 6ª Escola de Primavera de Transição e Turbulência EPTT (2008).

Sanchis, A., Johnson, G.W., and Jensen, A. The formation of hydrodynamic slugs by the interaction of waves in gas–liquid two-phase pipe flow. Int.J. Multiphase Flow 37, 358–368 (2011).

Sangalli, M., McCready, M. J. and Chang, H-C. Stabilization mechanisms of short waves in stratified gas–liquid flow. American Institute of Physics 9 (4), p. 919-939, 1997

Sanjou, Michio and Nezu, Iehisa. (2011). Turbulence structure and coherent vortices in open-channel flows with wind-induced water waves. Environmental Fluid Mechanics. 11. 113-131. 10.1007/s10652-011-9210-7.

Schicht, H. H., Stromungsbilder bei adiabater Zwei-phasenstromung Wasser/Luft in einem horizontalen Rohr, V erfahrenstechnik. Vol. 3, No. 4 (1969).

Schmid, P. J. and Henningson, D. S., Stability and Transition in Shear Flows. Applied Mathematical Sciences Vol. 142 Springer Verlag (2001).

Schmid, P. J., Henningson, D. S., and Jankowski, D. F. Stability and transition in shear flows. Applied mathematical sciences, Vol. 142, Appl. Mech.Rev. 55, B57 (2002).

Schlichting, H. Boundary layer theory. (7th ed.), McGraw-Hill, New York (1979).

Soleimani, A. and Hanratty, T. J. Critical liquid flows for the transition from the pseudo-slug and stratified patterns to slug flow. Int. J. Multiphase Flow 29 (1), 51–67 (2003).

Sommerfeld, A. Ein beitrag zur hydrodynamischen erklärung der turbulenten flüssigkeitsbewegungen. Atti del 4. Congr. Internat.dei Mat. III, Roma, (1908).

Strand, O. 1993. An experimental investigation of stratified two-phase flow in horizontal pipes. Ph.D. Thesis, University of Olso, 1993.

Taitel, Y. and Dukler, A. E., “A model for predicting flow regime transitions in horizontal and near horizontal gas-liquid flow,” AIChE J. 22(1), 47–55 (1976).

Tzotzi, C. and Andritsos, N. Interfacial shear stress in wavy stratified gasliquid flow in horizontal pipes. Int. J.Multiphase Flow 54, 43–54 (2013).

Ujang, P. M., Lawrence, C. J., Hale, C. P., and Hewitt, G. F. Slug initiation and evolution in two-phase horizontal flow. Int. J. Multiphase Flow32(5), 527–552 (2006).

Ursell, F. (1953). The long-wave paradox in the theory of gravity waves. Mathematical Proceedings of the Cambridge Philosophical Society, 49(4), 685-694.

Valluri, P., Spelt, P. D. M., Lawrence, C. J., and Hewitt, G. F. Numerical simulation of the onset of slug initiation in laminar horizontal channel flow. Int. J. Multiphase Flow 34(2), 206–225 (2008).

Wallis, G. B. and Dobson, J. E. The onset of slugging in horizontal stratified air-water flow. Int. J. Multiphase Flow 1(1), 173–193 (1973).

Wallis, G.B. (1969) One-Dimensional Two-Phase Flow. McGraw-Hill, New York, 243.Waves on Fluid Interfaces, Academic Press, New York (1983)

Weisman, J. Sketches of flow regimes for two-phase flow in a horizontal pipe. Source: Two-phase flow patterns. Chapter 15 in Handbook of Fluids in Motion, Cheremisinoff N.P., Gupta R. 1983. Ann Arbor Science Publishers.

Wetzel, J. M. and Arndt, R. E. A. Hydrodynamic design considerations for hydroacoustic facilities: Part I—Flow quality. J. Fluids Eng. 116(2),324–331 (1994).

Wu, X. and Moin, P. A direct numerical simulation study on the mean velocity characteristics in turbulent pipe flow. J. Fluid Mech, 608:81-112 (2008).

Yiantsios, S. G. & Higgins, B. G. 1988 Linear stability of plane Poiseuille flow of two superposed fluids. Phys. Fluids 31 (11).

12
Appendix - One dimensional model (Barnea and Taitel, 1993)

In the present literature review, the methodology developed by Barnea and Taitel (1993) was chosen to exemplify the application of linear stability analysis of two phase flows through pipes. This method is more didactic in the understanding of stability problem and is widely used for an estimative application in two-phase flow transition. In addition, the predictions provided by the work of Barnea and Taitel (1993) will be used in comparisons with the experimental results obtained in the present thesis. Thus, the methodology described by Barnea and Taitel (1993) will be briefly equated below.

The Stability analysis of stratified flow is performed on the "two-fluid model" equations (Ishii, 1980). The geometry attracted from Barnea and Taitel (1993) is illustrated in the figure below and a brief outline of this analysis follows.

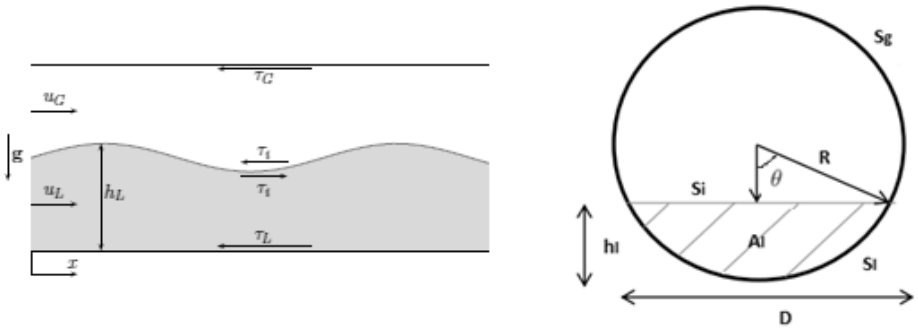

Figure 90 – Geometric parameters of methodology described by Barnea and Taitel (1993).

Since it is a one-dimensional model, the equations are described in terms of the pipe cross-section average. Where,

$$\theta = \arccos\left((1-2\frac{h_L}{D}\right) \tag{12.1}$$

$$A_L = \frac{D^2}{4}(\theta - sen\theta\cos\theta) \tag{12.2}$$

$$A_G = A - A_L \tag{12.3}$$

$$S_L = D\theta \tag{12.4}$$

$$S_i = D sen\theta \tag{12.5}$$

$$S_G = \pi D - S \tag{12.6}$$

According to Ishii (1980) the continuity and momentum equations in the one-dimensional form, considering the isothermal, irrotational and non-mass transfer hypotheses between the phases, can be rewritten as:

$$\frac{\partial}{\partial t}(\rho_j \alpha_j) + \frac{\partial}{\partial x}(\rho_j \alpha_j U_j) = 0 \tag{12.7}$$

$$\frac{\partial}{\partial t}(\rho_j \alpha_j U_j) + \frac{\partial}{\partial x}(\rho_j \alpha_j U_j U_j) = -\alpha_j \frac{\partial P_{ij}}{\partial x} - \alpha_j \rho_j g \frac{\partial h_L}{\partial x} - \frac{\tau_{wj} S_j}{A} \pm \frac{\tau_i S_i}{A} \tag{12.8}$$

Where *A*, is the cross sectional area of the tube, τ, the shear stress and *j*, the respective phase index.

The shear stresses are determined based on the friction factor, f, considering hydrodynamically developed flow, according to the expression a below.

$$\tau_{wj} = \frac{f_k}{2} \rho U_k |U_k| \tag{12.9}$$

$$\tau_i = \frac{f_i}{2} \rho_G (U_G - U_L) |U_G - U_L| \tag{12.10}$$

Assuming incompressible flow and combining both phases' momentum equations, the pressure terms can be eliminated using the approximate relation below.

$$P_{iL} = P_{iG} - \frac{\sigma}{R_i} \cong P_G - \sigma \frac{\partial^2 h_L}{\partial x^2} \tag{12.11}$$

Where, σ is the surface tension and *R* is the curvature radius, yields the following equation,

$$\rho_L \frac{\partial U_L}{\partial t} - \rho_G \frac{\partial U_G}{\partial t} + \rho_L U_L \frac{\partial U_L}{\partial x} - \rho_G U_G \frac{\partial U_G}{\partial x} + (\rho_L - \rho_G) g \cos\beta \frac{\partial h_L}{\partial x} - \sigma \frac{\partial^3 h_L}{\partial x^3} = F \tag{12.12}$$

Where,

$$F = -\frac{\tau_L S_L}{A_L} + \frac{\tau_G S_G}{A_G} + \tau_i S_i \left(\frac{1}{A_L} + \frac{1}{A_G} \right) - (\rho_L - \rho_G) g \sin\beta \tag{12.13}$$

Assuming that the flow is composed of base and a perturbed flow,

$$\alpha_L = \bar{\alpha}_L + \hat{\alpha}_L \tag{12.14}$$

$$U_L = \bar{U}_L + \hat{U}_L \tag{12.15}$$

$$U_G = \bar{U}_G + \hat{U}_G \tag{12.16}$$

$$h_L = \bar{h}_L + \hat{h}_L \tag{12.17}$$

Neglecting second-order terms using the linearization procedure and adopting geometric parameters, we can obtain the equations of perturbations.

$$\overbrace{\frac{A}{A'_L}}^{\varphi_1} \sigma \frac{\partial^4 \hat{h}_L}{\partial x^4} + \overbrace{\left(\frac{\rho_L \bar{U}_L^2}{\alpha_L} + \frac{\rho_G \bar{U}_G{}^2}{\alpha_G} - (\rho_L - \rho_G) g \cos\beta \frac{A}{A'_L} \right)}^{\varphi_2} \frac{\partial^2 \hat{h}_L}{\partial x^2} + \tag{12.18}$$

$$\overbrace{2\left(\frac{\rho_L \hat{U}_L}{\alpha_L} + \frac{\rho_G \hat{U}_G}{\alpha_G} \right)}^{\varphi_3} \frac{\partial^2 \hat{h}_L}{\partial t \partial x} + \underbrace{\left(\frac{\rho_L}{\alpha_L} + \frac{\rho_G}{\alpha_G} \right)}_{\varphi_4} \frac{\partial^2 \hat{h}_L}{\partial t^2} =$$

$$\underbrace{\left(-\frac{A}{A'_L} \frac{\partial F}{\partial \hat{h}_L} - \frac{\hat{U}_G \partial F}{\alpha_G \partial U_G} + \frac{\hat{U}_L}{\alpha_L} \frac{\partial F}{\partial U_L} \right)}_{-\varphi_5} \frac{\partial \hat{h}_L}{\partial x} +$$

$$\underbrace{\left(-\frac{1}{\alpha_G} \frac{\partial F}{\partial U_G} + \frac{1}{\alpha_L} \frac{\partial F}{\partial U_L} \right)}_{-\varphi_6} \frac{\partial \hat{h}_L}{\partial t}$$

Where, A'_L is $\frac{\partial A_L}{\partial h_L}$.

To linearize the above equation, it is assumed that the term F is composed only of mean values. The hypothesis is valid only if $\hat{h}_L$ is very small, so that the fluctuations have little influence on the shear stresses. We can represent the above equation in simplified form:

$$\varphi_1 \frac{\partial^4 \hat{h}_L}{\partial x^4} + \varphi_2 \frac{\partial^2 \hat{h}_L}{\partial x^2} + \varphi_3 \frac{\partial^2 \hat{h}_L}{\partial t \partial x} + \varphi_4 \frac{\partial^2 \hat{h}_L}{\partial t^2} + \varphi_5 \frac{\partial^2 \hat{h}_L}{\partial x} + \varphi_6 \frac{\partial^2 \hat{h}_L}{\partial t} = 0 \tag{12.19}$$

Where, α is the phase holdup and $\hat{h}_L$ is the perturbed liquid level. Substituting for the perturbed liquid level,

$$\hat{h}_L = \varepsilon e^{i(\omega t - kx)} \tag{12.20}$$

into Equation (12.18) yields the following dispersion equation,

$$\omega^2 - (\phi_1 k + \phi_2 i)\omega + \phi_3 k^2 - \phi_4 k^4 + \phi_5 k i = 0 \tag{12.21}$$

$$\omega_{1,2} = \frac{1}{2}(\varphi_1 k + \varphi_2 i) \pm \frac{1}{2}\sqrt{(\varphi_1 k + \varphi_2 i)^2 - 4(\varphi_3 k^2 - \varphi_4 k^4 + \varphi_5 k i)} \tag{12.22}$$

$$\omega = \omega_r + i\omega_i \tag{12.23}$$

Where, ε is the amplitude of the perturbation and k is the wavenumber and,

$$\varphi_1 = \frac{\phi_3}{\phi_4}\ \varphi_2 = \frac{\phi_6}{\phi_4}\ \varphi_3 = \frac{\phi_2}{\phi_4}\ \varphi_4 = \frac{\phi_1}{\phi_4}\ \varphi_5 = \frac{\phi_5}{\phi_4} \tag{12.24}$$

Choosing temporal analysis, we can determine the amplification rate $(-\omega_i)$ of the perturbations for a real wave number. The steady-state solution is unstable whenever the imaginary part of ω is negative, leading to exponential growth of the perturbed variable $\hat{h}_L$. In a stratified two phase flow pattern, as in the case of the present study, the growth of the disturbance may lead to the transition to intermittent flow. If the amplification factor is positive, the disturbance will not develop and the transition will not occur.